TECTONIC HISTORY OF
THE GREAT BOUNDARY FAULT, RAJASTHAN

A THESIS

Submitted in fulfilment of the
requirements for the award of the degree
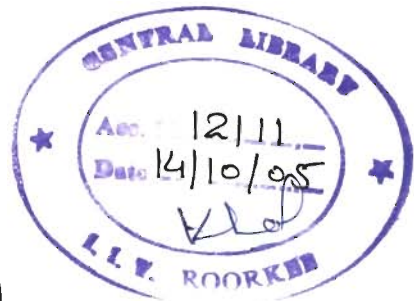*of*
DOCTOR OF PHILOSOPHY
in
EARTH SCIENCES

By

AMIT SAHAY

DEPARTMENT OF EARTH SCIENCES
INDIAN INSTITUTE OF TECHNOLOGY ROORKEE
ROORKEE-247 667 (INDIA)

MARCH, 2005

INDIAN INSTITUTE OF TECHNOLOGY ROORKEE
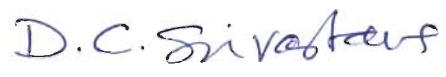
CANDIDATE'S DECLARATION

I hereby certify that the work which is being presented in the thesis entitled **"TECTONIC HISTORY OF THE GREAT BOUNDARY FAULT, RAJASTHAN"** in fulfillment of the requirement for the award of the degree of **DOCTOR OF PHILOSOPHY** and submitted in the **Department of Earth Sciences, Indian Institute of Technology Roorkee,** is an authentic record of my own work carried out during a period from January 2000 to March 2005 under the supervision of **Prof. D. C. Srivastava.**

The matter in this thesis has not been submitted by me for the award of any other degree of this or any other University/Institute.

Date: 14·03·05

(AMIT SAHAY)

This is to certify that the above statement made by the candidate is correct to the best of our knowledge.

(Dr. D. C. Srivastava)
Professor
Department of Earth Sciences
Indian Institute of Technology
Roorkee (INDIA)

The Ph.D. viva voce examination of **Mr. Amit Sahay** Research Scholar, has been held on _____

Signature of Supervisors   Signature of H.O.D.   Signature of External Examiner

Abstract

The Great Boundary Fault is a major tectonic lineament in the northwestern India that runs close to the contact between the Vindhyan sedimentary rocks (ca. 1400-600 Ma) and the pre-Vindhyan rocks. Despite the fact that the reactivated nature of this fault is indicated in some of the published accounts, the existing opinions on its tectonic evolutionary history and age are varied and conflicting.

This thesis makes an attempt to understand the tectonic history of the Great Boundary Fault by: (i) deciphering the characteristic deformation style of the fault zone and the fault related deformation zone, (ii) analyzing geometry, kinematics and dynamics of the mesoscopic structures developed during its initiation and reactivation in multiple phases, and (iii) analyzing the syntectonic fluid inclusions. The study area consists of three critical sections of the fault around Chittaurgarh, where the Vindhyan sedimentary rocks occurring on the footwall side show well developed fault zones and fault related deformation zone, and the Berach granite (ca. 2500 Ma), occurring on the hangingwall side, does not bear any significant imprints of the fault related deformation.

The Great Boundary Fault Zone contains different types of fault rocks, ductile shear zones, three successively developed folds groups (F_1 to F_3), and multiple sets of fractures and faults. The earliest structures are the mesoscopic scale ductile shear zones containing one or more sets of mylonite foliation. During the course of progressive ductile shearing, the mylonite foliation has been folded and refolded coaxially by the F_1 group folds. These ductile shear zones, along with the bedding surfaces, have been intensely folded into F_2 folds, and the superposition of F_2 folds over the F_1 folds has resulted into common development of type-2 interference pattern in the Great Boundary Fault Zone. F_3 folds are mild and their interference with F_2 folds shows development of broad culminations-depressions and coaptation folds.

Nature of the fault rocks within the Great Boundary Fault Zone is highly variable. Both, cataclasite and mylonite are commonly developed in the relatively competent lithounit caught up with in the fault zone. Fault breccia is relatively less common. The breccia/cataclasite and the mylonite have developed in alternate cycles, and the brittle deformation has acted as precursor to the ductile deformation, and the Great Boundary

Fault Zone has, in general developed in a brittle-ductile transitional zone. It is concluded that the Great Boundary Fault zone has a characteristic deformation style, which is defined by development of ductile shear zones, F_1 folds, type-2 interference patterns, and the cyclic development of cataclasite and mylonite in a brittle-ductile regime.

The fault related deformation zone contains two phases of folds, but three groups of brittle faults and fractures that were developed during the three successive phases of reactivation on the Great Boundary Fault. The low angle thrust faults represent the signatures of the first phase of reactivation on the Great Boundary Fault. The second group of brittle structures comprise striated fault/fractures, brittle-ductile shear zones and en-échelon veins. This group of structures is inferred to have developed during the second phase of reactivation on the Great Boundary Fault in a major strike-slip regime. The third group of structures include thrust and fault related kink folds that were developed during the third phase of reactivation on the Great Boundary fault in a thrust regime.

Paleostress analyses of the striated faults imply that the first and the third phase of reactivation occurred in thrust regimes in plane deviatoric and axial extensional states of stress, respectively. It is due to a major dextral strike-slip movement during the second phase of reactivation that the N-S trending F_2 folds in the fault related deformation zone assume a NNE to NE trend in the Great Boundary Fault Zone.

The fluid inclusion analyses on en-échelon veins, occurring within strike-slip shear zone of second phase, reveal that syntectonic fluids were highly saline and dense Na-Ca-Cl brines of intraformational origin. Interpretation of fluid inclusion data together with the estimates of the overburden thickness imply that the strike-slip faulting on Great Boundary Fault occurred at 2 km depth, 53 MPa pressure and 160-202°C temperature. These trapping conditions point to an anomalously high paleogeothermal gradient during the reactivation on the Great Boundary Fault.

In summary, amongst the four groups of successively developed mesoscopic structures, the earliest group of structures, i. e., the ductile shear zones and the F_1 folds, are related to initiation of the Great Boundary Fault in a possible thrust regime with top-to-the-SE sense of movement. The other three groups of structures, comprising successively developed brittle faults, are related to three successive events of reactivation of the Great Boundary Fault.

Acknowledgements

Contents

LIST OF FIGURES

vii

fluid inclusions show the presence of liquid phase and vapor phase at the room conditions.

LIST OF TABLES

xiii

Chapter 1

Introduction

1.1 Preamble

The concept that major fault lineaments represent zones of crustal weakness in continental regions, and evolve by tectonic reactivation was given by Hills (1956). It is now well established that the tectonic evolution of large-scale faults occurs commonly through different phases of reactivation that can either be similar or different with respect to nature of deformation and relative sense of displacement. For example, tectonic evolutionary history of the Outer Hebride Fault Zone, Scotland consists of five successive events of reactivation, which are characterised by distinct variations in style or nature of deformation and relative sense of displacement; namely, (i) top-to-the-NW ductile thrusting, (ii) top-to-the-SE brittle thrusting, (iii) top-to-the-NE sinistral strike-slip movement, (iv) top-to-the-SE brittle-ductile extension and (v) top-to-the-E brittle extension (Macinnes et al., 2000). By contrast, Wattle Gully Fault Zone, Australia, is a typical example where successive events of reactivation are characterised by similar nature of deformation, i. e., brittle reverse faulting (Cox, 1995).

According to Sibson (1985) and Sibson et al., (1988) pore-fluid pressure plays a crucial role in facilitating the reactivation of faults. The cyclic fluctuation in pore-fluid pressure between supralithostatic level to near hydrostatic level leads to successive reactivation of normal fault as high-angle reverse fault. By contrast, cyclic fluctuation in pore-fluid pressure between hydrostatic levels to below sub-hydrostatic levels leads to successive reactivation of thrust as low-angle normal fault.

Fault zone reactivation can occur well within intra plate regions, plate margin orogens as well as in the regions of active shallow subduction zones (Tandon et al., 2000). The Great Glen Fault Zone in Scotland is a typical example of an intraplate reactivated strike-slip fault (Stewart et al. 2000). Brevard Fault Zone in the southern Appalachians represents a plate margin fault, which records, (i) a thrust and dextral strike-slip movement in mid to late Paleozoic period and, (ii) a pure thrust type movement in the Alleghanian period (Bobyarchik, 1998). Fault zone in the Sierras Pampeanas regions of central Argentina, occur within active shallow subduction zones that have been reactivated as: (i) ductile reverse fault during Cambrian to Devonian, (ii) brittle normal fault and strike-slip fault during Carboniferous to Cretaceous and, (iii) high angle reverse fault during Tertiary period (Simpson et al. 2001).

The Great Boundary Fault of Rajasthan in the northwestern India is a well established intra plate tectonic lineament. In this thesis, an attempt is made to identify the characteristic deformation style of the Great Boundary Fault. Furthermore, the hypothesis that a crustal-scale fault, representing a major zone of weakness, evolves through successive phases of reactivation is tested in this thesis. The geometry, kinematics and

2

dynamics of different phases of reactivation events along the Great Boundary Fault are deciphered and its tectonic evolutionary history is reconstructed.

1.2 The Great Boundary Fault

Hacket (1877) coined the term 'Great Boundary Fault of Rajputana', for a prominent fault coinciding approximately with the western margin of the Vindhyan basin in Rajasthan. Surface trace of this fault is mappable for a strike length of more than 400 km, from Machilpur in the northeast to a little south of Chittaurgarh in the southeast of Rajasthan (Fig. 1.1a). The strike of Great Boundary Fault changes from NNE-SSW in the Chittaurgarh area to ENE-WSW or NE-SW in other parts (Fig. 1.1a). According to Sinha-Roy et al. (1995) the Great Boundary Fault is an imbricate zone that comprises a series of parallel steeply dipping reverse faults and intervening slices of sheared rocks. The maximum width of the fault zone is about 20 km in Karauli area and it decreases towards Chittaurgarh (Tiwari, 1995). The throw of the Great Boundary Fault is variable and the maximum throw of this fault is of the order of 1300-1400 m in the middle part of the fault zone near Mandalgarh, and it decreases both towards Chittaurgarh in the SW and Machilpur in the NE (Verma, 1996). Several metre-scale wrench faults occur sporadically all along the strike length of the Great Boundary Fault. Banerjee and Sinha (1981) suggest a pivotal nature of the Great Boundary Fault with the pivot located between Bundi and Chittaurgarh.
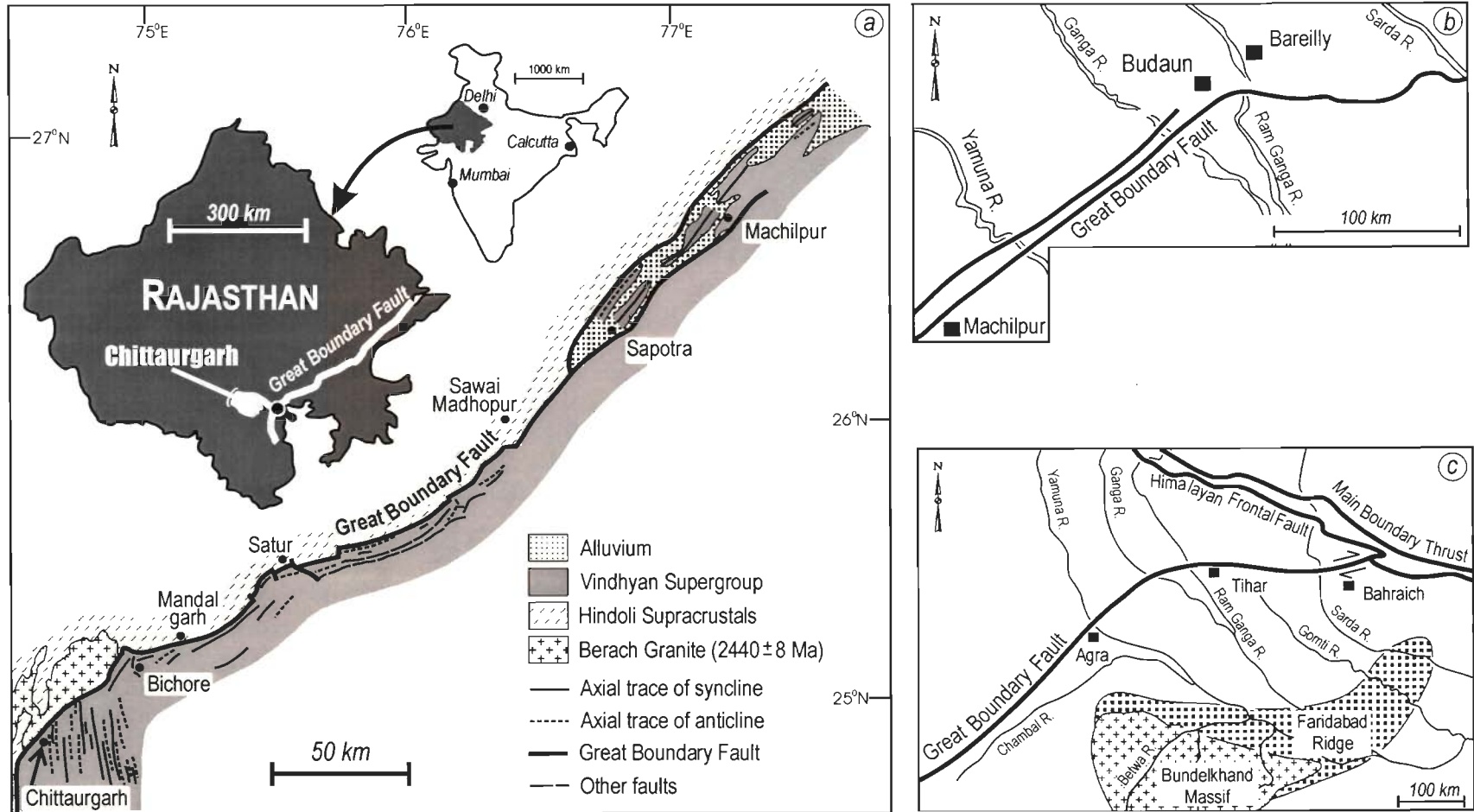
Fig. 1.1: (*a*) Geological setting of the Great Boundary Fault (compiled from Banerjee and Singh, 1981; Prasad, 1984; Tiwari, 1995). (*b*) Trace of the Great Boundary Fault beneath the gangetic alluvium (after Tiwari, 1995). (*c*)Trace of the Great Boundary Fault in Rajasthan and its linkage with the active Himalayan Frontal Fault (after Valdiya, 1998).

Recent seismic reflection studies by Tiwari (1995) show northeastward continuation of the Great Boundary Fault for another 400 km, from Machilpur upto Sarada river, under the Gangetic alluvium (Fig.1.1b). The subsurface trend of the Great Boundary Fault remains NE-SW or E-W under the Gangetic alluvium, with minor kinks and curvatures (Tiwari, 1995). Further, the geophysical studies indicate that the Great Boundary Fault dips at very steep angle towards northwest and cuts a thick section of the crust up to a near Moho depth (Choudhury and Datta, 1975; Gokarn et al. 1995; Reddy et al. 1995). Valdiya (1998) hypothesises an eastward extension of the Great Boundary Fault and its linkage with the presently active Himalayan Frontal Fault (Fig. 1.1c).

The Great Boundary Fault, in general, runs close to the boundary between sedimentary rocks of Vindhyan Group (ca.1400–600 Ma, Venkatachala et al. 1996) and the granites, the metavolcanics and the metasedimentary rocks belonging to the Paleoproterozoic or Archean age. In the southwestern sector, the Great Boundary Fault runs along the contact between the Archean basement, namely, Berach granite (ca. 2440 ± 8 Ma, Wiedenbeck et al., 1996), and the Mesoproterozoic cover sequence corresponding to the lower and middle Vindhyan Supergroup (Fig. 1.1a). For most of its stretch in the central sector, the Great Boundary Fault follows the contact between the Archean rocks or the Paleoproterozoic supracrustals of the Hindoli Group and the Neoproterozoic sedimentary sequences of the upper Vindhyan Supergroup. In the northeastern sector, the Great Boundary Fault comprises two sub-parallel faults, one of which cuts through the Neoproterozoic sedimentary sequence of upper Vindhyan Group and the other runs along the interface of the Paleoproterozoic Hindoli supracrustals and the Neoproterozoic sedimentary sequence of the upper Vindhyan Supergroup (Fig. 1.1a).

There are several opinions regarding the tectonic evolution of the Great Boundary Fault. Heron (1953) correlated the evolution of the Great Boundary Fault to the uplift of Aravalli ranges in the Mesozoic Era. Pascoe (1959) suggested that the development of the Great Boundary Fault is syntectonic with respect to folding of the Aravalli and Delhi rocks (ca. 2000–1450 Ma, Roy, 1988). According to Sinha-Roy (1986a), the Great Boundary Fault developed as a consequence of impingement of Bundelkhand massif with the Vindhyan cover rocks as a result of regional crustal deformation due to collision and jamming of the Indian plate with the Eurasian plates (ca. 60 Ma, Rowley, 1996).

Fermor (1930) was the first proponent of the hypothesis that the Great Boundary Fault is a pre-Vindhyan structure that has reactivated during and after the sedimentation of the Vindhyan Supergroup rocks (ca. 1400-600 Ma). Iqbaluddin et al. (1978) proposed that the Great Boundary Fault initiated as a normal gravity fault that activated as a reverse fault during the deposition of Bhander Group of rocks in the Lower Paleozoic period. They ascribe the reactivation to the centrifugal stress field in the Vindhyan basin margin. According to Prasad (1981), the Great Boundary Fault is a post-Vindhyan fault that cuts through various stratigraphic formations and runs athwart to major structural elements such as large scale folds in the Vindhyan Group of rocks. Verma (1996) considers that the Great Boundary Fault was initiated as a normal fault during the rifting of the Aravalli Basin (ca. 2500 Ma.), and it reactivated as a reverse fault during the Delhi orogeny (ca. 1400 Ma). Choudhuri and Guha (2004) opine that the Great Boundary Fault originated as a thrust in a brittle-ductile/ductile regime and reactivated as a normal fault.

1.3 Scope of the present work and objectives

A review of the previous work, detailed in the preceding section, amply demonstrates the lack of concurrence on nature and evolution of the Great Boundary Fault. The main reasons for conflicting and divergent views on Great Boundary Fault are: (i) lack of detailed geological and structural map of the Great Boundary Fault Zone, (ii) lack of structural analysis in the Great Boundary Fault Zone and, (iii) the fact that most opinions regarding the evolution of the Great Boundary Fault Zone are based solely on the regional geologic considerations. No attempt has so far been made to identify different phases of reactivation on the basis of structural or microstructural studies.

Criteria for recognition of reactivation events and possible processes leading to crustal weakening along the zones of crustal-scale faults are now well established (Holdsworth, 1997). During the last two decades, several methods, based on numerical inversion of geological data, have been developed and tested for determination of palaeostress in rocks. (Etchecopar et al., 1981; Lisle, 1987; Angelier, 1990, 1994; Dune and Hancock, 1994; Arlegui and Simon, 1998; Vandycke and Bergerat, 2001; Vandycke, 2002; Orife et al., 2002; Orife and Lisle, 2003). With the availability of techniques for palaeostress determination from mesoscopic geological structures, it is now possible to analyze different phases of reactivation within the Great Boundary Fault Zone. The geometric, kinematic and dynamic analyses of major events of reactivation, arranged in relative chronological order, help reconstruct the tectonic evolutionary history of the Great Boundary Fault.

7

In view of a great deal of scope for detailed structural work along the Great Boundary Fault Zone, following lines of approach are planned for unravelling its tectonic evolutionary history:

(i)   To establish the characteristic style of deformation within the Great Boundary Fault Zone.

(ii)   To identify the multiple phases of reactivation on the Great Boundary Fault, and decipher the nature and dynamics of reactivation in each phase.

(iii)   Understand the nature and source of fluids, pressure-temperature, paleogeothermal and pore-fluid conditions during the deformation along the Great Boundary Fault, with the help of fluid inclusion technique.

1.4 Selection of the study area

The area around Chittaurgarh town is selected for detailed study, because it exposes one of the most complete sections of the Great Boundary Fault in a relatively narrow strip (Fig. 1.2). The rock types exposed in the study area, exhibit the imprints of both ductile and brittle deformation. Whereas the ductile deformation is represented by several generations of successively developed folds and mylonite foliations; the brittle deformation is represented by abundant fractures, striated faults and en-échelon veins.

The study area is bounded by latitude N 24° 51′ to 25° 02′ and longitude E 74° 35′E to 74° 48′E. It falls on Topographic sheets 45 L/9, 45 L/13, 45 K/12 and 45 K/16 of the Survey of India at 1:50,000 scale. The effect of denudation and erosion is very well
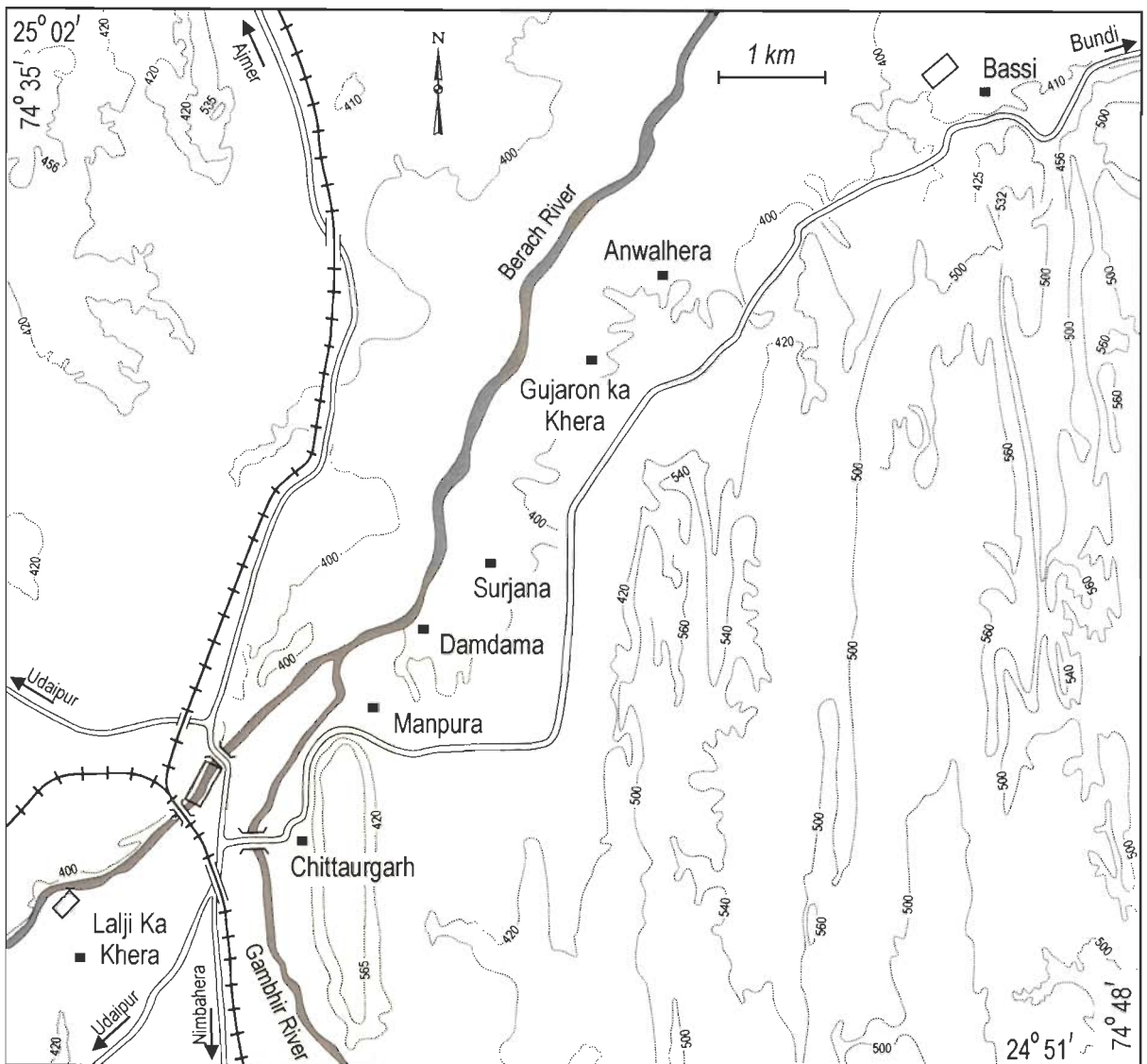
Fig. 1.2: Topography and location of the study area. The three sections studied in this thesis are shown by the rectangles around Chittaurgarh, lalji ka Khera and Bassi towns, respectively..

marked by the anticlinal valleys and the synclinal ridges with characteristically flat tops. In general, the anticlinal valleys are made up of the shale and the limestone beds, and the synclinal ridges are made up of the sandstone beds. The approximate elevation of the ridge is about 565 m above the mean sea level (Fig. 1.2).

Geological and structural setting

2.1 Regional geology

The Aravalli Mountain Range in Rajasthan is presently exposed as a horst-like structure, which was developed during continental rifting around 2500 Ma. According to Verma and Greiling (1995), the Great Boundary Fault defines the eastern margin of this horst. As discussed in the first chapter, this fault runs close to the contact between the Vindhyan Supergroup and pre-Vindhyan rocks. Vindhyan Supergroup consists of the unmetamorphosed sedimentary sequence, the pre-Vindhyan rocks are made up of the Berach granite, the metasedimentary rocks, and the metavolcanic rocks of the Hindoli Group.

Berach Granite

The Berach granite, referred as, Chittor gneiss by Hacket (1881), Bundelkhand gneiss by Gupta (1934) and Heron (1936) and, Berach granite by Pascoe (1968), occurs as the crescent bodies outcroping in and adjacent to the Berach valley near Chittaurgarh,

where it covers an area of about 300 km^2 (Sinha-Roy et al. 1998). This granite is dated as 2440 ± 8 Ma by ion microprobe analysis on Zircon and ^{207}Pb / ^{206}Pb data (Wiedenbeck et al., 1996). In the study area around Chittaurgarh the contact of Berach granite with the Vindhyan sedimentary rocks is mostly tectonic in nature and extends from a little northwest of Bhojunda (N 24° 50' 45''; E 75° 35' 45'') to a little southwest of Barundini (N 25° 10'; E 74° 56'). Towards south of Chittaurgarh, near Saraipipli (N 24° 13'; E 74° 37') and Dholapani (N 24° 16'; E 74° 40'), respectively, the contact of Berach Granite is represented by an unconformity with the andesitic flows marks the onset of the Vindhyan sedimentation and sandstone (Prasad, 1984).

Hindoli Group

The Hindoli Group occurs in an arcuate belt containing the felsic and the mafic metavolcanics and the metagreywackes forming a turbidite sequence (S. N. Gupta, 1981; Bose and Sharma, 1992). Heron (1917) correlated this formation with the Gwalior series of central India, while B. C. Gupta (1934) considered it to be a part of the Aravalli Supergroup. Bose and Sharma (1992) classified the rocks of the Hindoli Group into three facies, namely, the turbidite facies, the stable shelf facies and the mafic-felsic volcanics including tuffs. Opinions on the relationship between the Hindoli Group with the Berach Granite are divided. Raja-Rao et al. (1971), S. N. Gupta (1981), Prasad (1981, 1984, 1987) opine that the Berach granite intrudes the Hindoli Group. This opinion is contested by Sharma and Roy (1986), Roy (1988) and Bose and Sharma (1992) who suggest Berach granite forms a basement for the Hindoli Supracrustals.

12

The Vindhyan sedimentary sequence of Rajasthan occurs within intracratonic basin, which is supposed to have initiated as transtensional rift around 1800 Ma (Ram et al. 1996). It is bounded by the Jhalawar lineament in the south and the Great Boundary Fault in the north (Ramasamy, 1995). It occupies an area of about 24,000 km^2 and has a cumulative stratigraphic thickness of about 3.2 km. The Vindhyan sedimentation started with volcanic activity representing a fissure type eruption, on an irregular basin floor (Prasad, 1984). The Vindhyan Supergroup comprises repetitive sequence of shale, limestone, sandstone and pyroclastic materials at various stratigraphic levels (Chakraborty et al. 1996). The depositional environment remained near shore to tidal flat under fluctuating marine conditions (Prasad, 1981). Kale and Phansalkar (1985) suggest an overall outer shelf environment for the Vindhyan rocks and shore or lagoonal environment for some of the intervening formations. A generalized lithostratigraphic succession of the region is shown in Table 2.1.

Table 2.1: Lithostratigraphy of the Precambrian rocks in Rajasthan (compiled from Prasad, 1984; Bose and Sharma, 1992).

Era	Super Group		Sub Group	Formation
Proterozoic	Vindhyan Supergroup	Upper Vindhyan	Bhander Group (ca. 1350-600 Ma)	Upper Bhander shale
				Upper Bhander limestone
				Sirbu shale
				Lower Bhander sandstone
				Samaria shale
				Lower Bhander limestone
				Ganurgarh shale

		Rewa Group		Upper Rewa sandstone
				Jhiri shale
				Lower Rewa sandstone
				Panna shale
		Kaimur Group (ca. 940-900 Ma)		Kaimur sandstone
	Lower Vindhyan	Semri Group (ca. 1400-1140 Ma)	Khorip	Suket shale
				Nimbahera limestone
				Nimbahera shale
				Jiran sandstone
			Lasrawan	Binota shale
			Sand	Palri shale
				Sawa sandstone
			Satola	Bhagwanpura limestone
				Khardeola sandstone
				Khairmalia andesite
	————— Great Boundary Fault ? —————			
Archean	**Hindoli Supracrustal**			Slate, quartzite, phyllite metagreywacke and metavolcanics (ca. 2000)
	Berach granite			(ca. 2440 ± 8 Ma)

2.2 Geology of the study area

The study area exposes the Berach granite as the basement, and the Vindhyan sedimentary sequence as the cover rocks (Fig. 2.1). The Berach granite is mostly massive, competent and porphyritic and it does not exhibit any perceptible imprints of deformation related to Great Boundary Fault, except local brecciation in the small domains. By contrast, Great Boundary Fault related structures, ranging in the scale from a few mm to several km, are developed extensively in the Vindhyan sedimentary sequence. Table 2.2 gives the stratigraphic sequence, important megascopic and microscopic characteristics, thickness and age of various formations exposed in the study area.

Legend:
- Panna shale
- Kaimur sandstone
- Suket shale
- Nimbahera limestone
- Nimbahera shale
- Binota shale
- Sawa shale
- Sawa sandstone
- Bhagwanpura limestone
- Hindoli Group
- Berach granite

- XX Brittle deformation
- ▲▲ Fault breccia
- ◆ Axial trace of anticline
- ⊥ Axial trace of syncline
- GBFZ
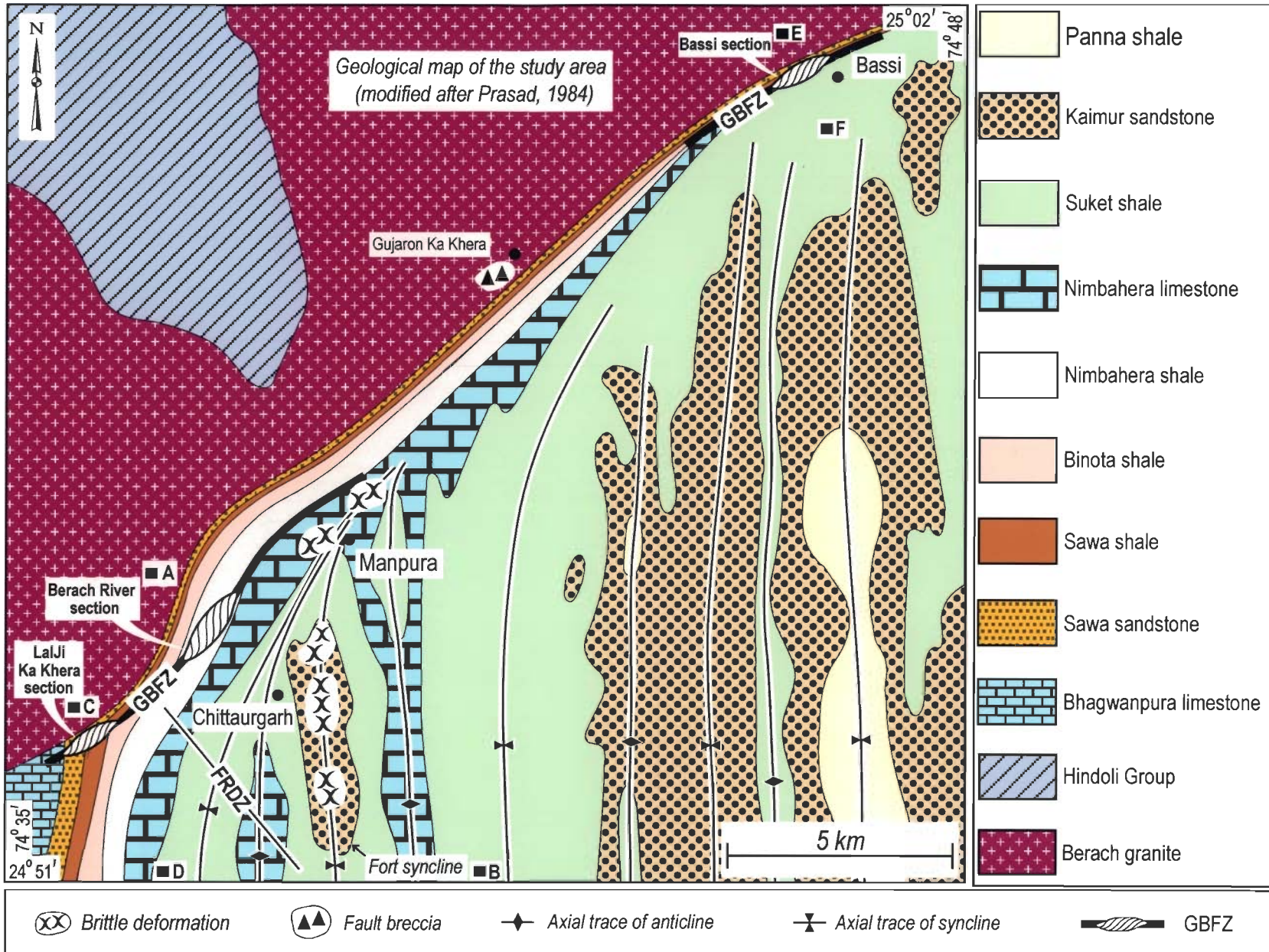
Fig. 2.1: Geological and structural setting of the study area. The location of Berach river section, Lalji ka Khera section and Bassi section are marked. AB, CD and EF are reference point for cross sections shown in Fig. 2.5. GBFZ- Great Boundary Fault Zone. FRDZ- Fault related deformation zone.

Table 2.2: Description of the rock types in the study area.

Rock Type	Characteristic Features	Thickness and age
Panna shale	Compact and fissile. Green or pale green, brownish and purple in colour.	Individual bed: Not Known Cumulative: 20 m (Prasad, 1984) Age: Not Known
Kaimur sandstone	Massive, compact and hard. Reddish to pinkish in colour, ferruginous, medium to coarse grained. Cross bedding and symmetrical ripple marks are common. Quartz constitutes the bulk composition (95%) with subordinate K-feldspars. The quartz grains are subangular to rounded and show sutured contact (Fig. 2.2a). Cementing material is essentially ferruginous.	Individual bed: Not known Cumulative: 70 m (Prasad, 1984) Age: ca. 900-940 Ma (Venkatachala et al. 1996)
Suket shale	Hard and fragile, pale green or chocolate brown in colour, fine grained, interbedded with siltstone bands. Angular to rounded quartz grains constitute the bulk composition with a few flakes of muscovite (Fig 2.2b).	Individual bed: Not Known Cumulative: 120 m (Prasad, 1984) Age: Not known
Nimbahera limestone	Massive, compact and hard. Bluish grey or dark grey, fine-grained. Beds are generally separated by thin shale bands. Pyrite crystals (1-2 cm) are common. In thin section, bedding parallel stylolites are common (Fig. 2.2c).	Individual bed: 10 cm-1 m Cumulative: 148 m (Prasad, 1984) Age: Not Known
Nimbahera shale	Fissile and splintery. Typically khaki, purple or greenish purple in colour very fine-grained. Bedding parallel ferruginous bands and cross beds are common (Fig. 2.2d). Quartz grains show weak preferred orientation parallel to bedding surface.	Individual bed: Not Known Cumulative: 45 m (Prasad, 1984) Age: Not known

Binota shale	Fragile and splintery, olive green, brown, pink and purple in colour, very fine-grained. At places the bedding surfaces are intercalated with siltstone bands. Bedding parallel quartz veins, pressure solution and stylolite are common (Fig. 2.2e).	Individual bed: Not Known Cumulative: 250 m (Prasad, 1984) Age: Not Known
Sawa shale-porcellanite	Soft, pale yellow with greyish bands of porcellanite, which is extremely fine grained (Fig. 2.2f). Under high magnification, randomly oriented microcrystalline quartz and small shreds of mica are observable.	Individual bed: Not known Cumulative: 75 m (Prasad, 1984) Age: Not Known
Sawa sandstone	Massive, compact and hard, pink to white colour, medium to coarse-grained. Cross bedding is common. Quartz constitutes the bulk composition with subordinate K-feldspar ($\leq$10%). Quartz grains are generally subrounded to rounded and show planar to wavy contact, but angular grains are also common (Fig. 2.2g). Matrix is calcareous.	Individual bed: 0.5–2.5 m Cumulative: 100 m Age: ca. 1000–1300 Ma (Prasad, 1984)
Bhagwanpura limestone	Massive, compact and hard, grey, fawn, brown and pink in colour, fine-grained and stromatolitic. In thin section micritic groundmass of calcite/dolomite is common (Fig. 2.2h).	Individual bed: 15–50 cm Cumulative: 30 m Age: ca. 1000–1300 Ma (Prasad, 1975)
Berach granite	Massive, pink coloured, medium to coarse grained, equigranular hypidiomorphic granite. It range from granite to granodiorite, and at places gabrroic variety are also common. Quartz, K- feldspar, plagioclase, microcline are the common minerals with few biotite and muscovite. Feldspar grains are mostly weathered and quartz grains show undulose extinction (Fig. 2.2i).	Thickness: Not known Age: ca. 2440 $\pm$ 8 Ma (Wiedenbeck et al. 1996)

18
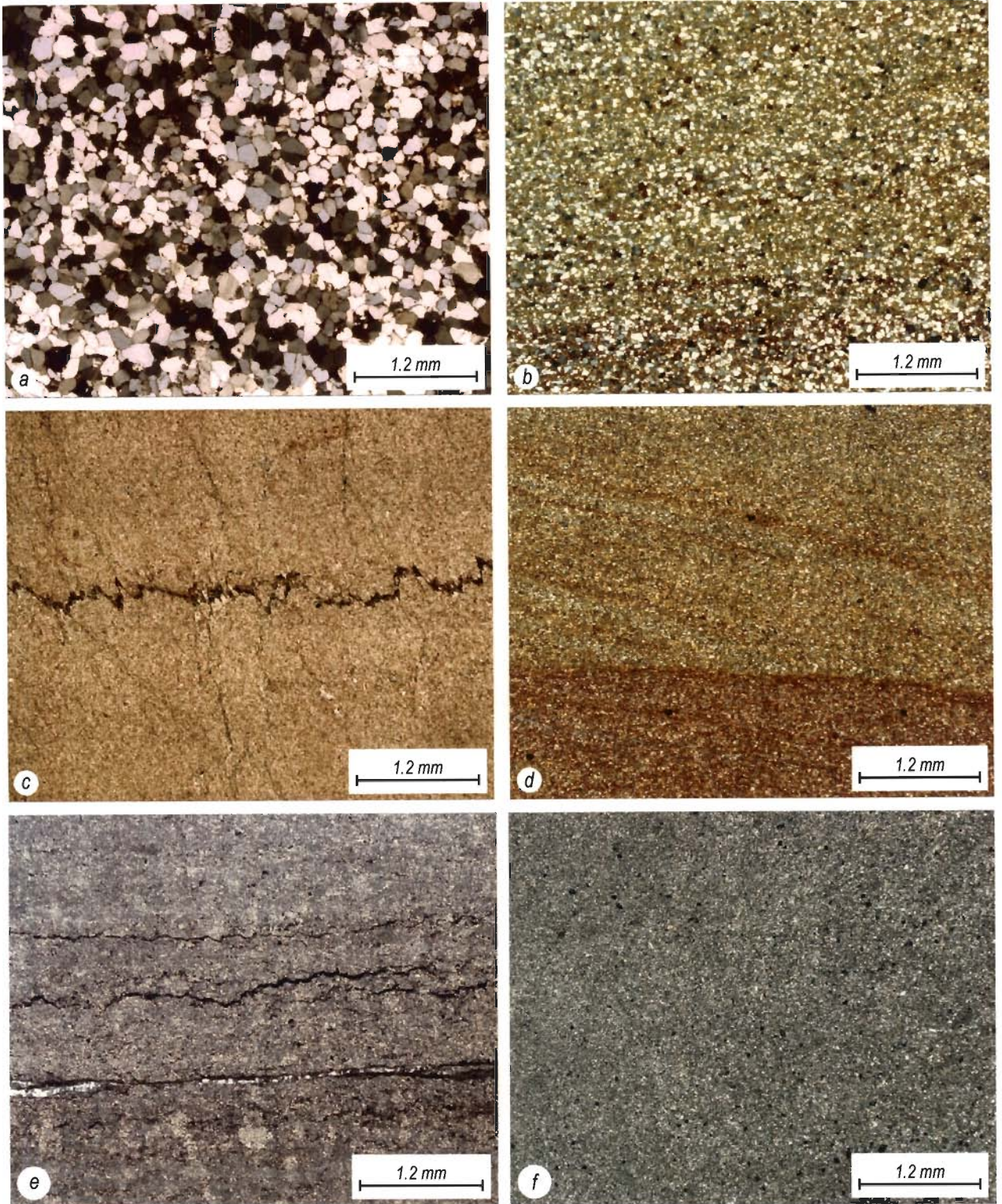
Fig. 2.2: *See captions on page 21*
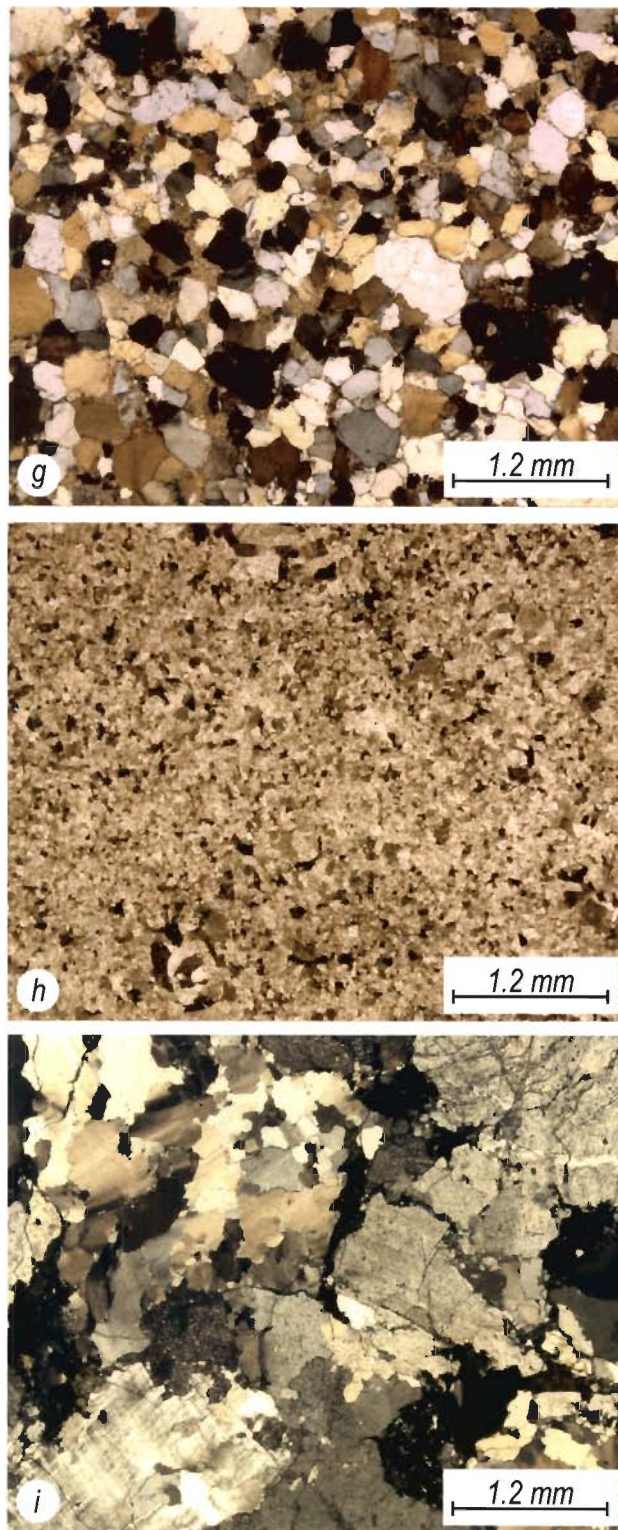
Fig. 2.2: Photomicrographs of the rock types in the study area (crossed polars). (***a***) Kaimur sandstone-medium to coarse grained and subangular to rounded quartz grains. (***b***) Suket shale- fine grained and angular to rounded quartz grains. (***c***) Nimbahera limestone- micritic limestone with well developed stylolite. (***d***) Nimbahera shale- showing cross bedding structure. (***e***) Binota shale-bedding parallel quartz vein and stylolite. (***f***) Sawa porcellanite- fine grained. (***g***) Sawa sandstone-medium to coarse grained and rounded to subrounded quartz grains showing planar or wavy grain contacts. (***h***) Bhagwanpura limestone- fine to medium grained micritic limestone. (***i***) Berach granite-K- feldspar and quartz grains showing weathered and undulose extinction, respectively.

21

2.3 Fault zone and fault related deformation zone

Large scale faulting commonly results into development of two structurally different zones of deformation (Newman and Mitra, 1993). First, a fault zone that consists of intensely deformed fault rocks. Second, a fault related deformation zone, in which rocks are relatively less intensely deformed than the fault zone rocks. The boundary between these two types of zones is seldom sharp and fault zones commonly grade into fault related deformation zones, which, in turn, pass into the rocks that bear no any imprints of deformation due to faulting. The thickness of either of these two types of zones can vary from cm to km scale.

In general, three different types of spatial relationships can be distinguished on the basis of the scale of development of fault zone and fault related deformation zone: (i) m-km thick fault related deformation zones on both hangingwall and footwall sides of a m-km thick fault zone (Fig. 2.3a), (ii) m-km thick fault related deformation zone on either of the hangingwall or footwall side of the m-km thick fault zone (Fig. 2.3b and c) and, (iii) a sharp fault zone with or without fault related deformation zones on either or both hangingwall or footwall sides (Fig.2.3d to g).

Different types of fault zones and fault related deformation zones are developed in different parts of the Great Boundary Fault. For example, in the northeastern part of the Great Boundary Fault, near Machilpur, where the fault cuts through the Vindhyan sedimentary rocks, the fault related deformation zone is likely to occur on both hangingwall and footwall sides of the well developed fault zone (Fig. 1.1a). In those sections, where Great Boundary Fault runs along the contact between the Vindhyan
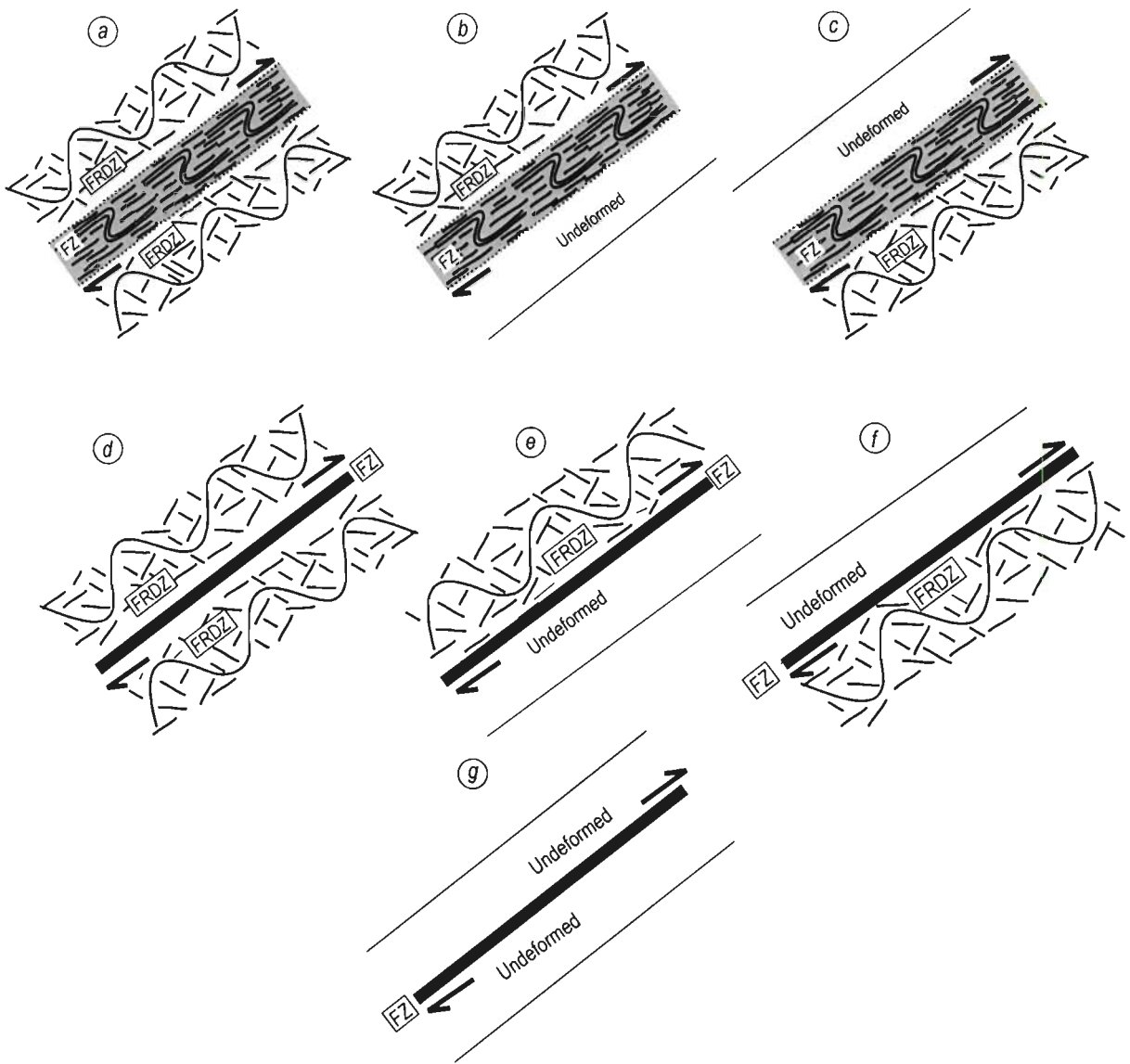
Fig. 2.3: (*a-g*) Schematic cross sections showing spatial relationship between fault zone (FZ) and fault related deformation zone (FRDZ). (*a*) FRDZ occurring on both hangingwall and footwall side of the FZ. (*b*) FRDZ occurring on hangingwall side of the FZ. (*c*) FRDZ occurring on footwall side of the FZ. (*d*) FRDZ occurring on both hangingwall and footwall side of a sharp fault. (*e*) FRDZ occurring on hanging wall side of a sharp fault. (*f*) FRDZ occurring on footwall side of a sharp fault. (*g*) A sharp fault without FRDZ.

sandstone and pre-Vindhyan quartzite, for example, in the Unli river section (N 25° 13' 7"; E 75° 14' 24") near Mandalgarh, the fault zone is represented by a sharp fault showing intense fracturing and brecciation within a few cm thick zone and, fault related deformation zone in the Vindhyan sedimentary beds occurring on the footwall side (Figs. 1.1a, 2.3f and 2.4). Finally, in those sections, where Great Boundary Fault runs along or close to the contact between the relatively incompetent Vindhyan sedimentary rocks and competent Berach granite, for example, near Chittaurgarh, the development of both the fault zone and the fault related deformation zone are confined within the relatively incompetent Vindhyan rocks occurring on the footwall side (Fig. 2.5). In these sections, there is no fault related deformation in the Berach granite on the hangingwall side.

This thesis concerns with a detailed study of the structural style of the Great Boundary Fault Zones in three different sections and the fault related deformation zones in one section. In all the three sections, both the Great Boundary Fault Zone and fault related deformation zones are confined within the Vindhyan cover rocks and do not, in general, extend into the granitic basement. Major structural characteristics of the two types of deformation zones are highlighted in Table 2.3.

Table 2.3: General description of the two types of deformation zones along the Great Boundary Fault.

Great Boundary Fault Zone	Fault related deformation zone
Characterised by numerous cm to m-scale discrete ductile shear zones and three groups of successively developed folds, namely, F_1, F_2 and F_3. Of the three phases of folding, F_2 folds are mostly dominant and the Great Boundary Fault runs parallel to the axial planes of these folds. The fault zone rocks vary from mylonite through cataclasite and breccia.	Characterised by km scale F_2 folds and, metre scale striated faults and en-echelon veins. Lack F_1 and F_3 folds, mylonites, cataclasite, or breccia is conspicuous. Intensity of F_2 folding is much milder than the corresponding folds in the fault zone. Furthermore, the F_2 folds trend N-S in the fault related deformation zone and NE-SW in the Great Boundary Fault Zone.

Three typical sections of the Great Boundary Fault Zone, selected for this study, are the Berach river section, the Lalji Ka Khera section and the Bassi section (Fig. 2.5a to c). In all the three sections, the Great Boundary Fault Zone is developed either close to or along the contact between the granitic basement and sedimentary cover rocks, albeit its development is restricted within the Vindhyan sedimentary rocks (Fig. 2.5a to c). In the Berach river section, the Great Boundary Fault Zone passes close to the contact between the Berach granite and the Vindhyan shale beds. Although it is likely, that a thin strip of shale also occur on the hangingwall side, the nature of deformation in the shale beds on the hangingwall side cannot be deciphered due to lack of outcrops. The Great Boundary Fault Zone in the Berach river section cuts through the Nimbahera shale, which shows ample evidence of mylonitization and successive folding. In the Lalji Ka Khera section and the Bassi section the Great Boundary Fault Zone cuts through the Sawa sandstone-shale-porcellanite sequence.

The structures present in the fault related deformation zone are also found to occur in the Great Boundary Fault Zone, but the vice-versa does not hold good. The structures in the fault related deformation zone are relatively less complex than those in the fault zone. Furthermore, the rocks in the fault zone are mostly thinly bedded Sawa sandstone-shale-porcellanite. In the fault related deformation zone, however, the thick and relatively competent rock units, such as Kaimur sandstone and Nimbahera limestone are present. These rocks show best development of successive mesoscopic scale structures that were developed during the multiple phases of reactivation of the Great Boundary Fault. For these reason, the reactivation history of the Great Boundary Fault is traced through the detailed study of structures in the fault related deformation zone.
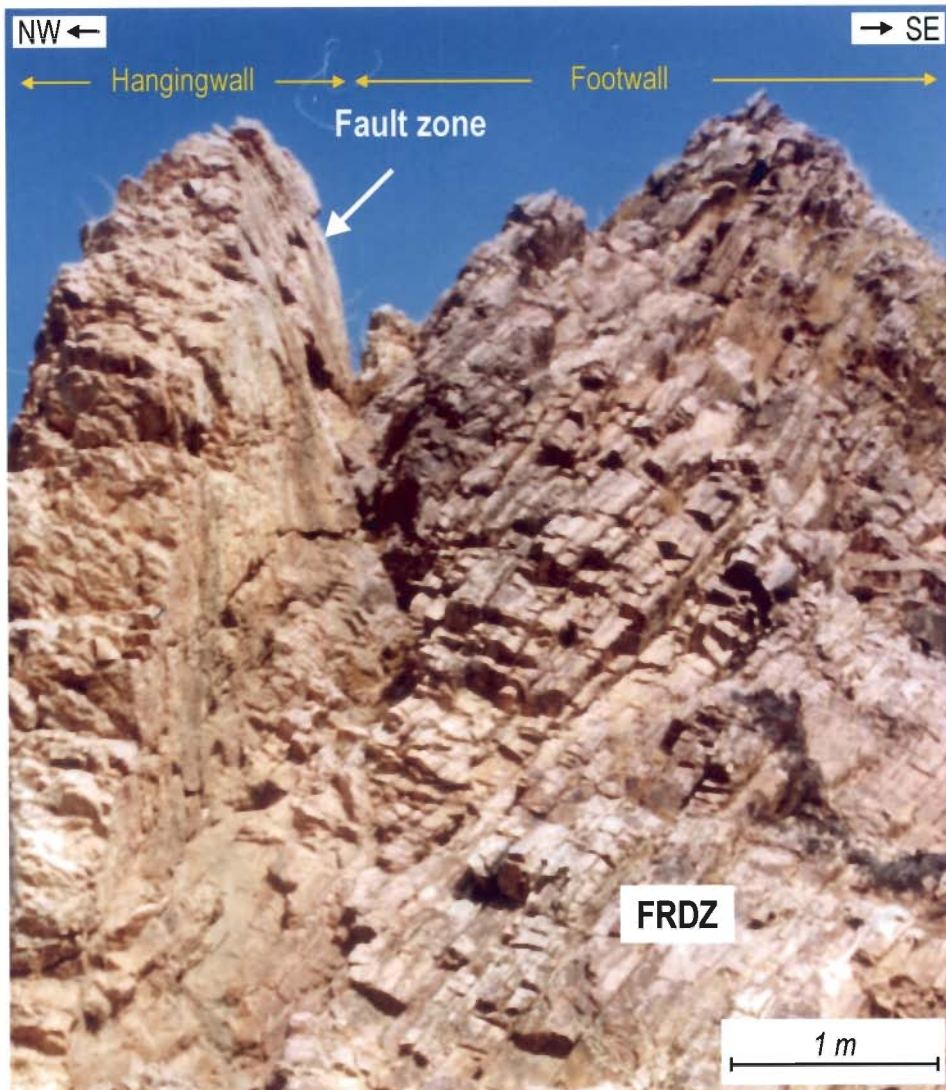
Fig. 2.4: An example of a sharp fault zone with fault related deformation zone (FRDZ) in the Vindhyan rocks on the footwall side. The pre-Vindhyan rocks occurring on the hangingwall side do not show any fault related deformation zone.
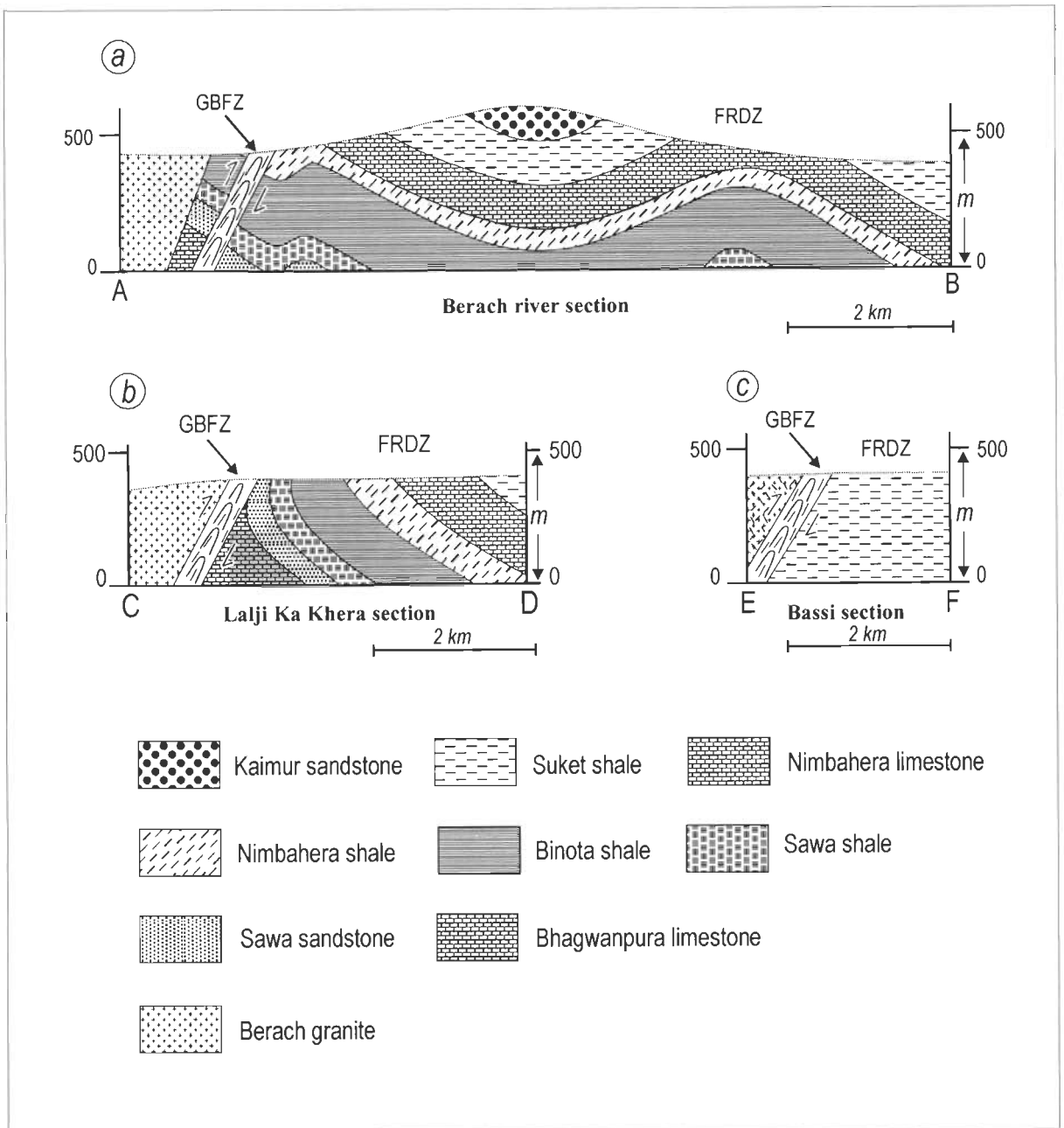
Fig. 2.5: (*a-c*) Schematic cross sections across the study area. The cross sections are drawn along the reference points AB, CD and EF (shown in fig. 2.1) for the Berach river section, the Lalji ka Khera section and the Bassi section, respectively. In Bassi section, Berach granite occur as gabbroic variety.

Structural style of the Great Boundary Fault Zone

The aim of work presented in this chapter is to explore a characteristic structural style, if any, of the Great Boundary Fault Zone. For this, three typical sections of the Great Boundary Fault Zone, namely, Berach river section, Lalji ka Khera section and Bassi section have been mapped and studied in details. The Great Boundary Fault Zone, in all these three sections, is preserved as a zone of intense ductile deformation that is cut by the multiple sets of fractures and faults. Although the Great Boundary Fault Zone in the Berach river section lies close to the Berach granite, it does not run along the contact of the Berach granite and the sedimentary rocks. Instead, it is developed within the Nimbahera shale beds that are exposed in the vicinity of the Berach granite. In Lalji ka Khera and Bassi sections the Great Boundary Fault Zone consists of the Sawa sandstone-shale-porcellanite sequence that is juxtaposed against the Berach granite.

3.1 Berach River Section

The Great Boundary Fault Zone in the Berach river section attains a maximum thickness of about 115m in its middle part and pinches out on either side to assume a

lenticular geometry (Fig. 2.1). It consists of the Nimbahera shale beds, which show abundant development of ductile and brittle structures.

3.1.1 Ductile structures

Mesoscopic scale overprinting relationships allow the classification of the ductile structures within the fault zone into two main groups: (i) early structures- related to ductile shearing and, (ii) late structures- developed subsequent to ductile shearing. The early structures include the ductile shear zones; a group of early folds, F_1, which contains two fold sets, F_{1A} and F_{1B} and; two sets of quartz veins. The late structures post-date the event of ductile shearing and include two successive groups of folds F_2 and F_3, that are well developed at the scales ranging from the outcrop to map.

Early structures: ductile shear zones and F_1 folds

Numerous lensoid, or, tabular ductile shear zones cut through the Nimbahera shale beds exposed within the Great Boundary Fault Zone (Fig. 3.1a). Although strike continuity of these shear zones can be traced up to several metres, their width varies from a few centimeters to a couple of decimetres. The ductile shear zones are mainly made up of sheared quartz veins, opaque concentrations and a few unsheared fragments of the Nimbahera shale beds (Fig.3.1a). Whereas the quartz veins, within ductile shear zones, are invariably mylonitised- the opaque bands, made up of goethite and pyrolusite, show

32
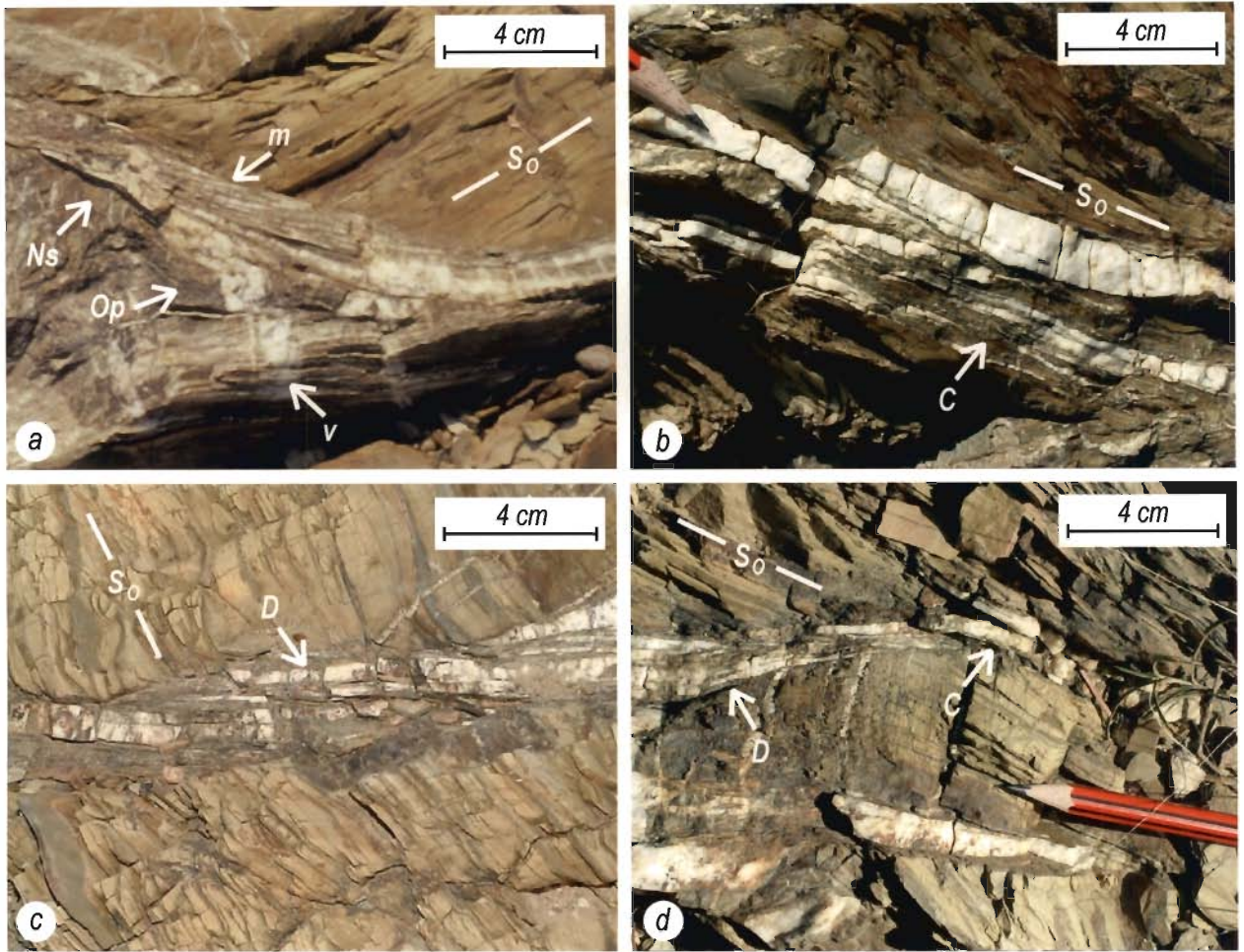
Fig. 3.1:(*a-d*) Ductile shear zones cutting through the Nimbahera shale beds in the Berach river section (crossed polars). (*a*) Ductilely sheared quartz veins (*V*), mylonite foliation (*m*), opaque bands (*Op*) and unsheared fragment of Nimbahera shale (*Ns*). (*b*) A concordant shear zone (*C*) containing mylonitised quartz veins and paralleling bedding surface (*So*). (*c*) A discordant shear zone (*D*) inclined at an angle to bedding surface (*So*). (*d*) discordant sear zones (*D*) grading into concordant shear zone (*C*).

little or no evidence of ductile shearing. It is evident, therefore, that the bulk of the strain related to ductile shearing is concentrated within the mylonitised quartz veins.

Two distinct types of ductile shear zones are mappable: (1) concordant, which run parallel to the bedding surfaces, and (2) discordant, which cut through the bedding surfaces at low to moderate angles (Fig. 3.1b and c). Because of inconsistent overprinting relationships, and the fact that many concordant shear zones grade into discordant shear zones along their strike length, these two types of ductile shear zones are inferred to have developed in a common deformational event (Fig. 3.1d). It is likely that although bulk of the quartz veins were developed parallel to the bedding surfaces, some were developed at low angles to the bedding surfaces. This lack of strict initial parallelism between the quartz veins has eventually resulted into a synchronous development of concordant shear zones and discordant shear zones.

As F_1 groups of folds are confined within the ductile shear zones, these folds are inferred to have developed during the course of progressive shearing. Similarly two sets of quartz veins, viz. bedding parallel veins and bedding perpendicular veins were also developed and mylonitised during the progressive ductile shearing. The details of the evolution of F_1 folds and quartz veins is discussed later in this chapter.

Late structures: F_2 and F_3 folds

These structures are represented by two fold groups, F_2 and F_3. F_2 folds are most predominant and control the outcrop pattern of the Great Boundary Fault Zone in the Berach river section (Fig. 3.2a). Open to gentle, upright F_2 folds occur as a series of NNE

to NE trending anticlines and synclines (Fig. 3.2b to d). F_3 folds, in general, occur as NW-SE trending upright warps, which plunge at variable angles towards SE (Fig. 3.2e).

Branching of hinge lines is a common characteristic of F_2 folds (Fig. 3.3a). The angular divergence between the branched hinge lines ranges from 42 to 74° (Fig. 3.3b). The change in F_2 fold geometry from anticline to syncline along a common axial trace due to branching of hinge lines has resulted into development of hourglass map pattern at a few outcrops (Fig. 3.3c). Although several processes, such as the superposed folding, the variation in compression across the axial plane, the folding on variably oriented S-surfaces, and the sheath folding can produce hourglass map pattern, none of these mechanism are responsible for the development of hourglass structure in the Great Boundary Fault Zone.

Several lines of evidence, such as the direct relationship between the bed thickness and fold wavelength, the class 1B geometry of folds, the occurrence of hinge line normal striae on the fold limbs, the bedding parallel shear offset of quartz veins and the branching of hinge lines imply that the F_2 folds were developed by flexural slip mechanism during the buckling of the Nimbahera shale beds (Fig. 3.3d). The flexural slip mechanism and branching of F_2 hinge lines, in turn, imply the development of hourglass structure due to interaction between the two out-of-phase fold waves during the buckling of the Nimbahera shale beds (Ghosh and Ramberg, 1968; Dubey and Cobbold, 1977; Sahay and Srivastava, 2005).
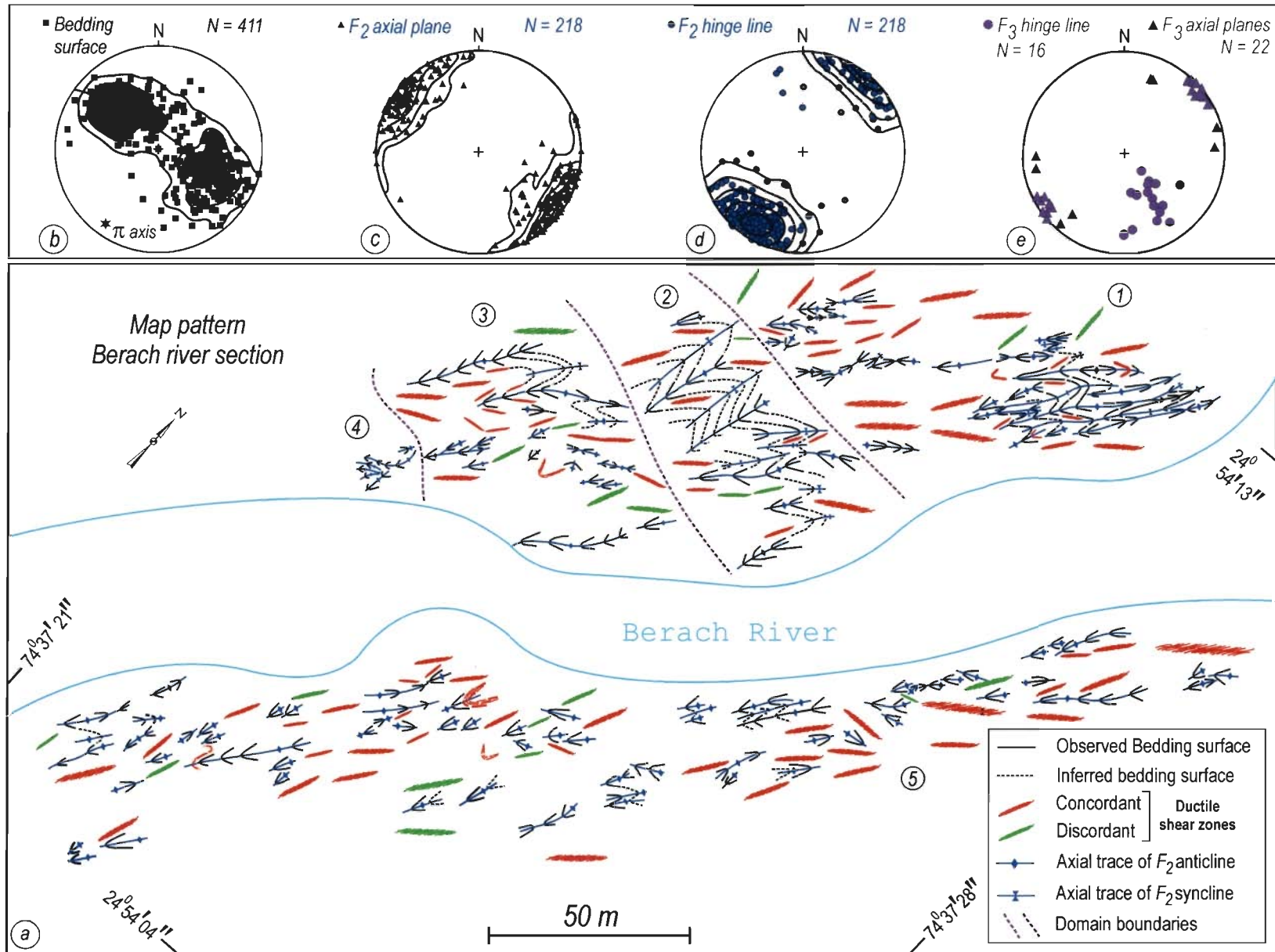
Fig. 3.2: (*a*) Structural map of Great Boundary Fault Zone in the Berach river section showing F_2 folds and ductile shear zones. (*b-e*) Lower hemisphere equal area plots for bedding surface, F_2 axial plane and hinge line, and F_3 axial plane and hinge line, respectively. (*1-5*) domains for structural analyses.
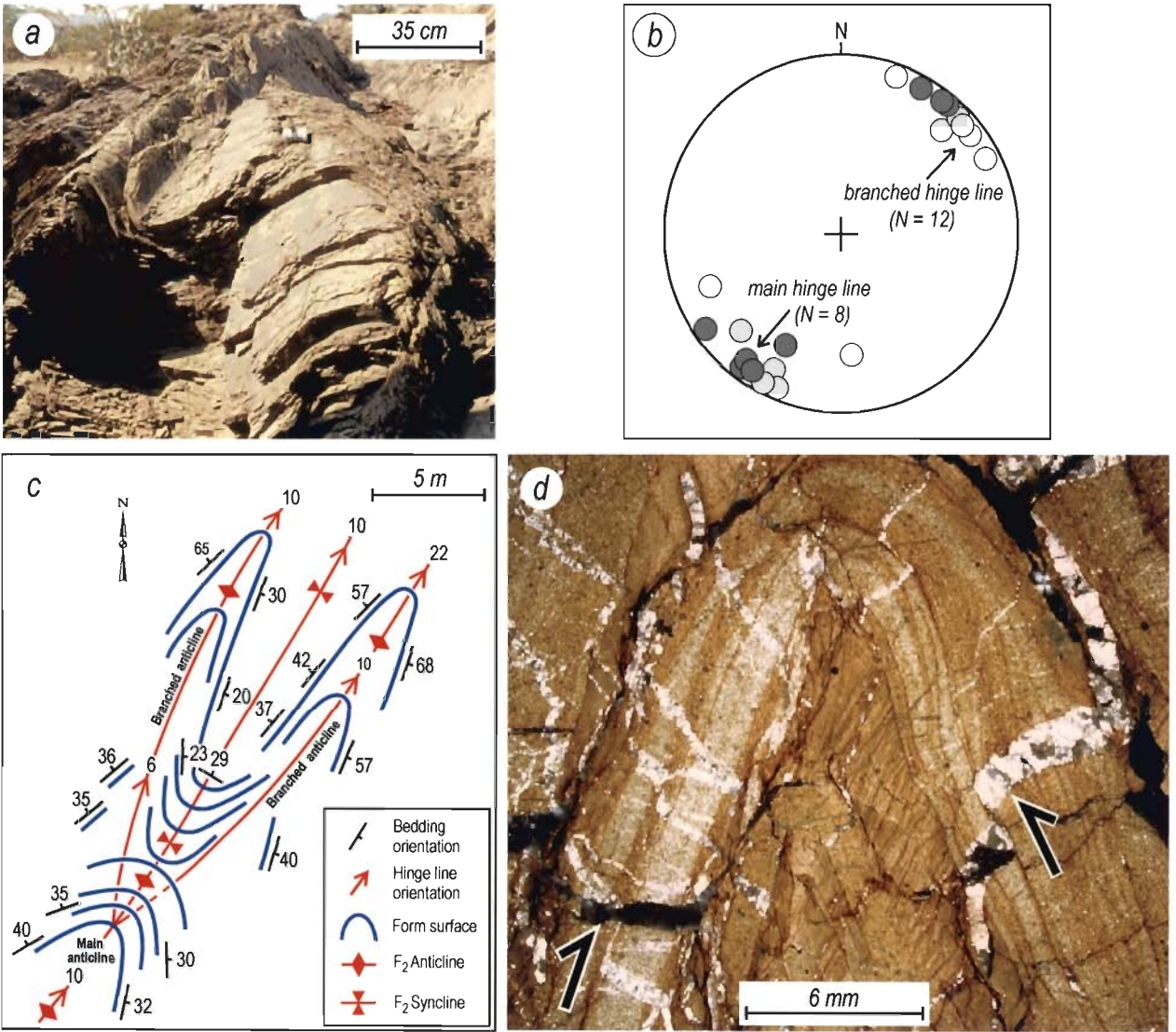
Fig. 3.3: (**a**) Branching of F_2 hinge line. (**b**) Lower hemisphere equal area plots for the main hinge lines and branched hinge lines of F_2 folds in the Berach river section. (**c**) Map pattern of an hourglass structure. (**d**) F_2 fold show shear offset of quartz veins on both limbs due to flexural slip folding (crossed polars).

39

The effect of F_2 folding on early structures is very conspicuous in the Berach river section. During the F_2 folding, the ductile shear zones were folded about F_2 hinge lines (Fig. 3.4a and b). The hinge lines of folds on concordant shear zones always parallel the hinge lines of F_2 folds on the bedding surfaces (Fig. 3.4c). The hinge lines of folds on discordant shear zones are, however, inclined at low angles to the hinge lines of F_2 folds on the bedding surfaces (Fig. 3.4d). This variation in orientations of hinge lines of the folds on concordant and discordant shear zones is because of the fact that the concordant and discordant shear zones were not parallel to each other before the onset of F_2 folding.

F_1 group of folds developed during ductile shearing was refolded during F_2 folding. Two types of overprinting relationships between F_1 folds and F_2 folds are most commonly observed: (i) interference pattern showing F_1 axial plane folding (Fig. 3.5a and b) and, (ii) deformed stretching lineations L_1 (Fig. 3.5c).

Interference pattern: As described later, the two sets of folds, F_{1A} and F_{1B}, developed during ductile shearing, show a coaxial relationship and type-3 interference pattern (Ramsay, 1967). By contrast, the F_2 folds and F_1 folds invariably show a non-coaxial relationship and interfere with each other to produce type-2 pattern(Fig. 3.5a and b). It is mainly because of the type-2 interference that the F_1 folds are now nonplane-noncylindrical (Fig. 3.5d).

Deformed L₁ lineations: Deformed L_1 lineations parallel F_1 hinge lines and occur on the folded surfaces of F_2 folds (Fig. 3.5c). Thin section studies reveal that L_1 lineations

define a stretching lineation, which is made up of stretched quartz grains and quartz ribbons. The unrolled patterns of the deformed L_1 lineations are obtained by overlaying a transparent sheet over the individual F_2 folds, marking the traces of L_1 lineations and F_2 hinge lines, and unrolling the transparent sheet to a planar configuration for removing the effect of F_2 folding. The geometric pattern of deformed lineations obtained in this manner, not only indicates the mechanism of F_2 folding but also represents the orientation of F_1 hinge lines prior to the onset of F_2 folding (Ramsay, 1967). Because F_2 folds invariably conform to class 1B geometry, it is clear that the effect of flattening was insignificant not much during development of these folds.

As the unrolled patterns of the deformed L_1 lineations are characteristically rectilinear at most of the outcrops (Fig. 3.6a), it is evident that the F_2 folds were developed dominantly by flexural slip mechanism (Ghosh and Chatterjee, 1985). Although the unrolled patterns of deformed L_1 lineations are variably directed, they consistently plunge at subhorizontal or low angles (Fig. 3.6b). It is, therefore, logical to infer that the F_1 hinge lines were noncylindrical and F_1 axial planes were dipping at low angles prior to the development of F_2 folds. The variation in F_1 hinge line orientation is, therefore, due to a combination of two main factors: (i) noncylindrical nature of F_1 folds before the initiation of F_2 folding and, (ii) rotation of F_1 hinge lines during the F_2 folding.

Effect of F_3 folds on F_2 and F_1 folds

F_3 folds occur as NW-SE trending gentle warps with wavelength of the order of several metres and cm-dm scale amplitudes (Fig. 3.7a). Because of the gentle nature F_3

42
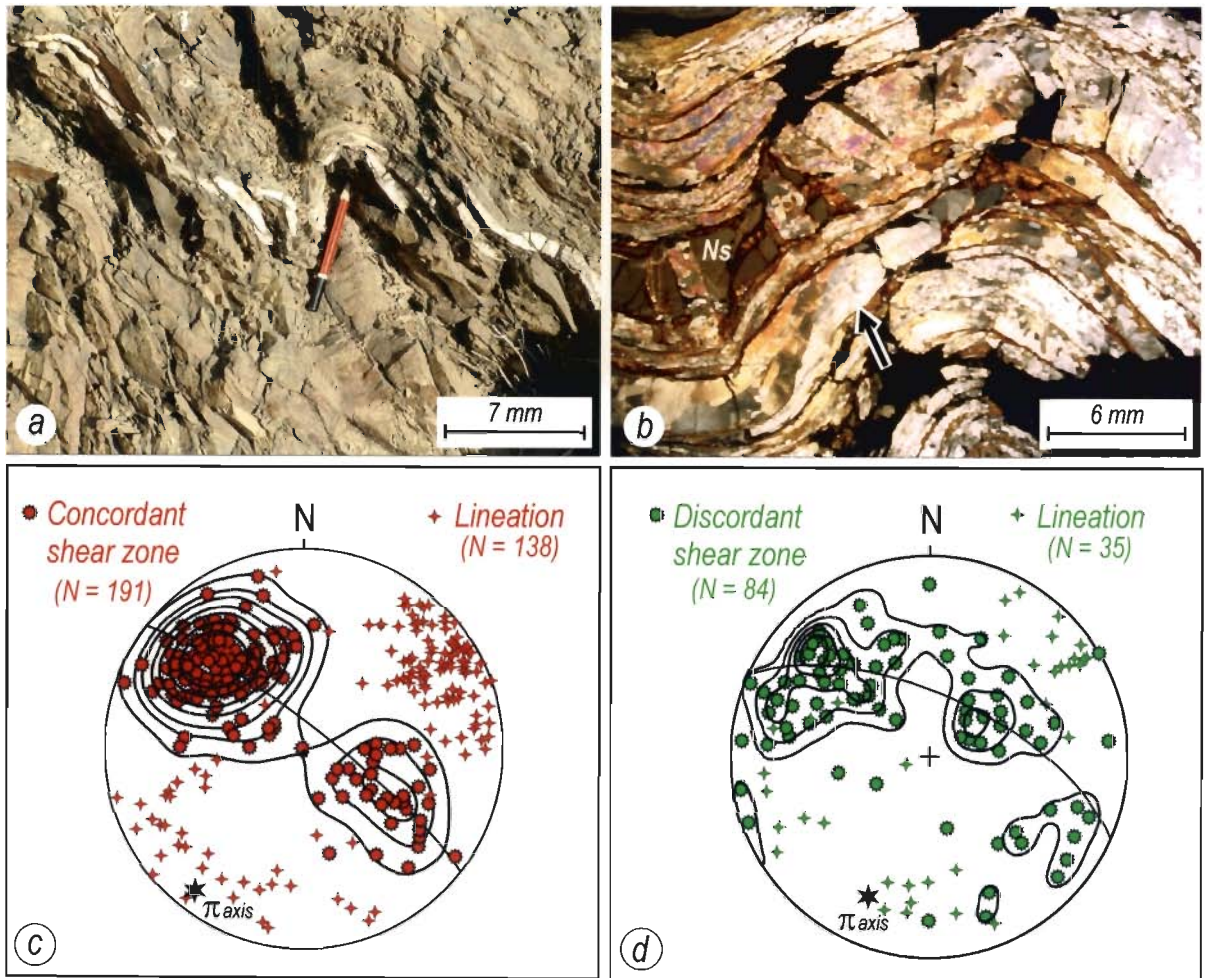
Fig. 3.4: (*a*) A mylonitised quartz vein folded by F_2 folds (pointed by pencil). (*b*) A F_2 fold on the quartz ribbons (pointed by arrow) defining mylonite foliation. *Ns*- relict fragment of Nimbahera shale (crossed polars). (*c-d*) Lower hemisphere equal area plots for ductile shear zones in the Berach river section. (*c*) π - axis of concordant shear zones parallels the π - axis of bedding surfaces (cf. fig. 3.2b). (*d*) π - axis of discordant shear zones is at a low angle to the π - axis of bedding surfaces (cf. fig. 3.2b).
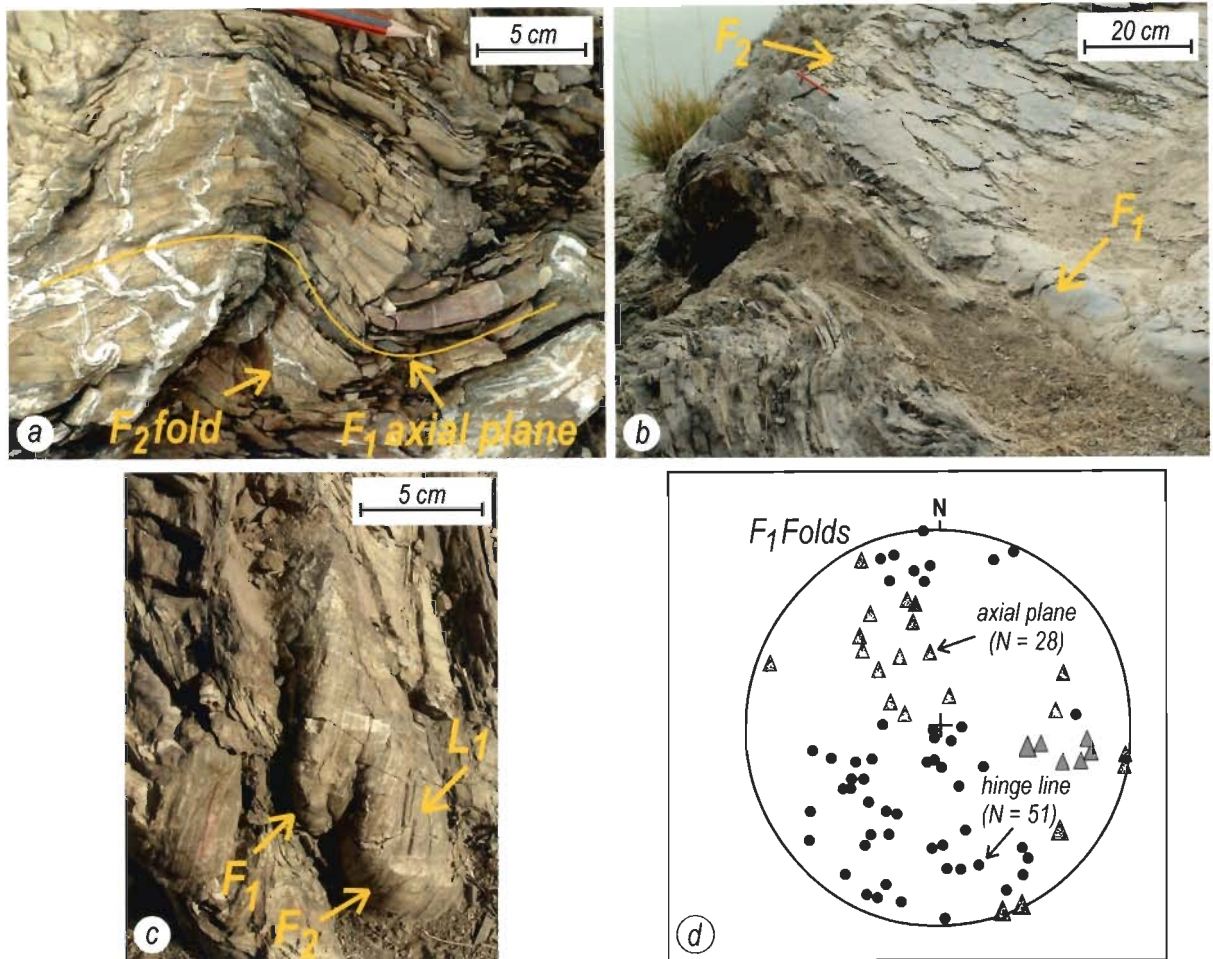
Fig. 3.5: (*a*) F_1 axial planes are folded by F_2 fold. (*b*) An open upright F_2 fold refolds the axial plane and hinge line of an isoclinal F_1 fold. (*c*) Deformation of stretching lineation, L_1, and F_1 hinge line by F_2 fold. (*d*) Lower hemisphere equal area plots for hinge lines and axil planes of F_1 folds in the Berach river section.
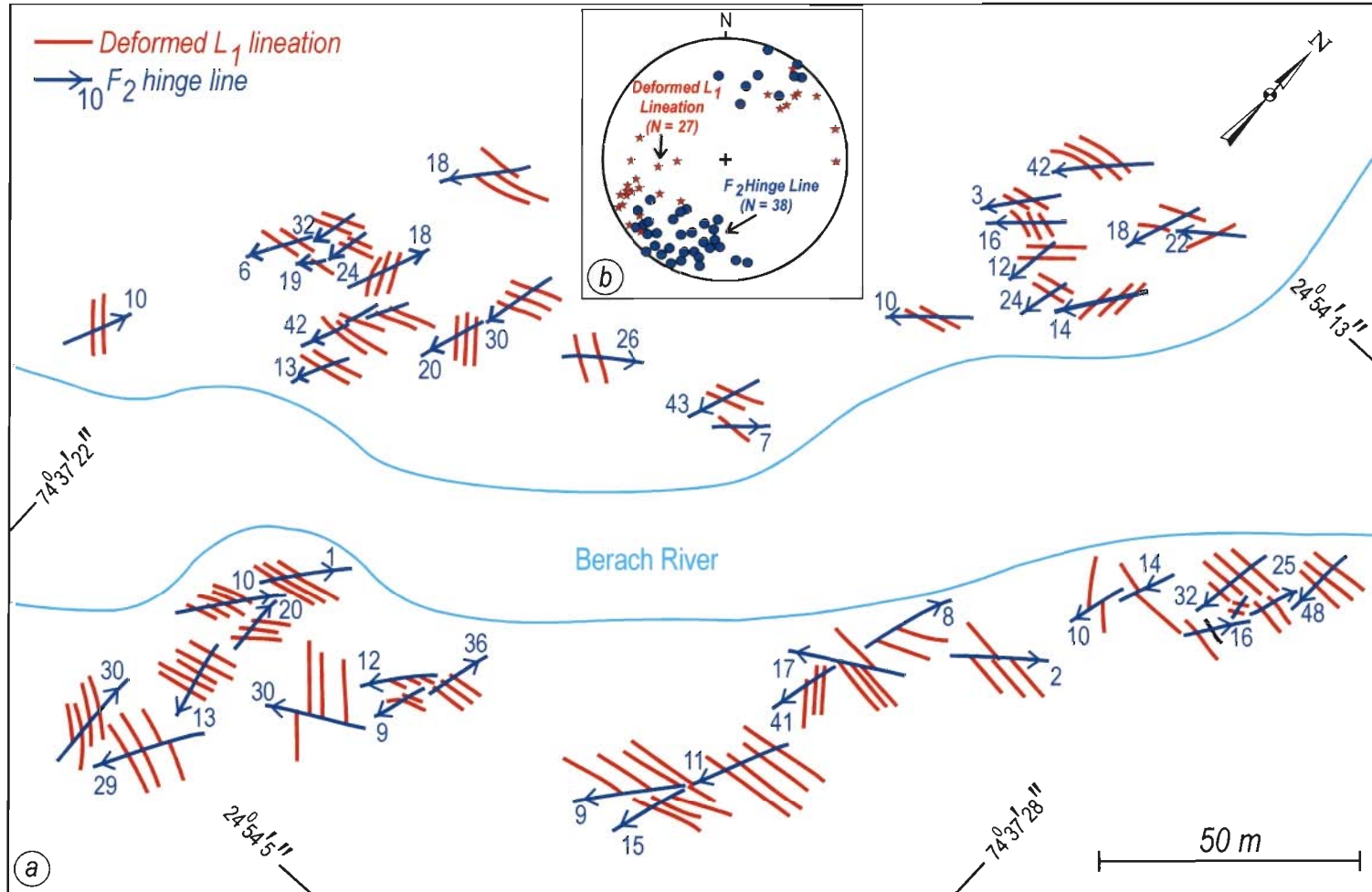
Fig. 3.6: (*a*) Unrolled rectilinear patterns of L_1 lineaions in the Berach river sction. (*b*) Lower hemisphere equal area plots of the F_2 hinge lines and the deformed L_1 lineations, occurring on the F_2 folds.
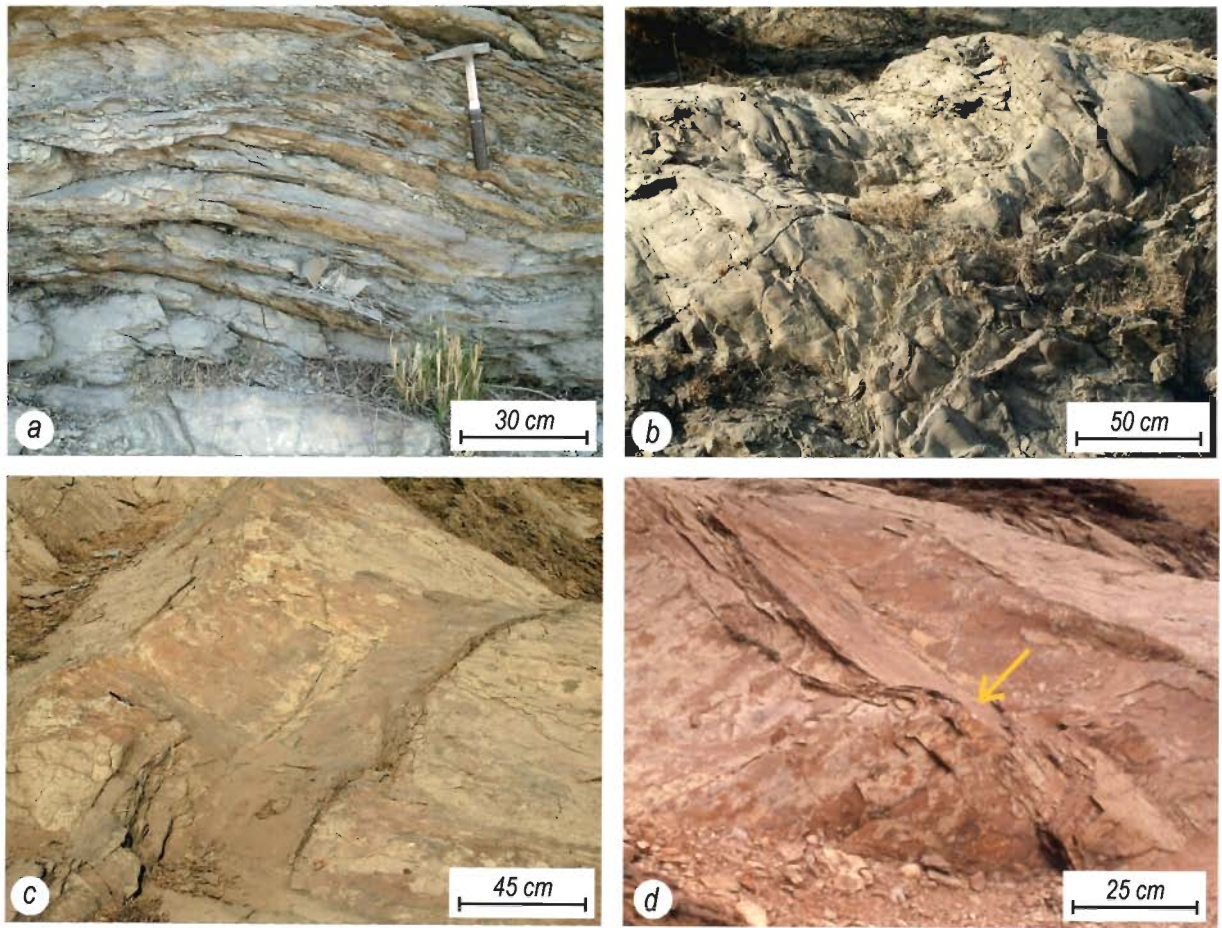
Fig. 3.7: (*a*) F_3 warp. (*b*) An F_2 anticlinal depression. (*c*) A broad dome-basin. (*d*) Coaptation/ curvature accomodation fold (pointed by arrow).

folds do not significantly modify the geometry of F_1 folds, which are invariably tight to isoclinal and developed in cm-dm scale. F_3 folds, however, modify the geometry of F_2 folds to some extent, particularly, in those domains, where these two fold groups occur at the comparable scales. In such domains, the anticlinal depressions, synclinal culminations, basins and domes and coaptation/curvature accommodation folds are common (Fig. 3.7b to d). These structures are, at least, partly formed due to superposition of NW-SE trending F_3 warps on NE-SW trending F_2 folds (Lisle et al., 1990).

Structural analyses

For the purpose of structural analysis, the Great Boundary Fault Zone in the Berach river section has been subdivided into five domains (Fig. 3.2a). The boundaries of these domains are delimited by considering the similarity in map pattern and the homogeneity with respect to the F_2 hinge line orientations. These domains are mapped at the scales ranging from 1:60-1:1200 depending upon the complexity and the scale of critical structures within each domain (Figs. 3.8 to 3.12). The characteristic map patterns, results of structural analysis and inferences regarding the fold geometry in each domain are summarized in Table 3.1.

Table 3.1: Structural analyses of the Great Boundary Fault Zone
in the Berach river section.

Domains	Map pattern	Ductile shear zones
Domain-1	The map pattern is controlled by the NE-SW trending F_2 folds that are characterised by steeply dipping axial planes and low plunging to nonplunging hinge lines (Fig. 3.8a and b). The map pattern also depicts a common occurrence of anticlinal culminations, anticlinal depressions, synclinal culminations and the hinge line bifurcations in F_2 folds.	The concordant shear zones are folded about F_2 hinge lines. The stretching lineations on these shear zones, despite a wide scatter, are inclined at low to moderate angles to the F_2 hinge lines (Fig. 3.8c). Discordant ductile shear zones, show inconsistent orientations (Fig. 3.8d).
Domain-2	F_2 folds in this domain trend NNE-SSW in the western part, and NE-SW in the eastern part and; F_2 hinge lines predominantly plunge at low angles towards SW (Fig. 3.9a and b). The variation in the trend of F_2 folds in this domain is due to relatively more pronounced effect of F_3 folding in the eastern part and local variation in amount of strike-slip movement of the Great Boundary Fault. Although culminations and depressions are rare to absent, an F_2 anticline, showing distinct bifurcation of hinge line, occurs on a mappable scale in central part of this domain.	Although concordant and discordant ductile shear zones dip predominantly towards SE in this domain, both are folded about F_2 hinge lines (Fig. 3.9c and d). The stretching lineations on both types of ductile shear zones are inclined at low angles to the F_2 hinge lines.
Domain-3	F_2 folds in this domain are characterised by anticlinal culminations and anticlinal depressions on mildly curviplanar axial planes (Fig. 3.10a). These culminations and depressions are	Bulk of the ductile shear zones are cofolded with F_2 folds on the bedding surfaces (Fig. 3.10a). The stretching lineations on these ductile shear zones are

	formed partly due to superposition of NW-SE trending F_3 warps on NE-SW trending F_2 folds, and partly due to complex nature of strain distribution during F_2 folding. As the culminations and depressions are very gentle, bulk of F_2 hinge lines plunge at low angles towards NE and SW and F_2 axial planes dip at steep angles towards NW and SE (Fig. 3.10b).	also rotated about the F_2 hinge lines (Fig. 3.10c and d).
Domain-4	Domes-basin and coaptation or curvature accommodation folds on radiating axial traces occur in the eastern and western part of this domain, respectively (Fig. 3.11a). Most of the F_2 fold hinge lines plunge at low angles towards SW (Fig. 3.11b). NNW plunging F_2 folds are, however, common in the coaptation/curvature accommodation folds. The complex geometry of F_2 folds in this domain is due to a combined effect of the nature of strain distribution during F_2 folding and superposition of NW-SE trending F_3 warps on the F_2 folds.	Absent
Domain-5	Despite the fact that this domain occupies the largest area, F_2 folds are planar (Fig. 3.12a). F_2 folds in this domain show characteristically simple geometry with NE-SW striking axial planes and hinge lines plunging at subhorizontal to low angles towards NE and SW (Fig. 3.12b). Axial culminations and depressions and branching of the hinge lines are relatively less common in this domain.	Concordant shear zones, folded about F_2 hinge lines, are most dominant. The stretching lineations, on both concordant and discordant shear zones are inclined at low angles to F_2 hinge lines (Fig. 3.12c and d).

3.1.2 Brittle structures

Although the ductile structures, described earlier, are predominant within the Great Boundary Fault Zone, several sets of steeply dipping, or subvertical, fractures cut through the Nimbahera shale beds in the Berach river section (Fig. 3.13). On the basis of relative orientation with respect to the NE to NNE directed F_2 hinge lines, these fractures can be classified into four main groups: (i) Strike fractures, trending NNE, (ii) cross-fold fractures, striking NW, (iii) oblique set-1 fractures, striking EW and, (iv) oblique set-2 fractures striking NNW.

3.1.3 Microstructures within ductile shear zones

At the mesoscopic scale, only one prominent set of mylonite foliation namely, m_1, and a group of isoclinal folds, F_1 are discernible within the ductile shear zones. At the microscopic scale, however, a multitude of structures are discernible within the ductile shear zones. These structures include: (i) two sets of successively developed mylonite foliations, m_1 and m_2; (ii) two sets of successively developed coaxial folds F_{1A} and F_{1B}, which together constitute the F_1 group and; (iii) two sets of quartz veins, V_1 and V_2. It may be mentioned here that the distinction between F_{1A} and F_{1B} fold sets is possible only in instances where these two fold sets exhibit a distinct overprinting relationships. Both the sets of mylonite foliations, m_1 and m_2, are defined predominantly by relatively thick quartz rich bands that are separated by thin mica rich bands. The quartz rich bands, mainly made up of quartz ribbons, vary in thickness from 0.25 to 1.25mm and show
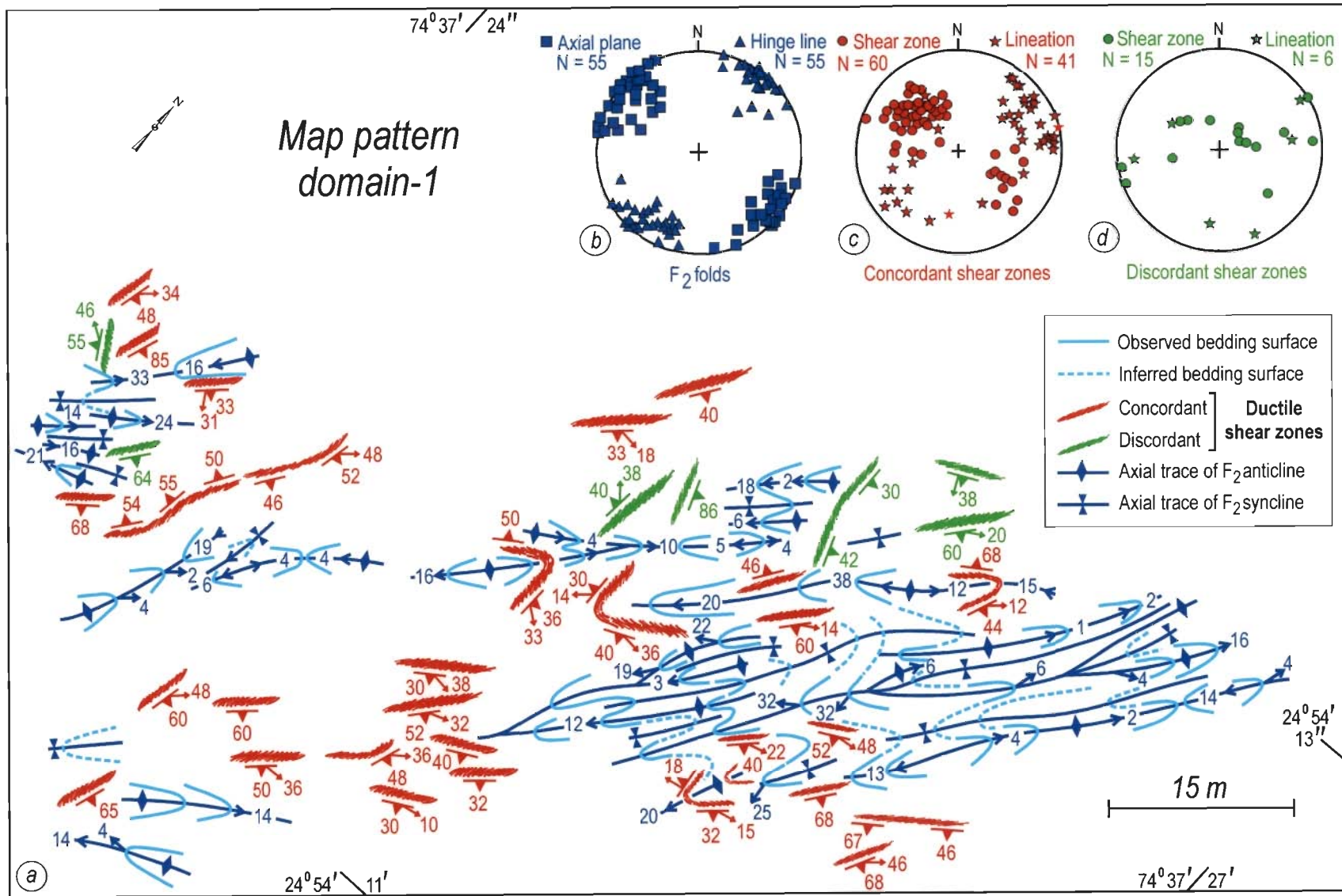
Fig. 3.8: (*a*) Structural map of domain-1 in the Berach river section. (*b-d*) Lower hemisphere equal area plots for F_2 axial planes and hinge lines, concordant shear zones and discordant shear zones, respectively.
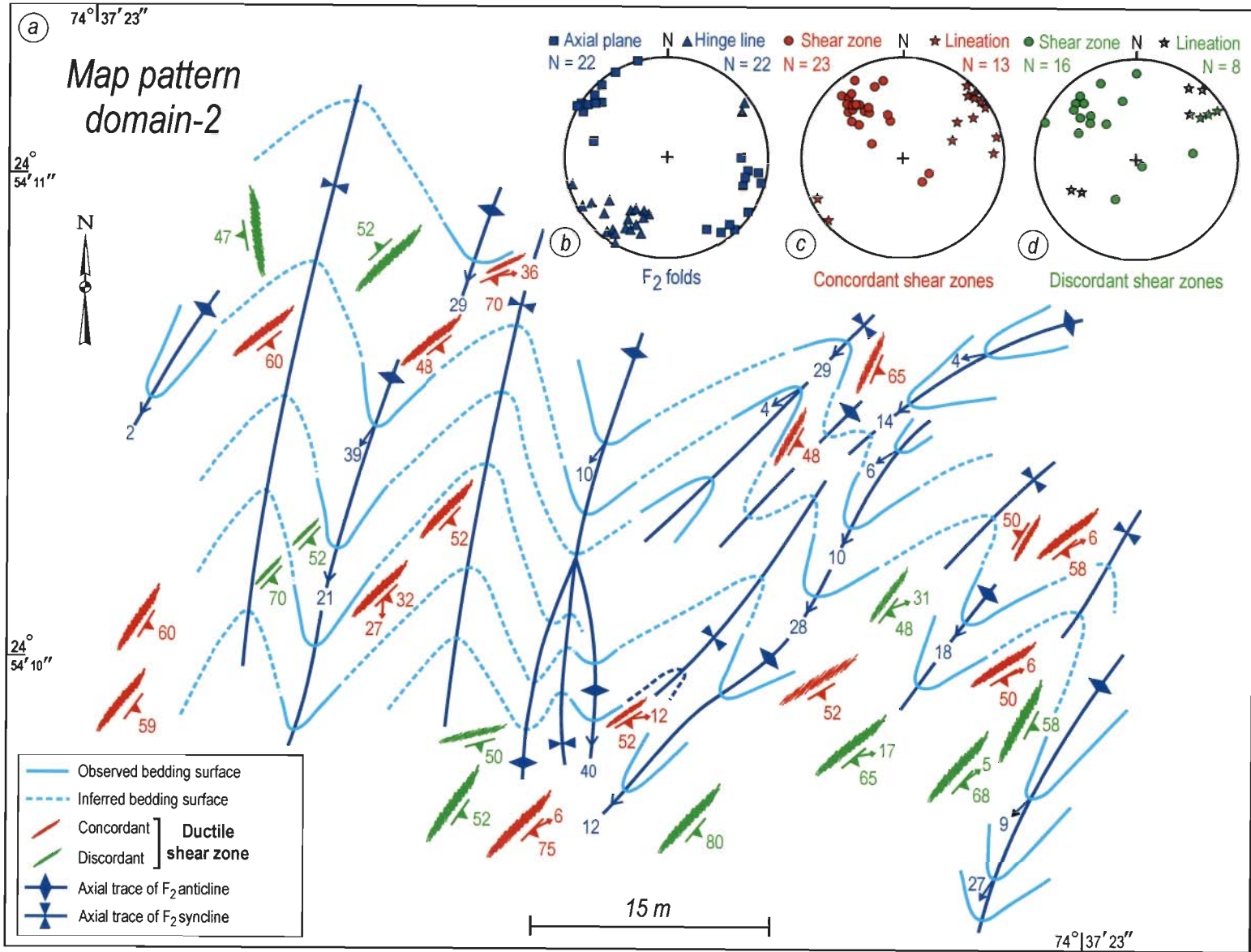
Fig. 3.9: (*a*) Structural map of domain-2 in the Berach river section. (*b-d*) Lower hemisphere equal area plots for F_2 axial planes and hinge lines, concordant shear zones and discordant shear zones.
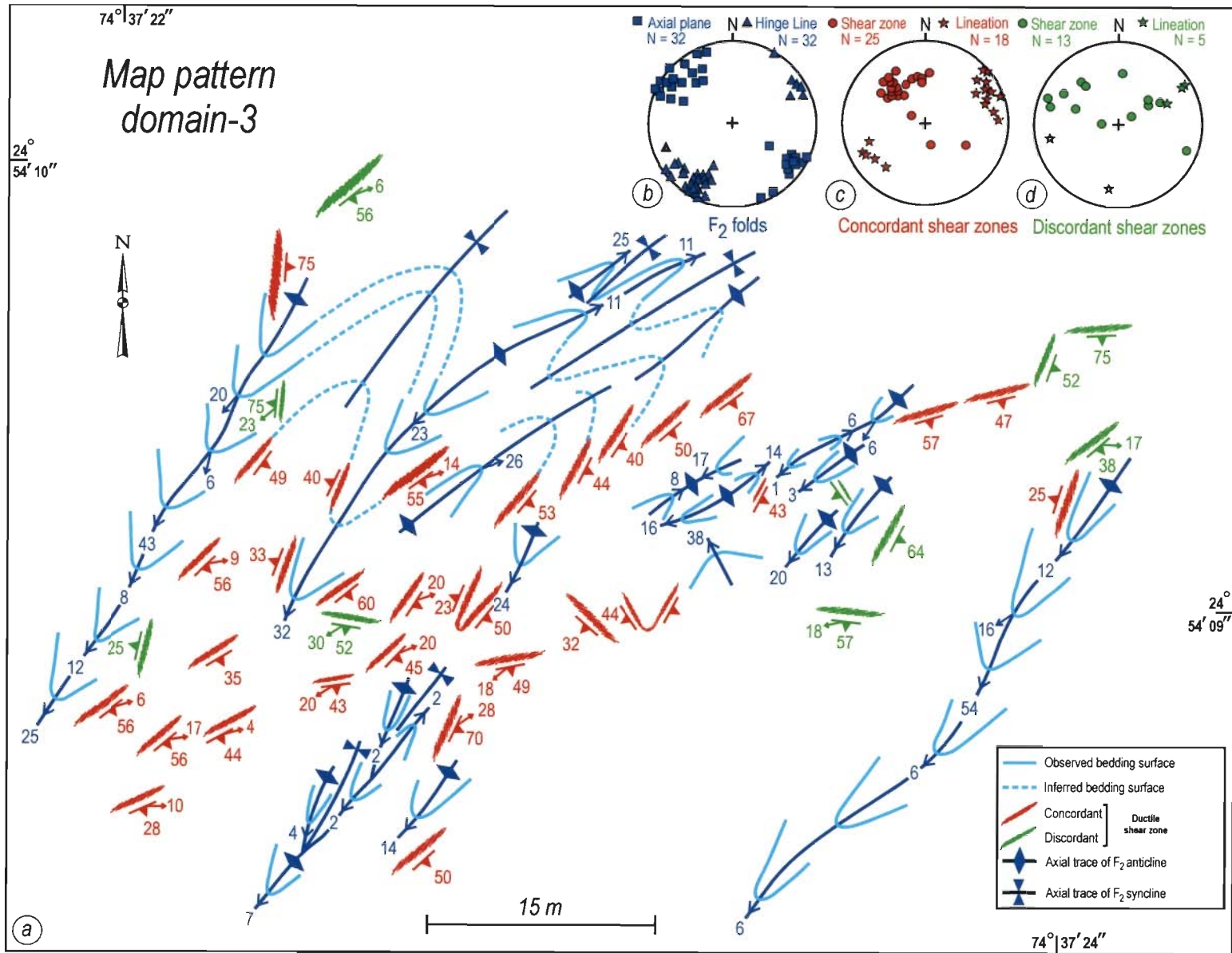
Fig. 3.10: (*a*) Structural map of domain-3 in the Berach river section. (*b-d*) Lower hemisphere equal area plots for F_2 axial planes and hinge lines, concordant shear zones and discordant shear zones.
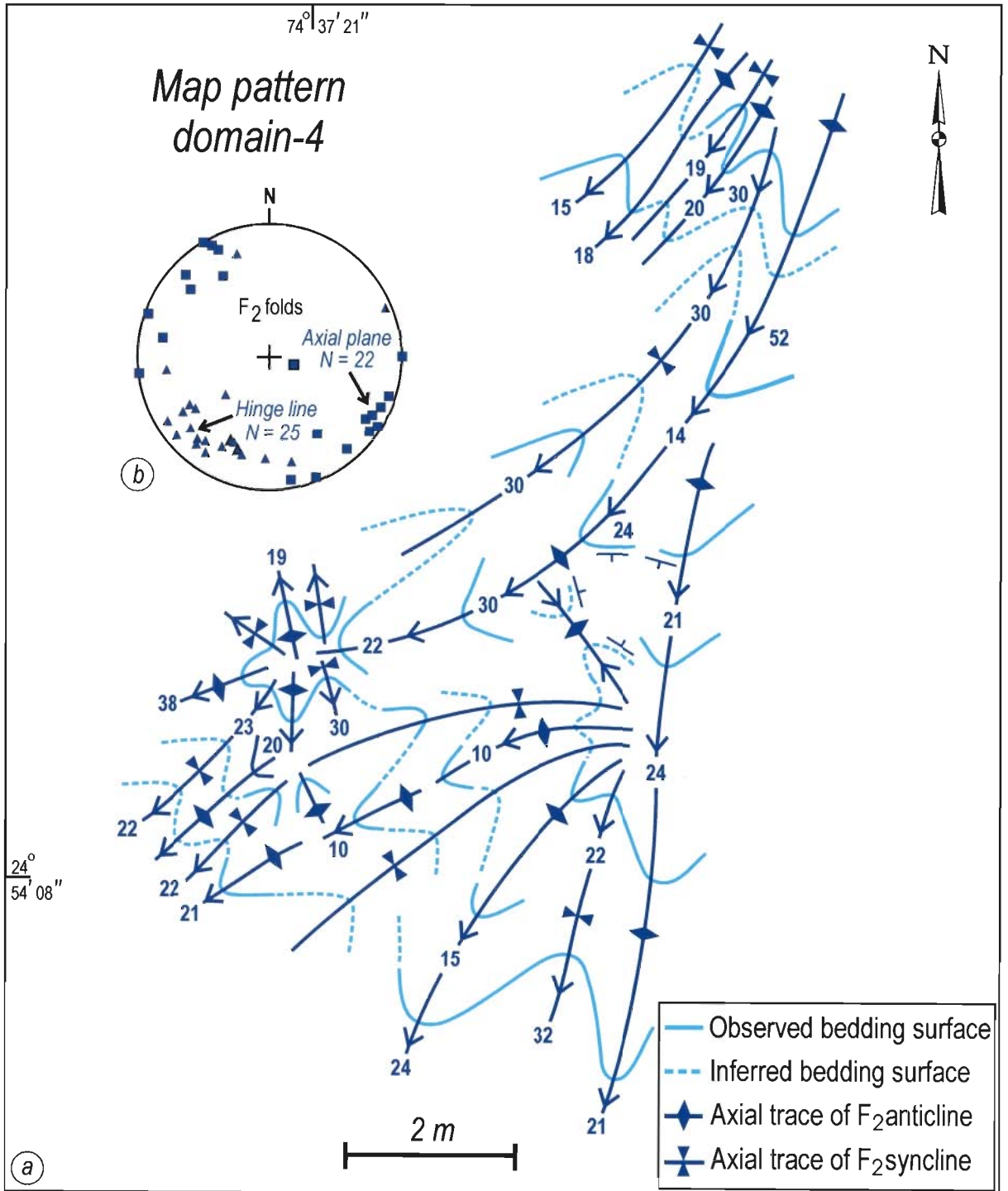
Fig. 3.11: (*a*) Structural map of domain-4 in the Berach river section. (*b*) Lower hemisphere equal area plots for F_2 axial planes and hinge lines.
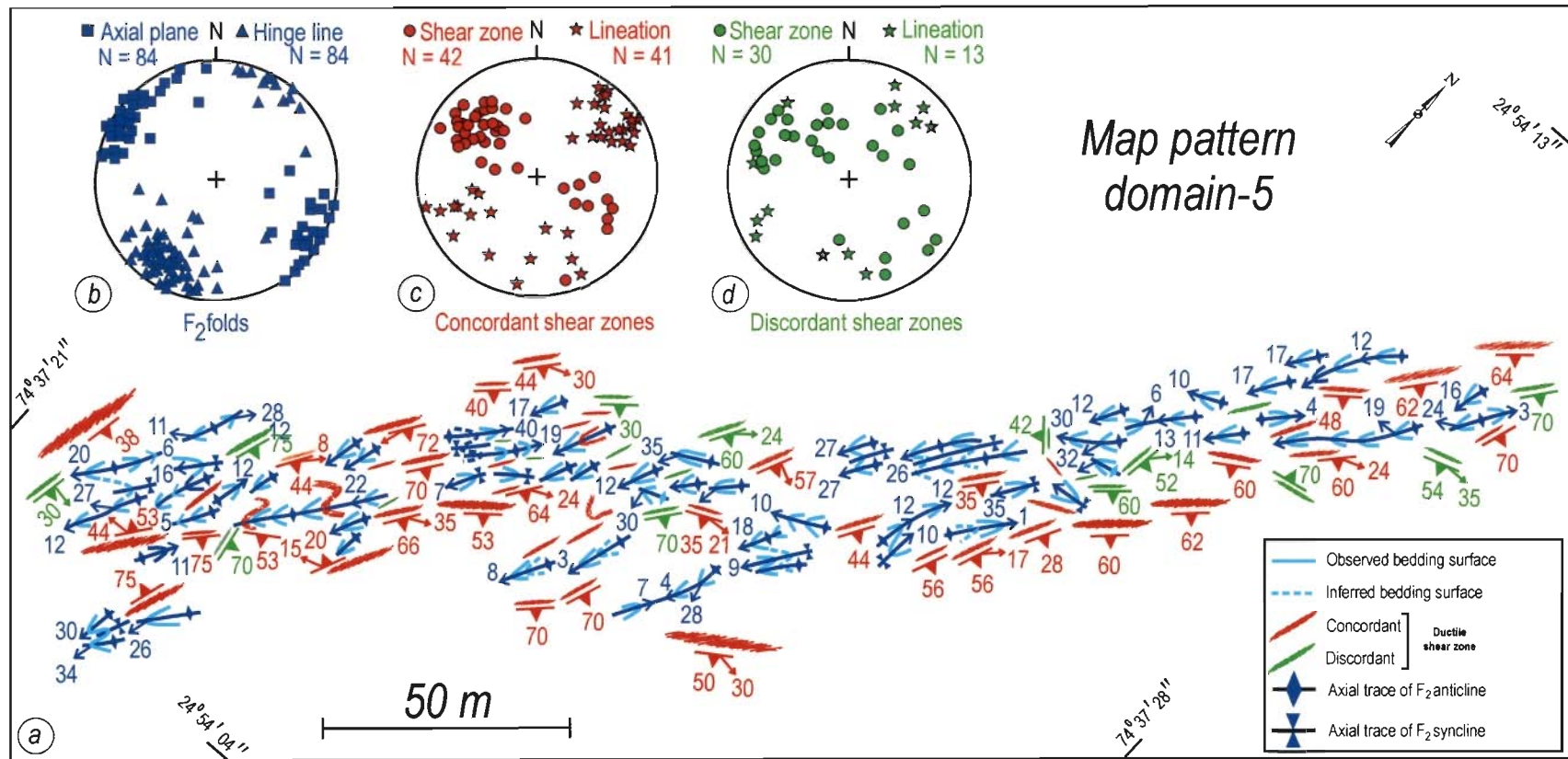
Fig. 3.12: (*a*) Structural map of domain-5 in the Berach river section. (*b-d*) Lower hemisphere equal area plots for F_2 axial planes and hinge lines, concordant shear zones and discordant shear zones.
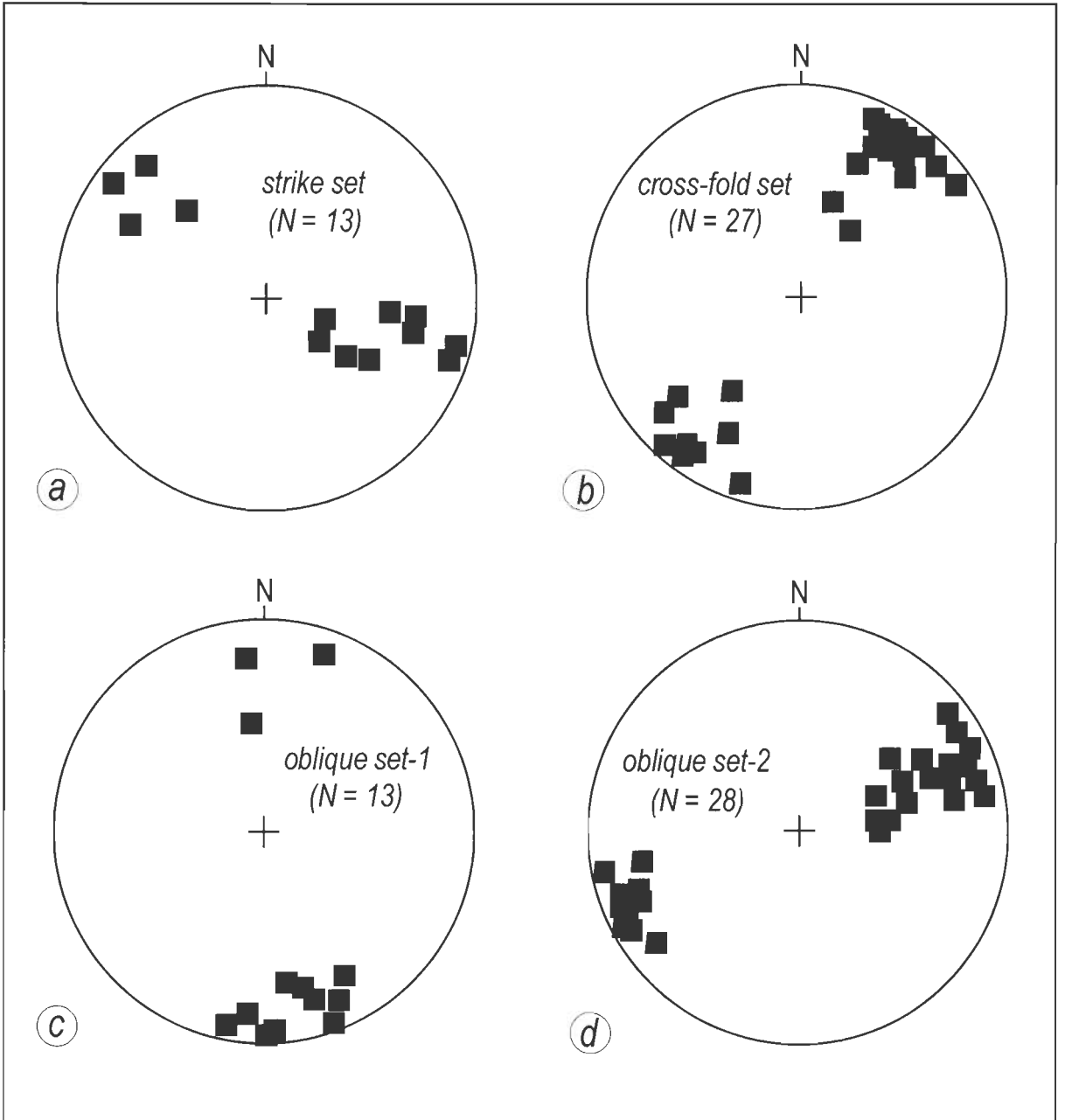
Fig. 3.13: (*a-d*) Lower hemisphere equal area plots for the poles to the different sets of fractures in the Berach river section.

characteristic development of deformation lamellae, subgrains and aggregates of fine grained recrystallised quartz. The mica rich bands contain white mica and biotite grains that are preferredly oriented in parallelism with the quartz ribbons.

S-C structure and asymmetric quartz boudins resembling fish structure are common within the mylonite foliation (Fig. 3.14a-b and c). Both *S-*and *C-* surfaces are distinct under the microscope and, the angle between these two surfaces decreases from 60 to 20° with progressive increase in the intensity of deformation (Lister and Snoke 1984; Fig. 3.14a and b). In those examples of *S-C* structures, where the *S-* surface is sigmoidal, the degree of sigmoidality of *S-*surface increases with the increase in the intensity of the ductile shearing. The sigmoidal *S-*surfaces, in a few examples, ride over one and other in a piggy back fashion to define a cleavage duplex (Nickelsen, 1986; Fig. 3.14d).

Microstructures representing different stages of recrystallisation are well preserved within the mylonites. An early stage is represented by the elongated quartz grains showing undulose extinction, subgrain development, deformation lamellae and serrated grain boundaries decorated with fine grained recrystallised quartz (Fig. 3.15a). The intermediate stage is represented by a core and mantle structure, where a few relict quartz porphyroclasts occur as the core in a mantle of fine grained recrystallised quartz grains (Fig. 3.15b). In the advance stage of dynamic recrystallisation, the elongated quartz grains are completely recrystallised into fine grained strain free quartz grains (Fig. 3.15c). Finally, the static recrystallisation process took over the dynamic recrystallisation and a foam texture, consisting of coarse quartz grains with straight boundaries and triple point junctions in a minimum grain boundary tension configuration, is produced (Hobbs et al. 1976, p. 111; Passchier and Trouw, 1998, p. 47; Fig. 3.15d).
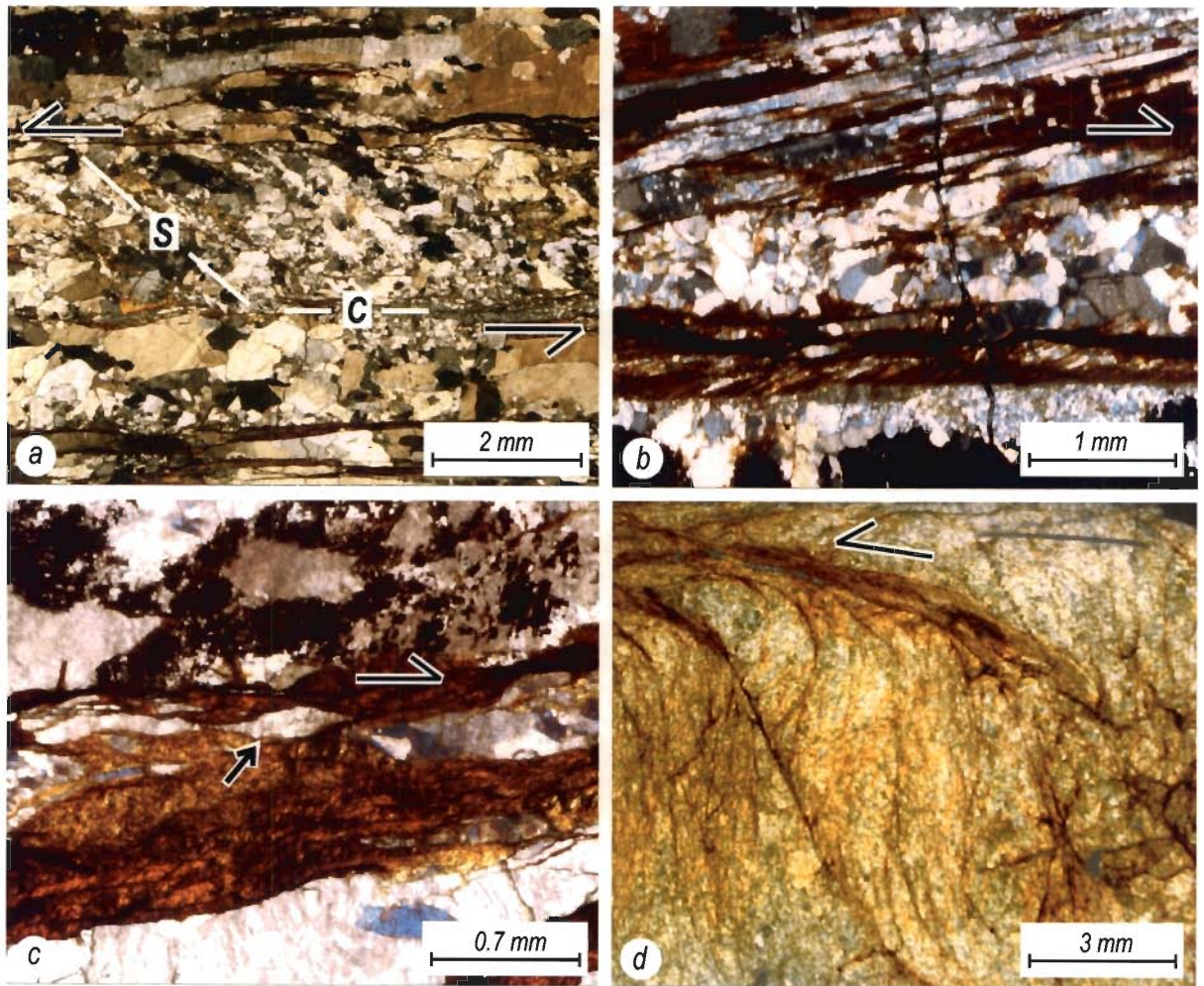
Fig. 3.14: (*a-b*) *S-C* structure in ductile shear zones (crossed polars). The angle between *S-* and *C-* surfaces decrease from 45° in **(a)** to 20° in **(b)** due to increase in the intensity of deformation. (*c*) An assymetric quartz boudin (pointed by arrow) surrounded by the pressure solution seams in the ductile shear zone (crossed polars). (*d*) Cleavage duplex (crossed polars).
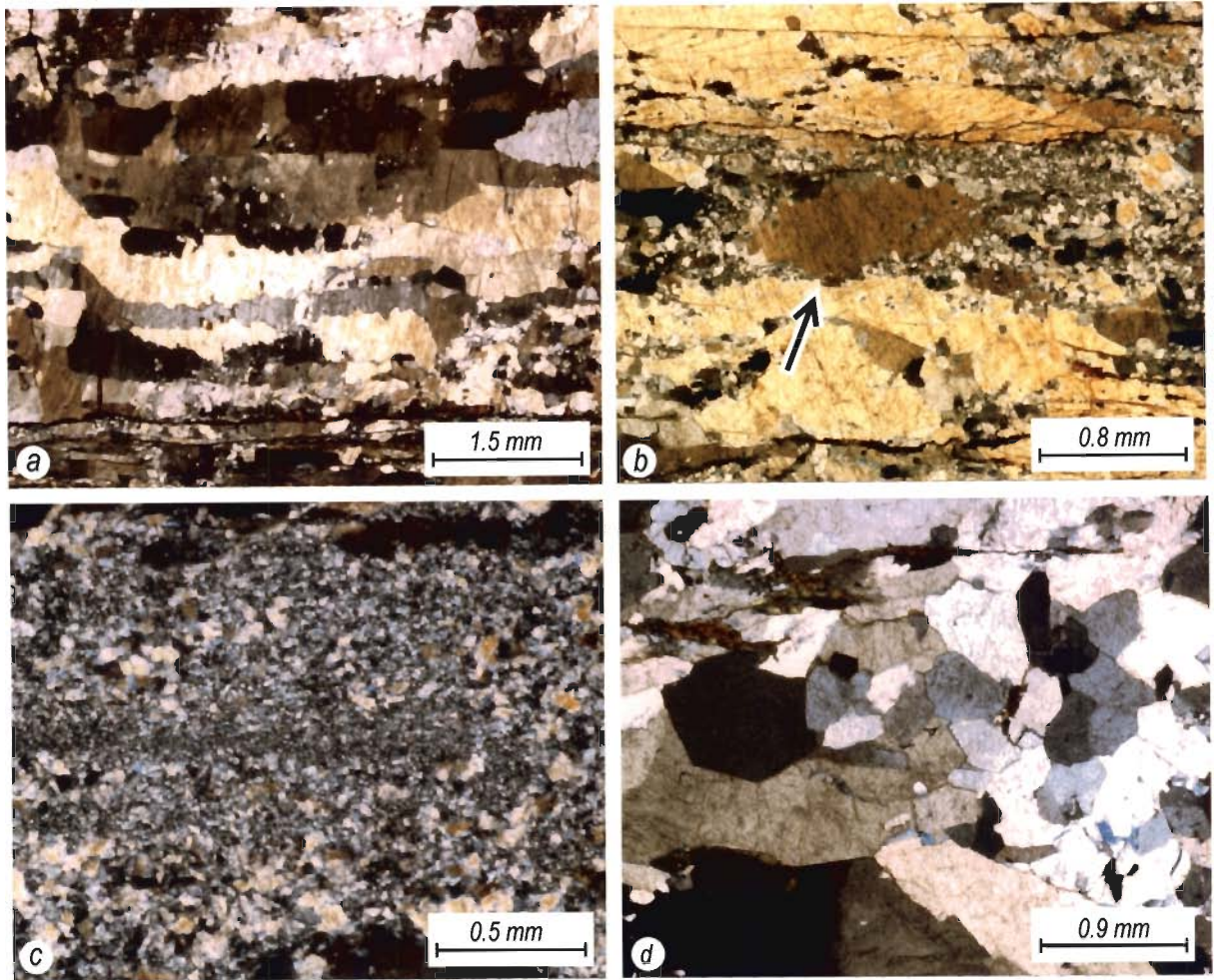
Fig. 3. 15: Different stages of recrystallisation (crossed polars). (*a*) Quartz ribbon showing serrated grain boundary. (*b*) Core and mantle structure (pointed by arrow), shows a relict quartz porphyroclast and recrystallised quartz grains along its margin. (*c*) Fine grained recrystallised quartz at the advance stage of dynamic recrystallisation. (*d*) Foam texture, resulting due to static recrystallisation, shows tripple point junction, at the contat of coarse quartz grains.

3.1.4 Structural evolution of ductile shear zones

The development of ductile shear zones seems to have initiated due to local stress gradients and circulation of intraformational pore-fluids in cm-m scale domains distributed sporadically within the ferruginous Nimbahera shale beds. The dissolution of SiO_2 by the pore-fluids in the domains of high stress concentration and its precipitation in the bedding parallel fractures within the low stress domains resulted into development of quartz veins V_1 in the Nimbahera shale beds (Fig. 3.16a and b). The opaque bands are mainly made up of the residual concentration of goethite and pyrolusite in the shale beds. The stress gradients and pore-fluid circulation gave way to the ductile shearing in bedding parallel veins, V_1, by a combination of pressure solution, cataclasis and recrystallisation processes. The mylonite foliation, m_1, developed during this process of ductile shearing, is the earliest recognizable tectonic fabric within the Great Boundary Fault Zone (Fig. 3.16c).

With the progressive ductile shearing, the mylonite foliation, m_1, folded into F_{1A} isoclinal folds and, a new mylonite foliation, m_2, developed axial planar to these folds (Fig. 3.17a to c). Furthermore a new set of fibrous quartz veins V_2 were developed perpendicular to F_{1A} axial planes due to extension along the F_{1A} axial planes (Figs. 3.16d and 3.17b). Finally, at advance stages of the progressive ductile shearing, a new set of isoclinal fold F_{1B} developed in a coaxial relationship with the preexisting F_{1A} folds (Figs. 3.16e and 3.17d).

3.2 Lalji Ka Khera Section

In this section, the Great Boundary Fault Zone contains an approximately 30m thick sequence of the Sawa sandstone-shale-porcellanite beds of the Lower Vindhyan Group, which is juxtaposed against the Berach granite (Fig. 2.1). These fault zone rocks are best described as an 'autoclastic mélange' because they show typical phacoid-in-sheared-matrix and do not contain any exotic block (Greenly, 1919; Raymond, 1984).

Outside the autoclastic mélange zone, the Sawa sandstone-shale-porcellanite beds lack any evidence of significant concentrated deformation. By contrast, within the autoclastic mélange zone, these rocks are invariably characterised by intense fracturing, brecciation, networking of veins, mylonitization and successive folding (Figs. 3.18a to c and 3.19a to b). The development of mylonite is most pronounced in relatively more competent lithounits, such as the Sawa sandstone beds. Mylonitisation in relatively less competent Sawa shale-porcellanite beds is, however, confined mainly to the quartz veins, which cut through these beds in diverse orientations.

The coarse-grained hypidiomorphic Berach granite, resting on the hanging wall side of the fault zone, occurs as scattered and weathered outcrops without any perceptible imprints of mesoscopic scale deformation. Under the microscope, however, the Berach granite also shows occasional brecciation in local domains (Fig. 3.19c).

3.2.1 Folding in fault zone rocks

The cataclasite/mylonite foliation parallels the bedding surfaces and traces the characteristic style of intricate folding within the autoclastic mélange zone (Fig. 3.20).
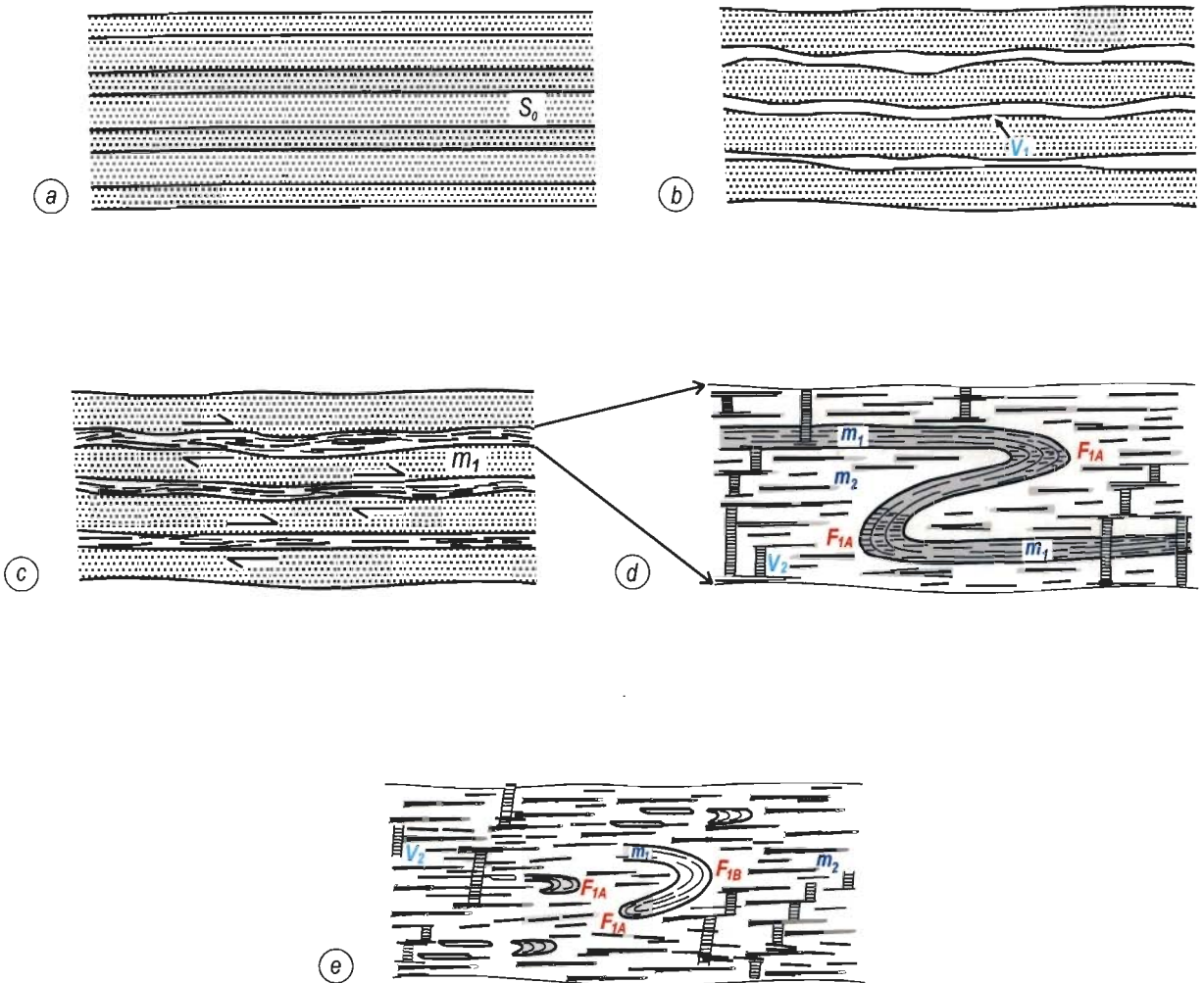
Fig. 3.16: Schematic diagram showing structural evolution of ductile shear zones in the Berach river section. (*a*) Nimbahera shale (*So*- bedding surface). (*b*) Development of bedding parallel quartz veins, V_1. (*c*) Ductile shearing of bedding parallel quartz veins, V_1, and development of mylonite foliation, m_1. (*d*) Development of F_{1A} isoclinal folds on mylonite foliation, m_1 and, a new mylonite foliation, m_2 axial planar to these folds. Bedding pependicular veins, V_2 developed at this stage due to extension along F_{1A} axial plane. (*e*) transposition of F_{1A} folds and development of F_{1B} isoclinal folds, which refold F_{1A} folds coaxially.
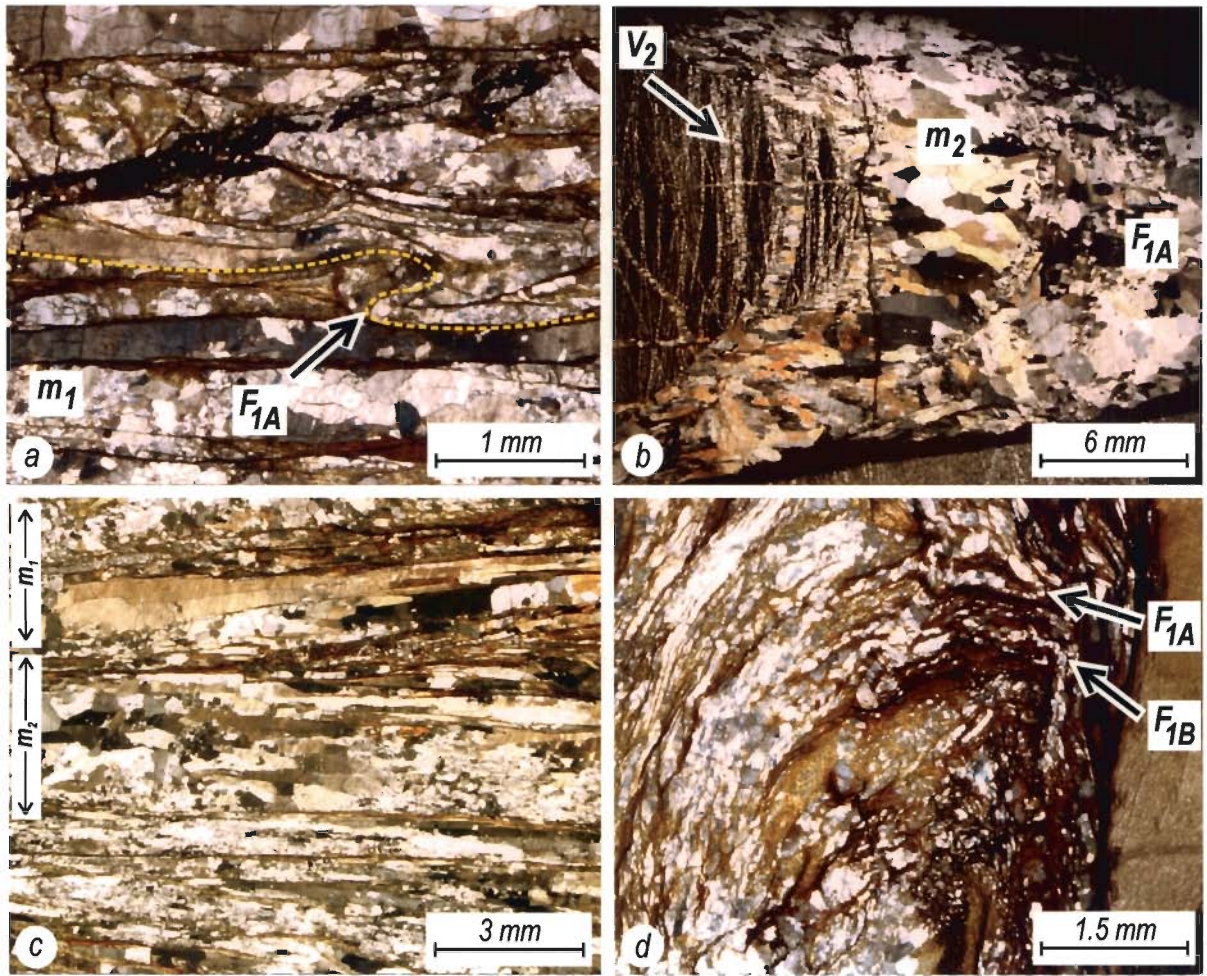
Fig. 3.17: Microstructures within ductile shear zones (crossed polars). (**a**) F_{1A} isoclinal fold traced by quartz ribbon (pointed by arrow and highlighted in yellow line). (**b**) Bedding perpendicular quartz veins, V_2 developed as a result of extension along F_{1A} axial plane. Note that the stretched quartz grains define m_2 mylonite foliation parallel to F_{1A} axial planes. (**c**) A late mylonite foliation, m_2 cuts through the early mylonite foliation, m_1. (**d**) A type-3 interference pattern between F_{1A} and F_{1B} folds traced by the mylontic foliation m_1.
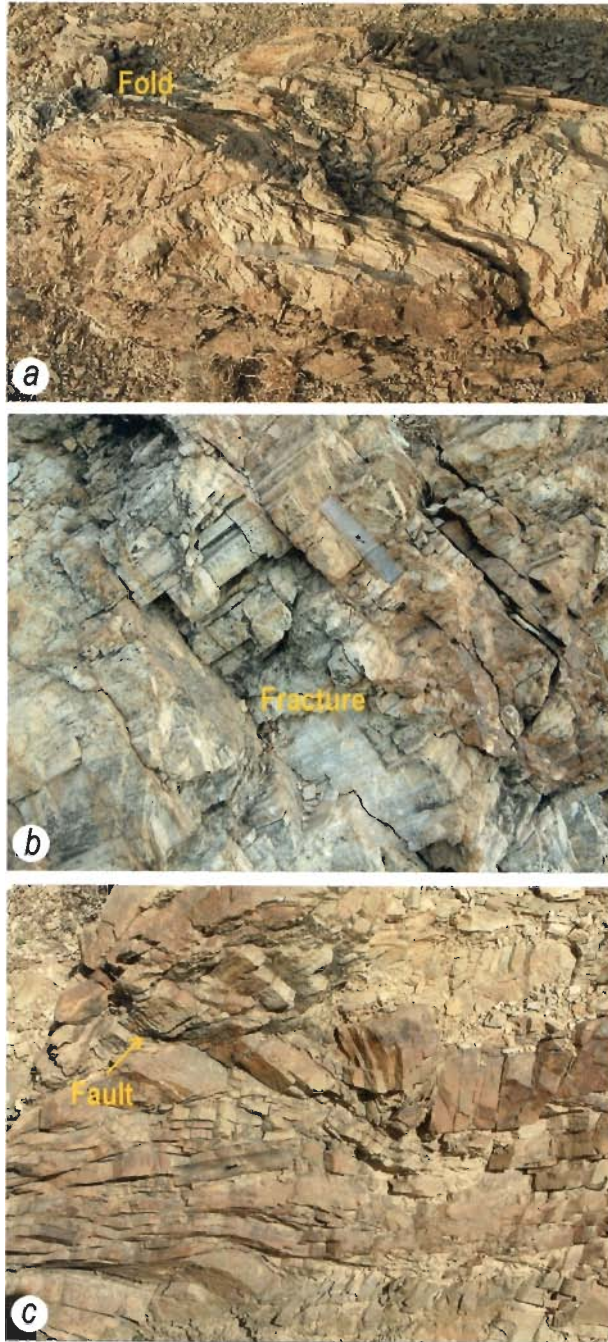
Fig. 3.18: (*a-c*) Field photographs showing intricate folding, fracturing and faulting in the Sawa sandstone-shale-porcellanite sequence of autoclastic melange zone in the Lalji ka Khera section.

77
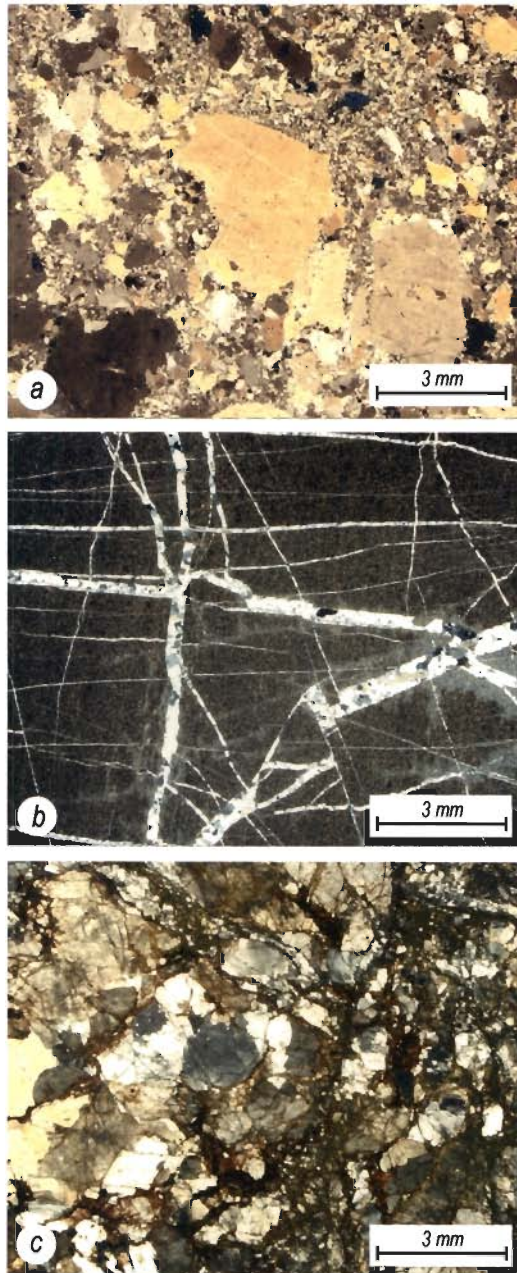
Fig. 3.19: Photomicrographs showing brecciation and veining in the rocks of autoclastic mélange zone in the Lalji Ka Khera section. (*a*) Brecciation in Sawa sandstone. (*b*) A network of quartz veins cutting through Sawa porcellanite beds. (*c*) Local brecciation in Berach granite.
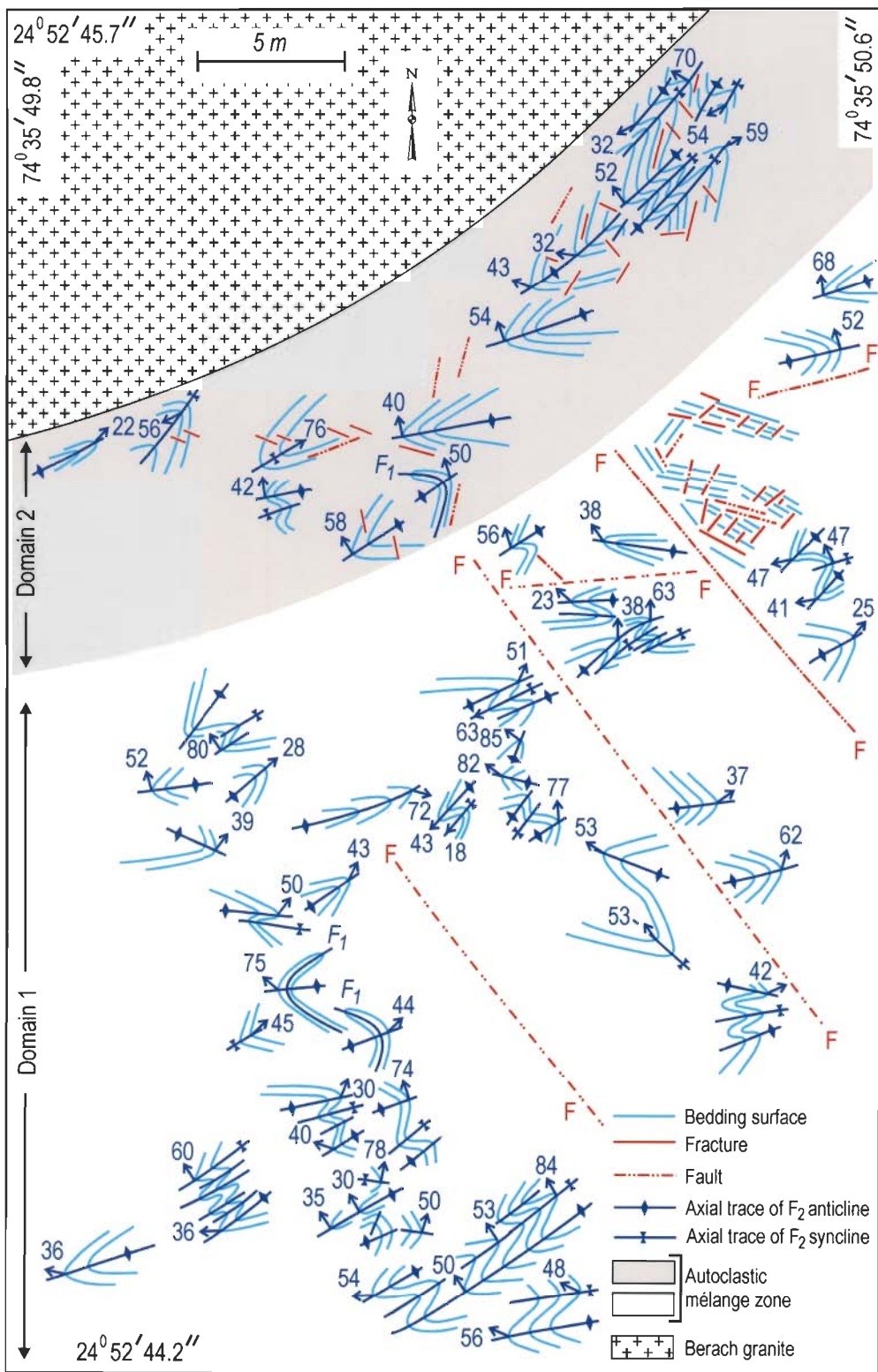
Fig. 3.20: Structural map of autoclastic mélange zone in Lalji ka Khera section. All folds are developed on bedding surface and/or bedding parallel cataclasite/ mylonite foliation.

81

On the basis of distinct overprinting relationships observed at several outcrops, these folds can be classified into three groups, namely, F_1, F_2 and F_3. Of these, F_3 folds, developed in local domains, do not control the deformation plan of the autoclastic mélange zone significantly.

F_1 folds are tight to isoclinal and F_2 folds are characteristically open to close type of conjugate kink folds. In general, both F_1 and F_2 hinge lines show considerable directional instability. Type-2 interference pattern, formed due to the superposition of F_2 folds on F_1 folds, are most common in the autoclastic mélange zone (Fig. 3.21a and b). A few outcrops, however, show type-3 interference between F_1 and F_2 folds (Fig. 3.21c and d). It is evident, therefore, that the angle between F_1 and F_2 hinge lines varies within the fault zone. The angular variation in F_1 and F_2 hinge lines is both due to the noncylindrical nature of F_1 folds before the onset of F_2 folding and, also due to the non-parallelism between the F_2 hinge lines of the two sets in conjugate pairs. As the F_1 and F_2 hinge lines are inclined at moderate angles to each other in most of the autoclastic mélange zone, the type-2 interference patterns are common.

Structural analyses

Based on the homogeneity with respect to the F_2 axial plane orientation, the autoclastic mélange zone has been divided into two domains, namely, domain-1 lying to the south and domain-2 lying to the north (Fig. 3.20). The intensity of deformation in domain-2 is distinctly much higher than in domain-1. Results of the structural analyses and inferences regarding the fold geometry in each domain are summarized in Table 3.2.

Table 3.2: Structural analyses of the Great Boundary Fault Zone
in the Lalji Ka Khera section.

Domains	Characteristic features
Domain-1 (lying in the vicinity and towards south of domain 2)	In general, F_1 folds are nonplane-noncylindrical and both the sets of F_2 conjugate pairs are plane-noncylindrical (Fig. 3.22a to c). The nonplanarity of F_1 folds is due to F_1 axial plane folding during the F_2 folding. The noncylindricity of F_1 folds is due to two main factors: (i) rotation of F_1 hinge lines during F_2 folding, and (ii) rotation of F_1 hinge lines due to shearing in the autoclastic mélange zone. F_2 folds occur as conjugate kinks, which, on average, have a modal dihedral angle of about 45° between the axial planes. The noncylindricity of F_2 folds is due to three main factors: (i) development of F_2 folds on diversely oriented limbs and hinge zones of F_1 folds, (ii) non-parallelism of the F_2 hinge lines in conjugate pairs sets, (iii) rotation of F_2 hinge lines during shearing in the autoclastic mélange zone. F_3 folds are scanty. These folds are plane-noncylindrical and occur in conjugate pairs of kink folds. The conjugate F_3 axial planes have a common NW-SE strike but dip at steep angle towards NE and SW, respectively (Fig. 3.22d). The variation in F_3 hinge lines orientation is relatively smaller as compared to the variation in F_2 hinge lines orientation. The initial non-parallelism of F_3 hinge lines in the conjugate pairs is the main reason for the observed variation in the F_3 hinge lines orientation. F_3 folds are only mildly developed and their effects on F_1 and F_2 folds are insignificant.
Domain-2 (in the vicinity of Berach granite)	This domain is characterised by a more intense nature of shearing. Because most of the F_1 folds have been obliterated during the F_2 folding and shearing, these folds are rare (Fig. 3.22e). F_2 folds are more abundant than in domain-1 (Fig. 3.22f and g). Both the sets of conjugate F_2 axial planes have been rotated towards the NNE

striking shear planes during the shearing in domain-2. As a sequel to this rotation, the dihedral angle between F_2 conjugate axial planes decreased to 26° in this domain.

The variation in F_2 hinge lines is due to: (i) initial non-parallelism between F_2 hinge lines of conjugate pairs, (ii) development of F_2 folds on non-parallel bedding surfaces corresponding to the limb and hinge regions of F_1 folds and, (iii) rotation of F_2 hinge lines towards the direction of maximum extension during the shearing in the autoclastic mélange zone.

3.2.2 Brittle structures

Several sets of fractures and faults cut through the rocks of autoclastic mélange zone (Fig. 3.20). On the basis of the angular relationship with respect to F_2 axial planes, these fractures and faults are classified broadly into two main sets: (i) a strike set, which comprises the fractures and the faults paralleling the F_2 axial planes and, (ii) a cross-fold set containing the fractures and faults, which are inclined at a moderate to high angles with respect to the F_2 axial planes. The fractures and faults belonging to strike set trend NE-SW and dip mostly at steep angles towards NW (Fig. 3.22h and i). The fractures and faults belonging to cross-fold set strike NW-SE and dip at steep angles towards SW and NNE, respectively (Fig. 3.22h and i). Lack of surface structures, such as plumose marking and twist hackles precludes the determination of the precise nature of fractures. Although a shear offset across several fractures is observable, it is not certain if these fractures initiated as shear fractures, or, the shearing is a phenomenon of reactivation on a

preexisting extension fractures. Lack of distinct overprinting relationship between fractures and faults of strike set and cross-fold set points to their synchronous origin.

3.2.3 Microstructural evolution of fault zone rocks

The tectonic evolution of the autoclastic mélange zone occurred in two or more cycles of deformation, such that each cycle consisted of three stages that are preserved as different sets of microstructures in these rocks. The first stage is represented by initiation and propagation of intragranular and transgranular microfractures alongwith brecciation and pressure solution leading to breakdown of quartz and K-feldspar grains into angular fragments (Fig. 3.23a). The intragranular microfractures can further be classified into two types: (i) extensional fractures, which are commonly filled with relatively strain free euhedral quartz grains of variable sizes and, (ii) hybrid extensional-shear fractures, which are filled with strained and elongated quartz grains inclined at low angles to the fracture boundary (Fig. 3.23b). The transgranular fractures are mostly shear type, but occasionally extensional type are also observable. The shear type transgranular fractures are invariably thinner than the extensional fractures and filled with very fine grained quartz grains that are aligned in a broad parallelism with the fracture boundary (Fig. 3.23c). The extensional type of transgranular fractures are filled with subangular and randomly oriented quartz grains showing weak undulose extinction (Fig. 3.23c).

The beginning of second stage of deformation, namely, cataclasis, is marked by widening of microfractures and their propagation to form a fracture network (Fig. 3.23d).
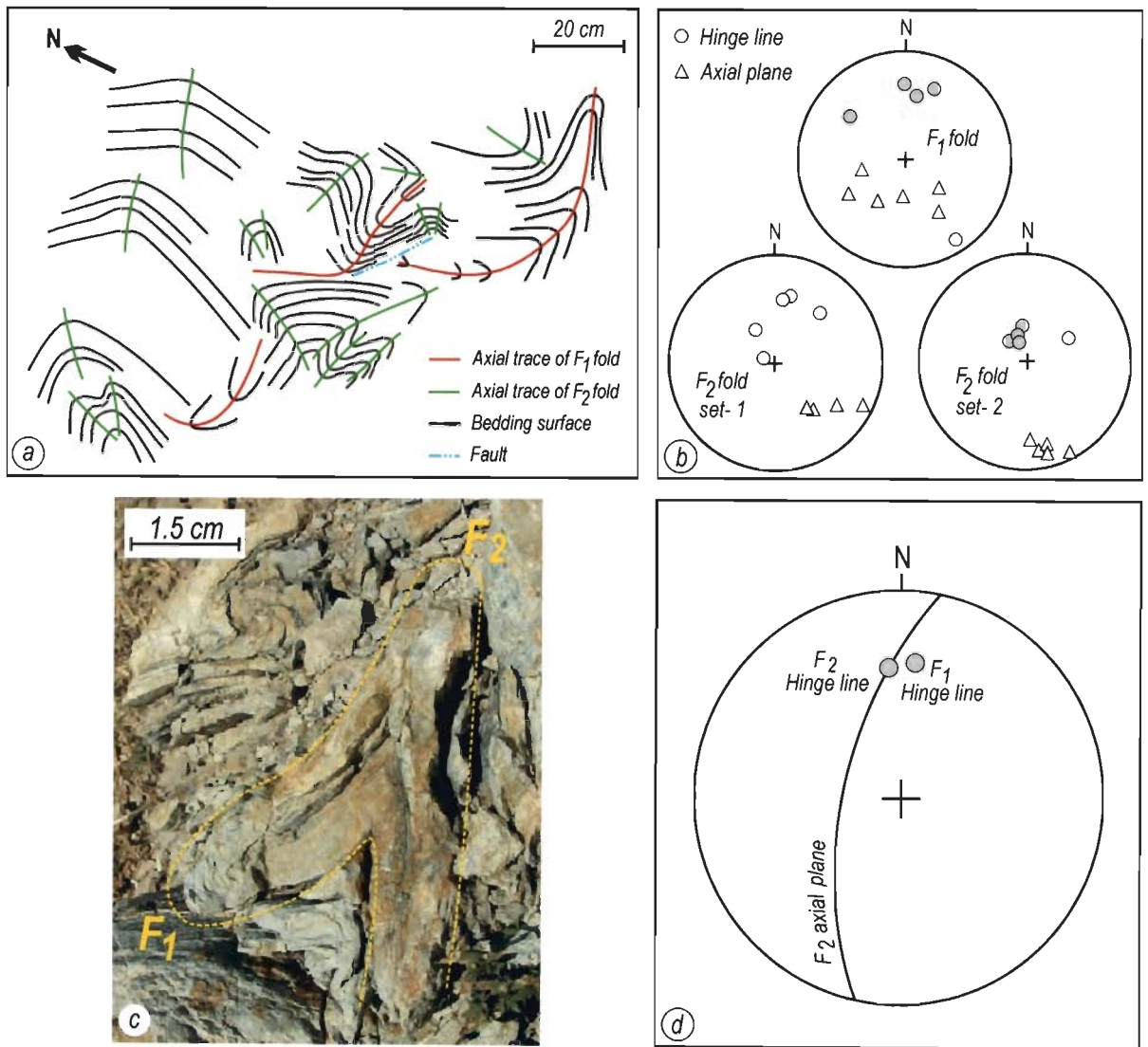
Fig. 3.21: (*a*) Field trace of a type-2 interference pattern in the Lalji ka Khera section. (*b*) Lower hemisphere equal area plots for hinge lines and axial planes of F_1 and F_2 folds in type-2 interference pattern shown in fig. (*a*). (*c*) Type-3 interference pattern. (*d*) Lower hemisphere equal area plots for hinge lines and axial planes of F_1 and F_2 folds in type-3 interference pattern shown in fig. (*c*).
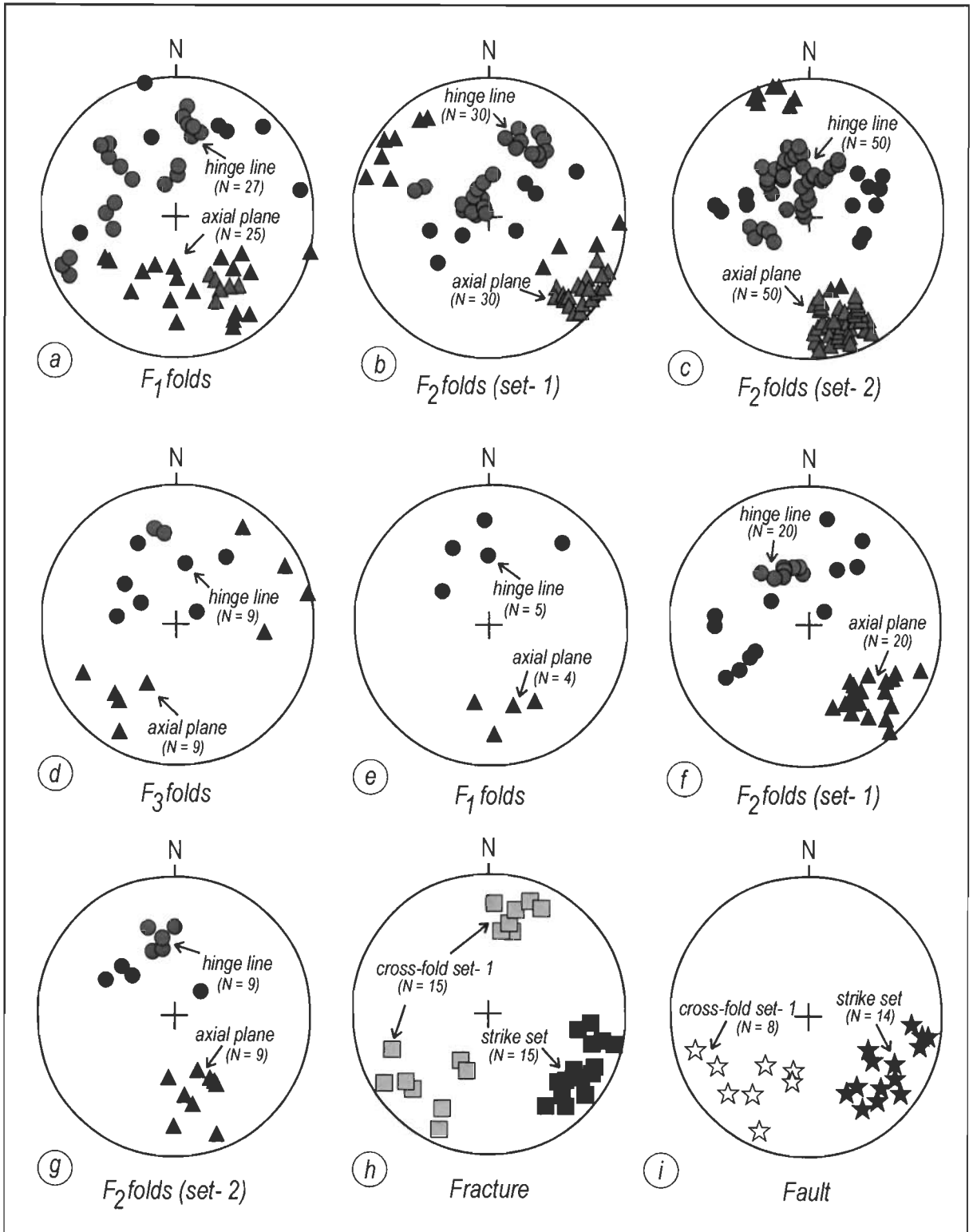
Fig. 3.22: Lower hemisphere equal area plots for folds, fractures and faults in Lalji Ka Khera section. (**a-d**) Axial planes and hinge lines of F_1, F_2 and F_3 folds in domain-1. (**e-g**) Axial planes and hinge lines of F_1 and F_2 folds in domain-2. (**h-i**) Fractures and faults in the entire Lalji ka Khera section.

At this stage, quartz and K- feldspar grains within the fracture zone, as well as, in the groundmass show subangular shapes of variable sizes. With increase in the intensity of deformation, diversely oriented fracture zones rotate to assume a crude parallelism with respect to each other (Fig. 3.23e). Due to enhanced fluid activity and pressure solution in these fracture zones, the grain size of quartz further reduces, the grain shape becomes less angular, and different components of fracture network merge with each other to form a cataclastic zone (Fig. 3.23f).

In the third stage, the deformation mechanism changes from brittle to ductile as a sequel to enhanced pressure solution and significant strain softening within the cataclastic zone. The initiation of ductile shearing results into reduction in size and alignment of fine grained quartz along the margin of the cataclastic zones (Fig. 3.23f). With increase in the intensity of shearing, the randomly oriented and coarse quartz grains also assume an inequidimensional shape, strong preferred orientation and, exhibit characteristic signatures of ductile deformation in form of undulose extinction, subgrain formation, deformation lamellae and recrystallisation (Fig. 3.23g). As a sequel to these changes, the rock fabric transforms from a cataclasite to a mylonite. The development of also mylonite marks the culmination of a typical cycle of deformation in the fault zone rocks of the Lalji ka Khera section.

The subsequent cycle of deformation again initiates with development of cataclasite through microcracking, brecciation, networking of fracture zones, and grain size reduction due to pressure solution. The microcracks and veins formed during this cycle distinctly cut through the mylonite foliation formed during the first cycle (Fig. 3.23h). The overprinting of mylonite by cataclasite and that of cataclasite by mylonite,
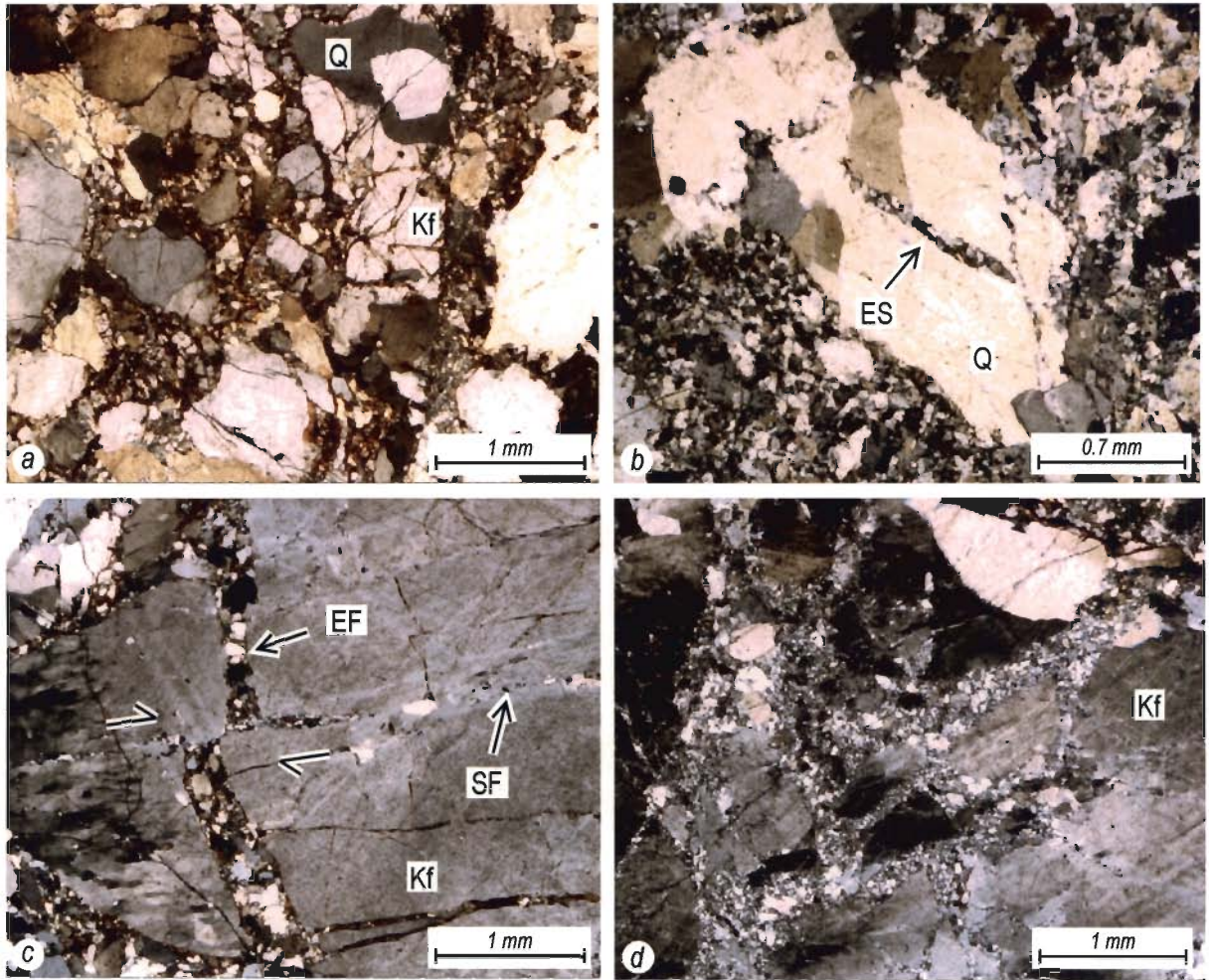
Fig. 3.23: (*a-h*) Photomicrographs showing evolution of fault rocks within autoclastic mélange zone in the Lalji ka Khera section (crossed polars). (*a*) Breakdown of K-feldspar (Kf) and quartz grains (Q) into angular fragments. (*b*) An intragranular hybrid extensional-shear fracture (ES) in a quartz grain (Q). (*c*) transgranular shear (SF) and extensional (EF) fractures. (*d*) Networking of fracture zones.

91
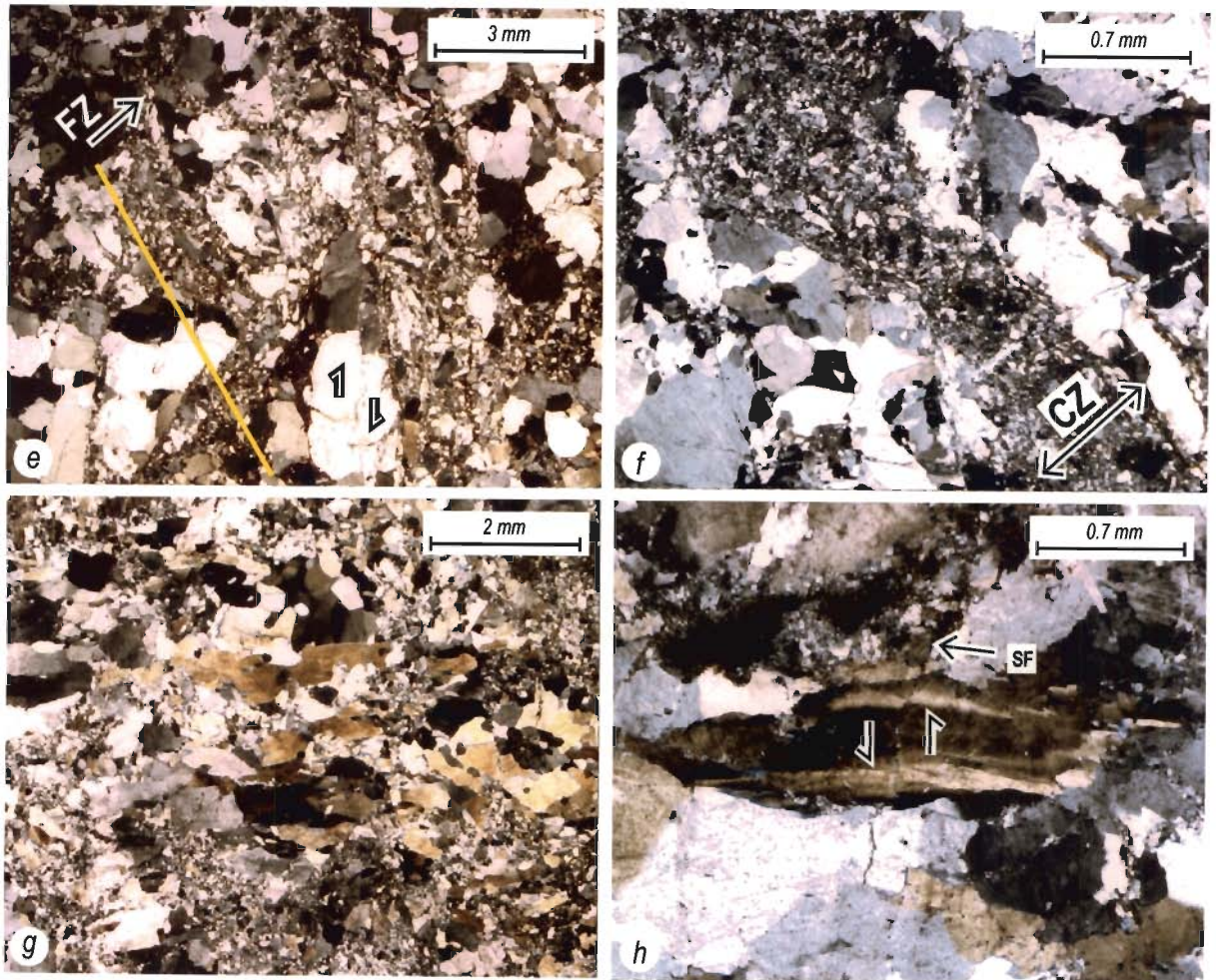
Fig. 3.23: (*e*) Different fracture zone (FZ) show a crude parallelism along the Yellow line. The pair of half arrows shows shear offset along a trnasgranular shear fracture (SF). (*f*) Cataclasite zone (CZ) containing relatively fine grained elongated quartz at the margin and coarse grained randomly oriented quartz at the median region. (*g*) Mylonite foliation containing preferredly oriented quartz grains deformed by crystal plastic deformation. (*h*) Overprinting of mylonite foliation by transgranular shear fracture (SF) pointed by arrow.
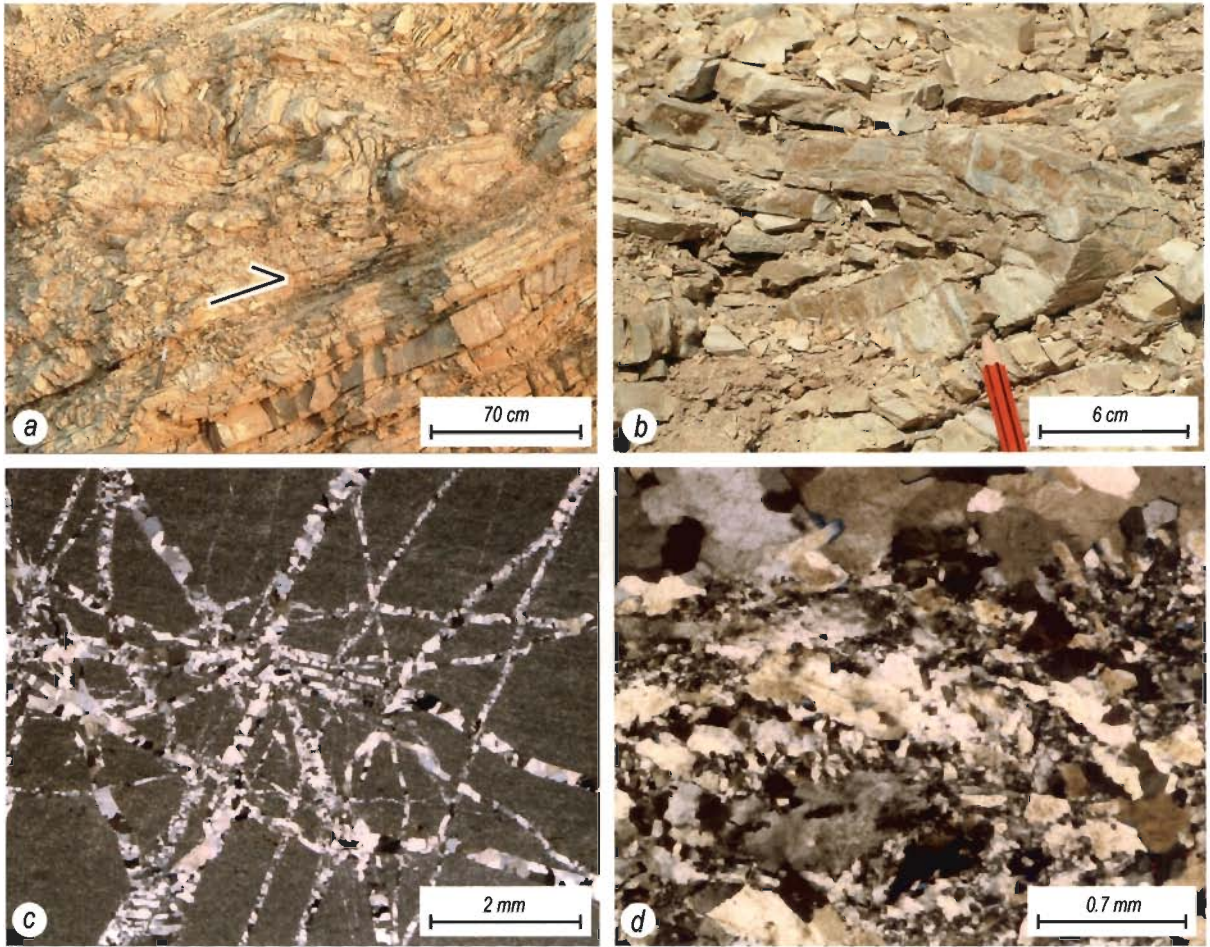
Fig. 3.24: Bassi section. (*a*) Brecciation and intense folding in Sawa sandstone-porcellanite beds on the hangingwall of a thrust. Thrust plane strikes N 340^0 and dips at 28^0 towards ENE. (*b*) A recumbent isoclinal fold on the bedding surfaces in the Sawa porcellanite bed. (*c*) Quartz veins in diverse orientation form a fracture network in the Sawa porcellanite beds. (*d*) Mylonite foliation within a ductile shear zone parallels the bedding surfaces in the Sawa sandstone beds.

are both common. This kind of cyclic generation of cataclasite and mylonite indicates the rocks in the autoclastic mélange zone evolved within the brittle-ductile transition zone (Takagi et al., 2000).

Several lines of microstructural evidence, such as the occurrence of microfractures, quartz filled veins, pressure solution seams, subgrains, serrated grain boundary and core and mantle texture all imply that the deformation within the autoclastic mélange zone occurred in a low temperature deformation regime (Groshong, 1988). The predominantly ductile behavior of quartz grains and brittle behavior of K-feldspar grains further indicate that the cataclasite and mylonite foliation were developed at an approximate temperature of about 300 to 350°C (Wang and Ludman, 2004). Each cycle of deformation within the autoclastic mélange zone, initiated by brittle fracturing and pressure solution, culminated in crystal plastic deformation and mylonitization. Brittle deformation in these rocks, therefore, acts as precursors to the ductile deformation (Guermani and Pennacchioni, 1998).

3.3 Bassi section

This section of the Great Boundary Fault Zone is exposed on either face of the railway line near Bassi railway station. It comprises 20-30 metre thick zone of Sawa sandstone-shale-porcellanite sequence of the Lower Vindhyan Group that are exposed in the vicinity of a gabbroic component of the Berach granite (Fig. 2.2). The geological setting of the Great Boundary Fault Zone in this section is similar to that of Lalji ka Khera section.

3.3.1 Fault zone rocks

The rocks within the fault zone are characterised by intricate folding, local brecciation and; cataclasis and mylonitisation, particularly, in the northeastern part of the section, where relatively competent Sawa sandstone-porcellanite beds are dominant (Fig. 3.24a and b). At the outcrop scale, however, there are no mappable boundaries of the ductile shear zones nor, there is any development of autoclastic mélange zone. In this regard, this fault zone is somewhat different in structural style than those in the Berach river section and Lalji ka Khera section.

The fault zone rocks, under the microscope, however, show distinct networking of veins, brecciation and, the development of cataclasite and mylonite foliation parallel to bedding (Fig. 3.24c and d). The development of mylonites is restricted either to the Sawa sandstone beds or to the quartz veins cutting through the Sawa porcellanite beds. Similar to Lalji ka Khera section, the mylonites, in this section too, have evolved through one or more cycles of multistage processes of fracturing, pressure solution, brecciation, cataclasis, crystal plastic deformation and recrystallisation.

3.3.2 Folding in fault zone rocks

Distinct overprinting relationships, observed at several outcrops, reveal that the Great Boundary Fault Zone in this section bears the imprints of three successive groups of folding, namely, F_1, F_2 and F_3. Individual mesoscopic F_1 folds are, in general, tight to

isoclinal, recumbent, or, low plunging reclined folds (Fig. 3.24a). At the scale of entire section or domains (defined later), these F_1 folds are characteristically nonplane-noncylindrical. Both F_2 and F_3 folds are open to close and occur in conjugate pairs of low plunging kink folds. The conjugate axial planes of F_2 folds strike E-W and dip at low to steep angles towards N and S, respectively. By contrast, the conjugate axial planes of F_3 folds strike NW-SE and dip at moderate to steep angles towards NE and SW, respectively.

Depending upon the angular relationship between F_1 and F_2 hinge lines, the superposition of F_2 folds on F_1 folds has resulted into the development of type-2 or type-3 interference patterns at different outcrops (Fig. 3.25a to d). Wherever the angle between F_1 and F_2 hinge lines is moderate or high, a type-2 interference pattern has developed. By contrast, wherever the F_1 and F_2 hinge lines parallel each other, a type-3 interference pattern has developed. It is mainly due to the folding of F_1 axial planes and rotation of F_1 hinge lines during F_2 folding that F_1 folds are nonplane-noncylindrical. At least, a part of angular variation in F_1 and F_2 hinge lines is also attributable to the initial non-parallelism between the hinge lines of conjugate pairs of F_2 kink folds.

Structural analyses

Based on the homogeneity with respect to orientation of axial planes of F_2 and F_3 folds, the Bassi section has been divided into two domains, namely, domain-1 lying northeastern and, domain-2 lying southwestern parts of the fault zone (Figs. 3.26a and

3.27a). In domain-1, both F_2 and F_3 folds occur on the mappable scale and their axial planes strike E-W and NW-SE, respectively. By contrast, in domain-2, only F_3 folds on NNW-SSE striking axial planes occur on the mappable scale. The structural analyses and inferences regarding the fold geometry in each domain are summarized in Table 3.3.

Table 3.3: Structural analyses of the Great Boundary Fault Zone in the Bassi section.

Domains	Characteristic features
Domain-1	In general, F_1 and F_2 folds are nonplane-noncylindrical (Fig. 3.26b and c). The noncylindricity and nonplanarity of F_1 folds is mainly due to two factors: (i) rotation of F_1 hinge lines and F_1 axial planes during F_2 and F_3 folding and, (ii) rotation of F_1 hinge lines due to shearing on the Great Boundary Fault Zone. The noncylindricity and nonplanarity of F_2 folds is mainly because of combined effect of: (i) initial non-parallelism between hinge lines and axial planes of the conjugate pairs of F_2 folds and, (ii) minor rotation of F_2 folds during F_3 folding (Fig. 3.26d).
Domain-2	In this domain NNW-SSE trending F_3 folds are dominant (Fig. 3.27a). F_3 folds refold earlier folds but the exact designation of early folds, i. e., F_1 or F_2, in individual interference patterns is not decipherable (Fig. 3.27b). It is because of the relatively higher amount of shearing in this domain that the conjugate sets of F_3 axial planes have been rotated into a common NNW orientation and the F_3 folds have assumed a tight geometry (Fig. 3.27c). This rotation has resulted into a distinctly greater homogeneity with respect to the orientation of F_3 axial planes in domain-2 as compared to domain-1.
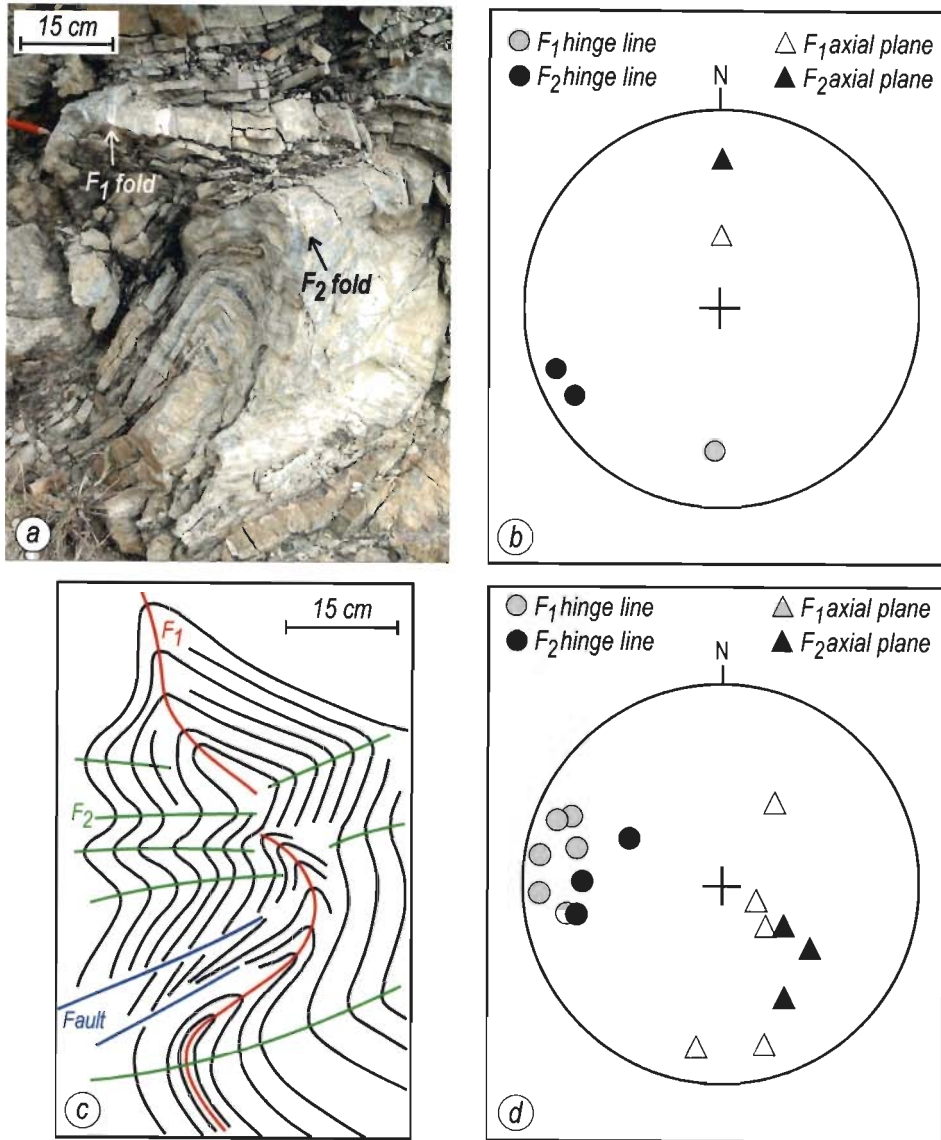
Fig. 3.25: Bassi section. (*a*) Type-2 interference pattern. (*b*) Lower hemisphere equal area plots for hinge lines and poles to the axial planes of F_1 and F_2 fold in type-2 interference pattern shown in fig. (*a*). (*c*) Field trace of a type-3 interference pattern. (*d*) Lower hemisphere equal area plots for hinge lines and poles to the axial planes of F_1 and F_2 folds in type-3 interference pattern shown in fig. (*c*).

...
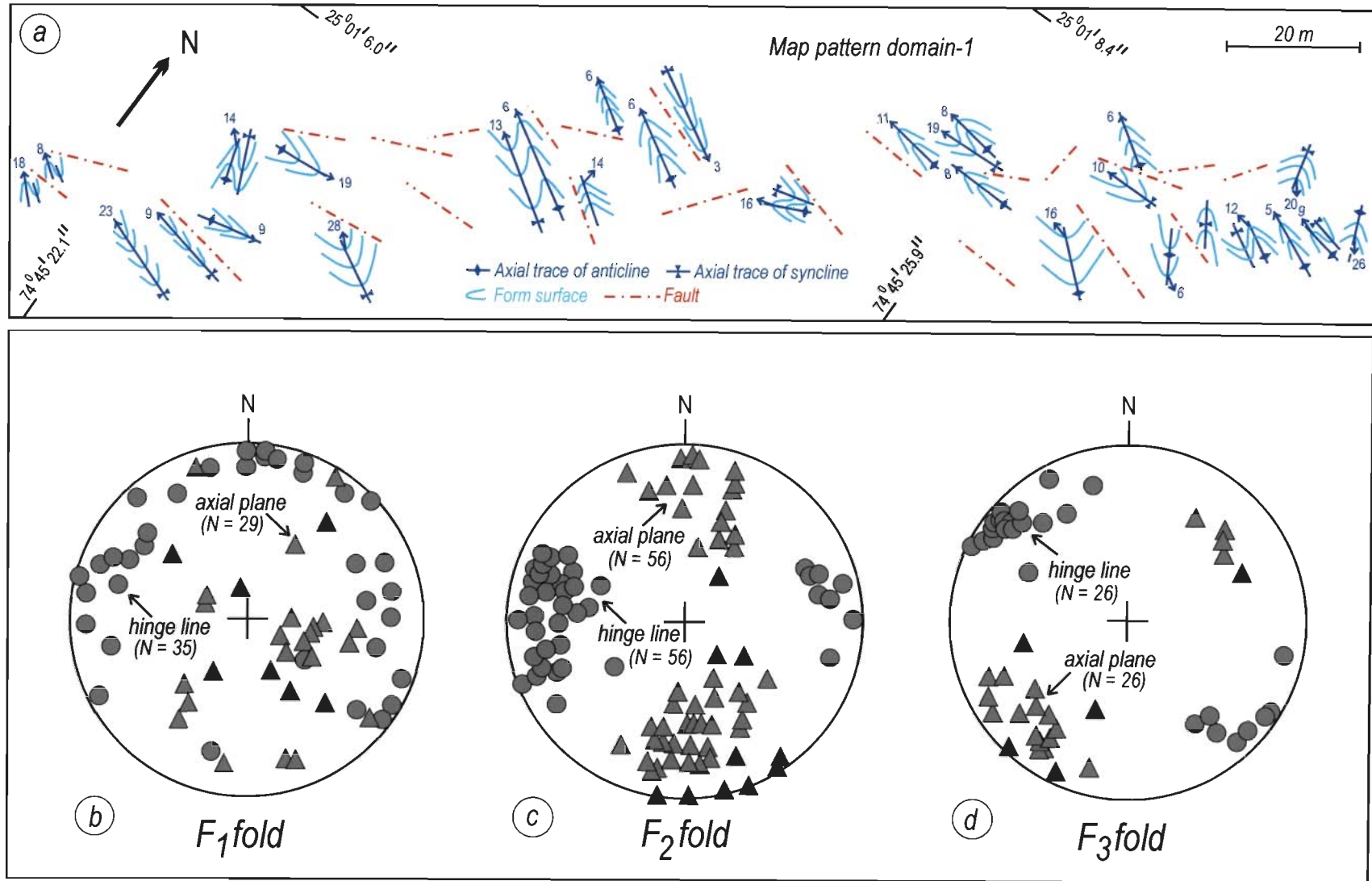
Fig. 3.26: (*a*) Structural map of domain-1 of Great Boundary Fault Zone in the Bassi section. Form surface is defined by bedding surfaces and bedding parallel cataclasite/mylonite foliation. (*b-d*) Lower hemisphere equal area plots for hinge lines and pole to the axial planes of F_1, F_2 and F_3 folds in domain-1.
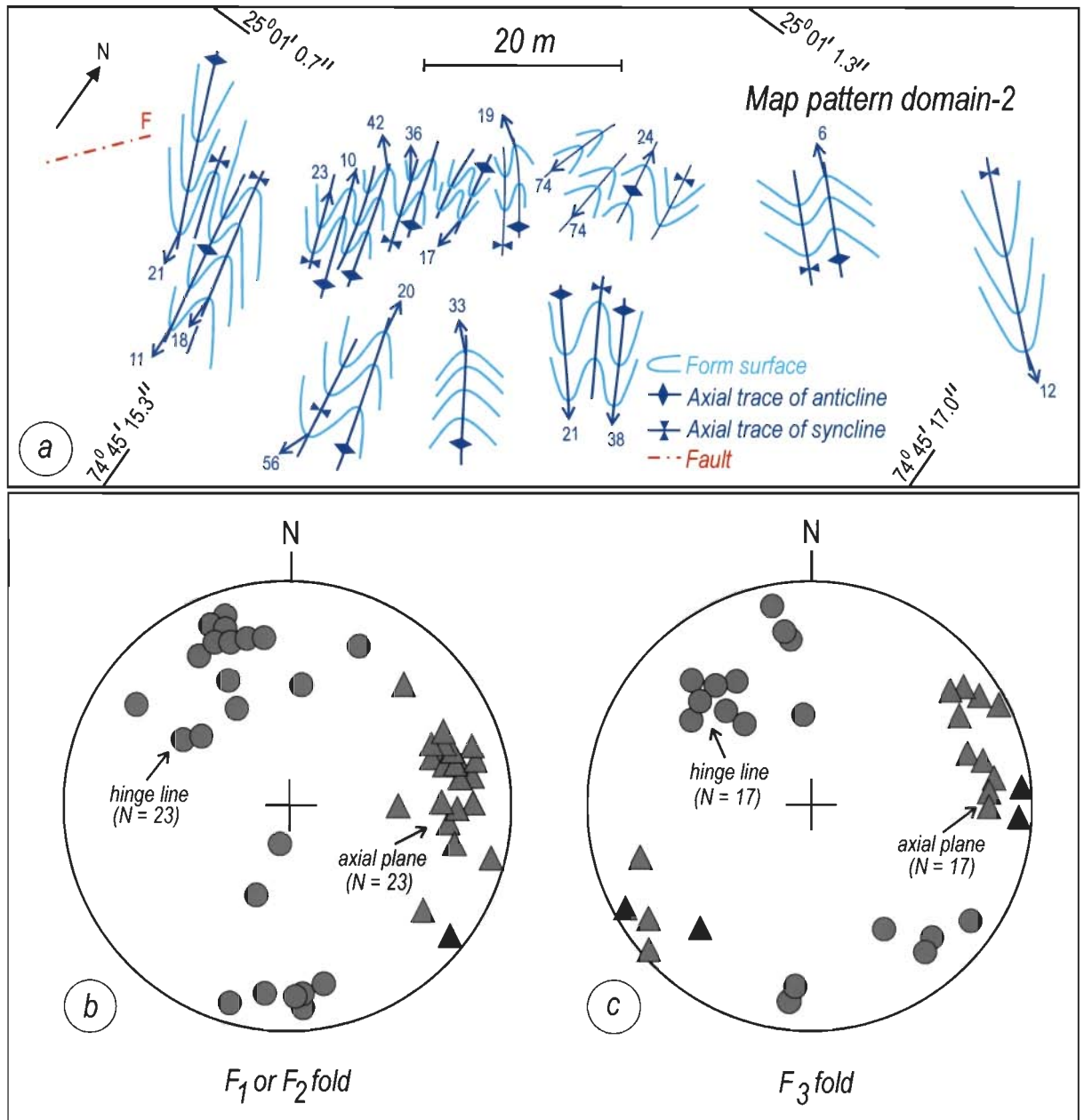
Fig. 3.27: (*a*) Structural map of domain-2 of Great Boundary Fault Zone in the Bassi section. Form surface is defined by bedding surfaces and bedding parallel cataclasite/mylonite foliation. (*b-c*) Lower hemisphere equal area plots for hinge lines and pole to the axial planes of F_1/F_2 and F_3 folds in domain-1.

3.3.3 Brittle structures

Three main sets of faults cut through the rocks within the fault zone in Bassi section, namely, set-1, set-2 and set-3 (Fig. 3.28 a to c). Of these, the two sets parallel F_2 and F_3 axial planes, respectively and; the third set, cuts through all the folds, represents the youngest set of faults in the Bassi section (Fig. 3.28d and e). The slip-lineations on faults of all the three sets show a wide range in orientation. Such a variation in the rake of slip-lineation on fault surfaces can occur either due to folding of fault planes, or, due to change in the direction of movement during the faulting, or, due to reactivation of diversely oriented planar discontinuities into different types of faults in a common stress regime. As the mesoscopic faults are neither folded nor contain curvilinear slip lineations, it is inferred that the observed variation in the rake of slip lineation is due to reactivation of diversely oriented planes into different types of faults, e. g., strike-slip, normal and thrust. The sense of movement on most of these faults is difficult to decipher because of lack of suitable markers on either side of the faults and/or fault surface structures (Petit, 1987; Doblas, 1998).

Summary: In summary, the fault zone rocks in all the three sections are deformed in a broadly common deformation plan, which consists of ductile shearing, successive folding and fracturing/faulting. In details, however, the structural geometry of the Great Boundary Fault Zone in the Berach river section is at variance with the structural geometry in the other two sections. These differences are mainly due to the fact that the Great Boundary Fault Zone, in the Berach river section, consists of relatively

incompetent Nimbahera shale beds. In the other two sections, relatively competent beds of Sawa sandstone-porcellanite sequence constitute bulk of the section.

In all the three sections, the cataclasite/mylonitisation parallels the bedding surfaces. The development of these bedding parallel mylonites, in Berach river section, is confined to cm-dm scale ductile shear zones that cut the Nimbahera shale beds sharply. In other two sections cataclasite/mylonite foliation is developed in local domains consisting of sandstone beds and, the boundaries of mylonite zones are neither sharp nor well defined.

The fault zone rocks in all the three sections are deformed by F_1, F_2 and F_3 folds during the successive phases of folding. Furthermore, in all the three sections, F_2 folds are most predominant and, F_1 folds are rare because of transposition during the post-F_1 deformation. F_3 folds are relatively most mild in all the three sections. F_1 folds in Berach river section are observed only within cm-dm scale ductile shear zones. In the other two sections, F_1 folds are also observable on bedding parallel cataclastic/mylonite foliations. F_2 folds occur as upright culmination and depression in the Berach river section, but in the other two sections, these folds occur as conjugate pairs of kink fold. Similarly, F_3 folds occur as open warps in the Berach river section but as conjugate kink folds in the Lalji Ka Khera and Bassi sections. Both F_2 and F_3 folds are relatively more homogeneous with respect to their orientations in the Berach river section, in comparison to the other two sections.

Type-2 interference is developed due to overprinting of F_2 folds on F_1 folds, is the most common style of fold superposition in all the three sections. Occasionally, however, type-3 interference patterns have also been observed between these two fold groups. It is
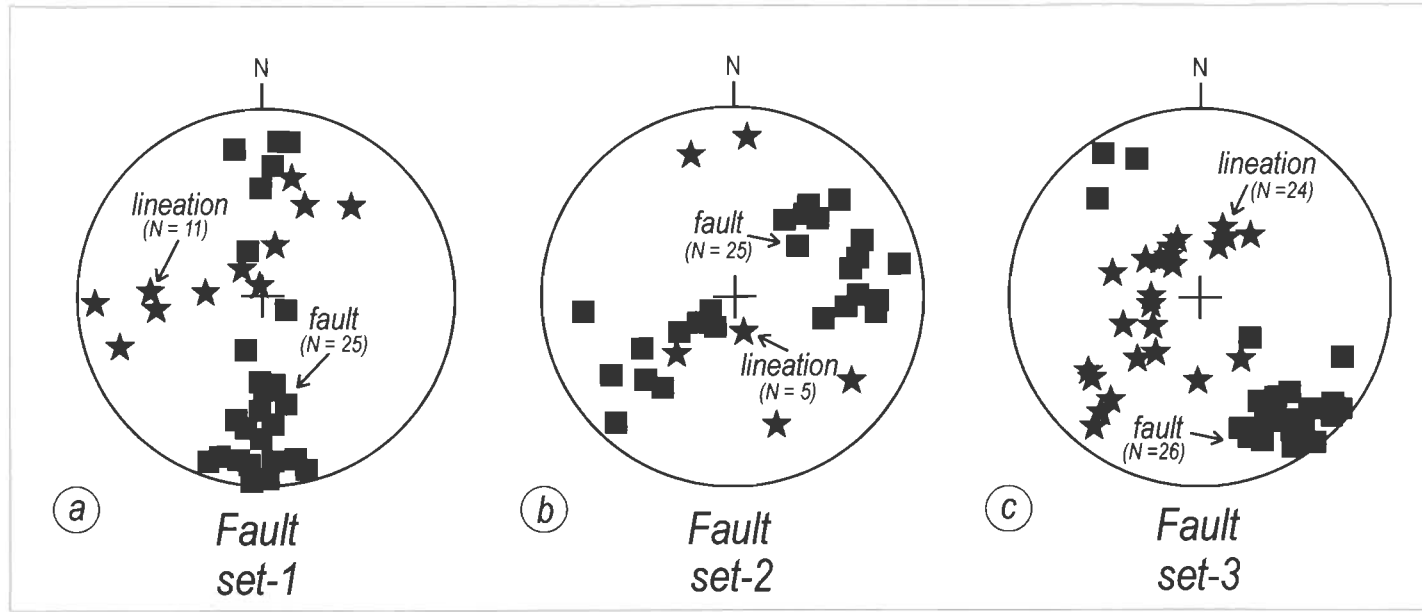
Fig. 3.28: Bassi section. (*a-c*) Lower hemisphere equal area plots for slip-lineations and pole to three sets of fault planes. (*d*) An F_2 axial planar fault (pointed by arrow). (*e*) A set-3 fault striking NNW and dipping at subvertical angle. Pencil points to straie on the fault plane.

only in the Berach river section that the superposition of F_3 over F_2 folds has resulted into development of broad culminations and depressions.

Detailed microscopic studies clearly reveal that the mylonitization of the relatively competent Sawa sandstone beds and the quartz veins in the bedding parallel ductile shear zones is the earliest event in the structural history of the Great Boundary Fault Zone. Whereas the F_1 folds were developed during the ductile shearing, F_2 and F_3 folds post-date the event of ductile shearing.

The fault zone rocks are cut by, at least, two to three sets of fractures/faults. These brittle structures show a consistent relationship with respect to the orientation of F_2 folds in all the three sections. The density of brittle structures is relatively highest in the Bassi section and lowest in the Berach river section, because the relative thickness of competent beds, such as sandstone is maximum in the Bassi section and minimum in the Berach river section.

Structural style of fault related deformation zone

The fault related deformation zone, in the Berach river section, consists of a deformed sequence of Nimbahera limestone, Suket shale and Kaimur sandstone beds. It is distinguished from the Great Boundary Fault Zone by a distinct decrease in the complexity and intensity of folding, lack of ductile shear zones and F_1 folds and, profuse development of brittle fractures and faults, particularly, in the relatively competent rock units, namely, the Nimbahera limestone beds and the Kaimur sandstone beds. It is due to thickly bedded nature of the sandstone and the limestone units in the fault related deformation zone that the bedding surfaces are folded into km scale F_2 folds, which are characterised by open upright, N-S trending and nonplunging to low plunging geometry.

This chapter concerns with the fault related deformation zone of the Berach river section, where the successively developed brittle structures cut through the sandstone and the limestone beds of the Fort syncline and the Manpura anticline, respectively (Fig. 2.1). Because of scanty nature of outcrops, the fault related deformation zone in Lalji Ka Khera and Bassi section are not studied.

4.1 Three phases of brittle structures

Distinct overprinting relationship reveals that three successive groups of brittle structures cut through the Vindhyan sedimentary rocks within the fault related deformation zone. Each group, consists of a set of dynamically compatible brittle structures that are demonstrated to have developed during a particular phase of reactivation of the Great Boundary Fault. Structures of the first phase include: (i) mesoscopic kink bands on N-S trending axes, and (ii) mesoscopic faults dipping at low angle (Fig. 4.1). Structures of the second phase consist of: (i) fractures, (ii) brittle-ductile shear zones containing en-échelon vein arrays and, (iii) steeply dipping strike-slip faults (Fig. 4.2). Structures of the third phase include thrust faults and thrust-related kink folds on E-W trending axes (Fig. 4.3).

Criteria for classification of these brittle structures in three successive phases are based on two distinct types of cross-cutting relationship: (i) the brittle-ductile shear zones of second phase structures consistently cut the thrust fault of first phase. (Fig. 4.4a) and, (ii) thrust faults of the third phase offset and drag the steeply dipping veins of the second phase (Fig. 4.4b).

4.1.1 First phase structures

Kink bands on N-S axes

Numerous compressional type kink bands occur as parasitic folds at the limbs of the large-scale F_2 folds, exemplified by Fort Syncline (Fig. 4.1a). These kink bands occur

114
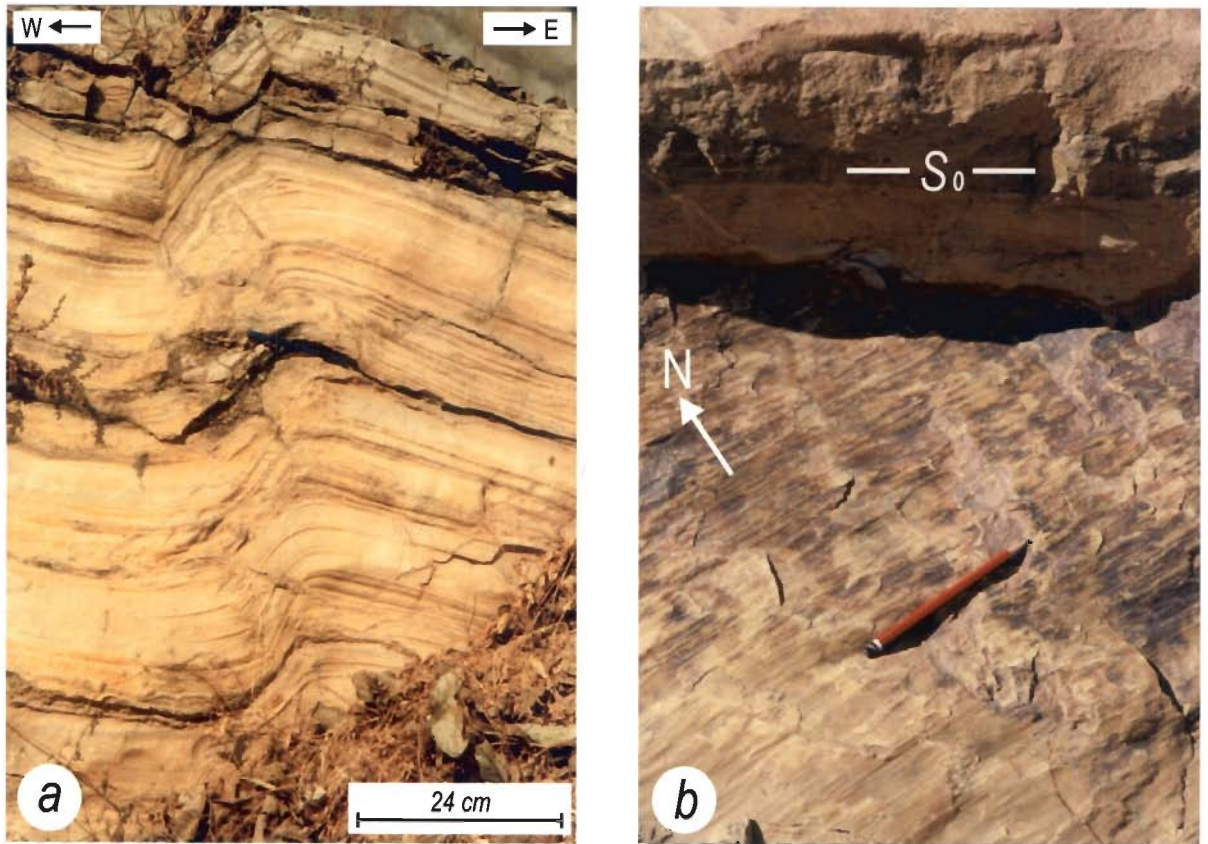
Fig. 4.1: First phase structures. (*a*) Profile section of a top-to-the-west kink band in the limestone beds. The kink axis is horizontal/N-S. (*b*) A low-angle thrust fault cutting through the kaimur sandstone bed on the western limb of the Fort syncline. *So*- trace of the bedding surface. Pencil parallels the slicken/groove lineations indicating an up-dip movement of the missing block.

Fig. 4.2: Second phase structures. (*a*) Plan view of a conjugate pair of vein arrays cutting the Kaimur sandstone bed on the eastern limb of the Fort syncline. Individual veins and array boundaries are subvertical. Thin extension veins (EV) in the upper part of the photograph bisect the dihedral angle between the complementary arrays. Note that almost all fibres are parallel. (*b*) A dextral strike-slip fault in the Kaimur sandstone bed on the western limb of the Fort syncline. The fault-surface is vertical and the slicken/groove lineations are subhorizontal.
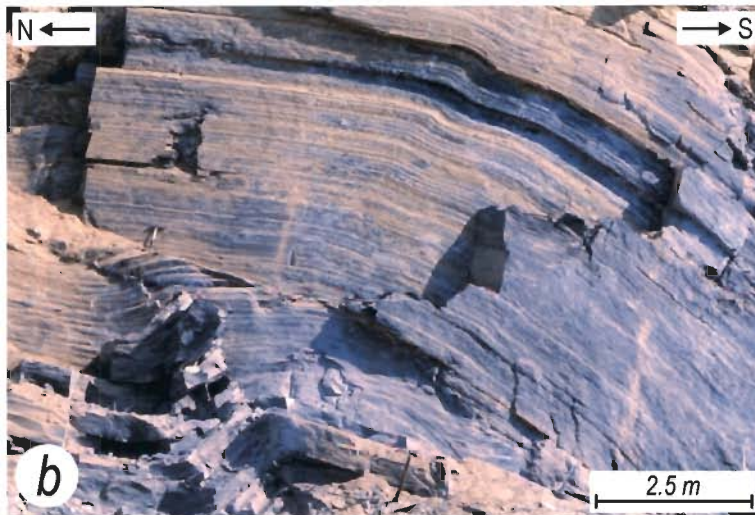
Fig. 4.3: Third phase structures. (*a*) Profile view of kink bands and the associated thrust faults in the limestone beds above the decollement surface (pointed by arrow). The kink axes are horizontal/E-W. (*b*) Top-to-the north thrust and associated kink band in the limestone beds (profile view).

119
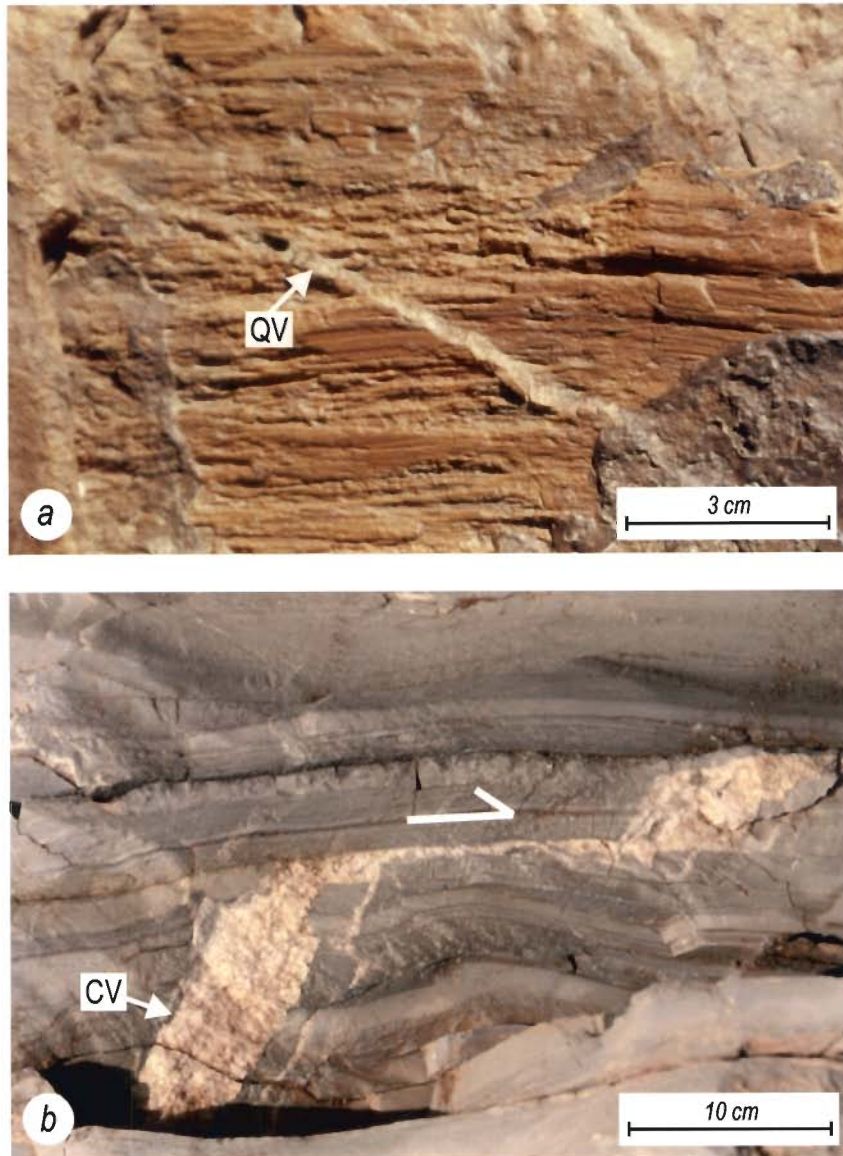
Fig. 4.4: (*a-b*) Overprinting relationships. (*a*) Strike-slip quartz veins (QV) of second phase cut through the striated and grooved first phase thrust in the Kaimur sandstone beds. (*b*) A subhorizontal bedding parallel thrust of thrid phase offsets and drags the steeply dipping calcite veins (CV) of the second phase in the Nimbahera limestone bed.

in two conjugate sets, which are characterised by top-to-the-west and top-to the-east sense of movement, respectively. The axes of kinks in both the sets are non-plunging and N-S trending. On the eastern limb of the Fort Syncline, an axial plane cleavage and a bedding/cleavage intersection lineation are developed parallel to the kink planes and kink axes, respectively.

Low angle fault

Faults belonging to the first phase dip characteristically at shallow angles $\leq 45°$, and these structures are best exposed in the Kaimur sandstone beds on the western limb of the Fort Syncline (Fig. 4.1b). The fault surfaces display profuse lineations in the form of ridges, grooves and slicken-lines, which imply a consistent top-to-the-up-dip sense of movement.

Paleostress analyses of the first phase structures

As the conjugate pairs of the first phase kink bands possess a characteristic orthorhombic symmetry, these structures qualify for the paleostress analysis by the method proposed by Ramsay (1962). The results of paleostress analysis reveal that these kink bands were developed in a thrust-type tectonic setting, such that the maximum and the intermediate principal stresses, σ_1 and σ_2 were horizontal and trending E-W and N-S, respectively; and the minimum principal stress, σ_3 was vertical (Fig. 4.5a). That the
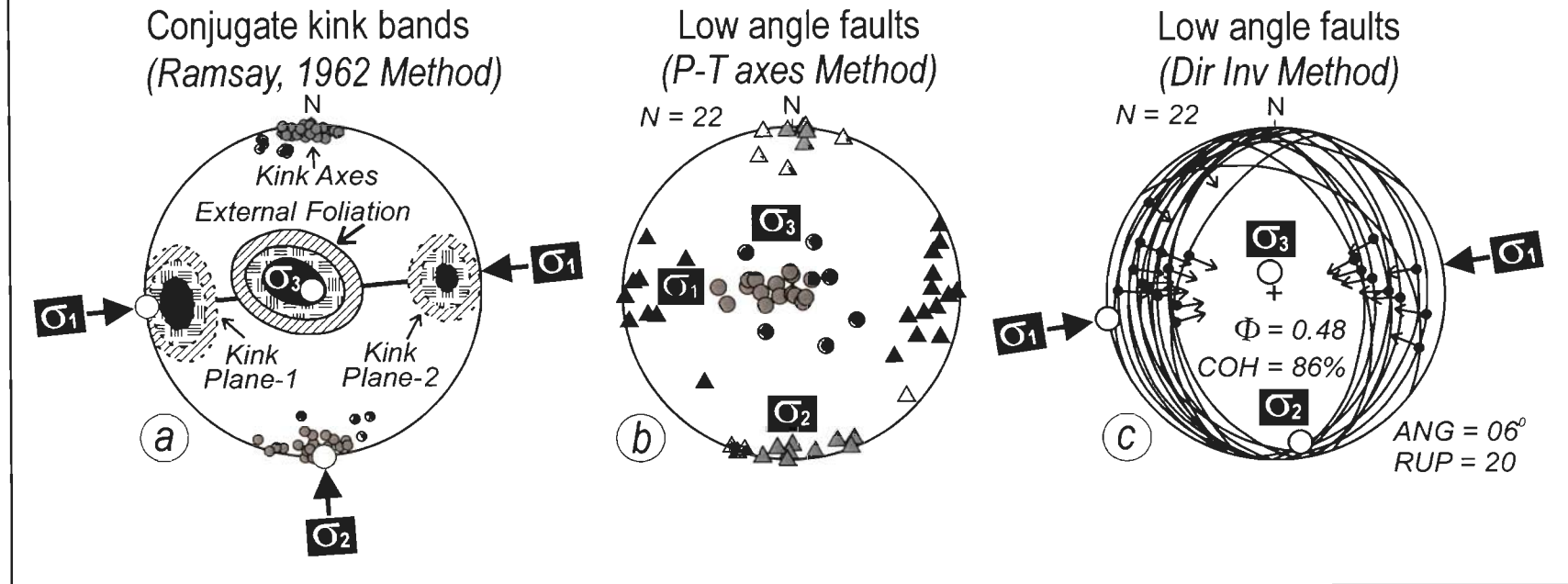
Fig. 4.5: Paleostress analyses of the first phase structures. (**a**) Kink plane-1 and kink plane-2 are complementary sets of conjugate pairs. Contouring by Kamb method. For kink plane-1, N = 31 and contours at 5-10-15σ ; σ = 1.6. For Kink plane-2, N = 58 and contours at 7-14-21σ ;σ = 1.3. For external foliation, N = 50 and contours at 7-14-21σ ; σ = 1.27. For kink axes, N = 58. White circles-principal stresses. (**b-c**) Stress analysis of the low angle faults. (**b**) P-T axes method; black triangle- σ_1- axis; grey triangle- σ_2 axis; grey circle- σ_3 axis. (**c**) Direct inversion method; great circle- fault surface; arrow on black dot- direction and sense of movement on the fault surface, white circles- principal stresses. See text for the definition of Φ , COH, RUP and ANG.

symmetry of these kink bands is orthorhombic is reaffirmed by the results of paleostress analysis, which show that the intermediate and minimum principal stresses, σ_2 and σ_3 parallel the kink axes and the pole to external foliation, respectively (Fig. 4.5a).

The first phase thrusts are also treated by both graphical and numerical methods, such as the P-T axes method and the direct inversion method, respectively (Turner, 1953; Angelier, 1990, 1994). Only those faults that indicate unambiguous sense and direction of movement are considered for the paleostress analysis. Three basic assumptions that are implicit in the application of the P-T axes method can be enumerated as: (i) the intermediate principal stress σ_2 lies on the fault plane at an angle of 90° from the slip-lineation, (ii) the movement plane contains slip-lineation, maximum principal stress σ_1, minimum principal stresses σ_3, and the pole to the fault plane, and (iii) on the movement plane, the σ_1-axis lies at an angle of 45°- (ϕ/ 2) from slip direction, measured in the direction of movement of footwall, where ϕ is the angle of internal friction. In this work, ϕ is assumed to be equal to 30°, which is the

common value for the angle of internal friction in most sedimentary rocks (Ragan, 1985).

The direct inversion method is based on the principle of determining a stress tensor by minimizing the angle between the theoretically calculated direction of maximum shear stress and the practically observed slip-lineation (Angelier, 1994). This method yields a reduced stress tensor with four components; namely, the three orientations of the principal stresses, and the shape factor Φ, which is the ratio of two differential stresses (σ_2-σ_3) / (σ_1-σ_3). One distinct merit of the direct inversion method is

its independence from the condition that the intermediate principal stress σ_2 must lie in the fault plane. The other merit is its applicability to faults that are developed as fresh ruptures, as well as to those faults that are reactivated along pre-existing discontinuities in rocks. Furthermore, the quality of results yielded by this method can be evaluated quantitatively by parameters COH, ANG and RUP, which are acronyms for quality estimators in the TENSOR program of Angelier (1994). For a given population of faults, COH indicates the total percentage of those faults, which agree with the stress solution. Both ANG and RUP indicate the misfit angle, i. e, angle between the theoretically calculated direction of maximum shear stress and the practically observed direction of slip lineation. RUP is considered a better indicator of the quality of stress solution than ANG because it not only describes the misfit angle but also indicates the magnitude of relative shear stress.

Results from both the P-T axes and the direct inversion methods are consistent with a stress configuration with E-W/horizontal maximum principal stress σ_1, N-S/horizontal intermediate principal stress σ_2, and a vertical minimum principal stress σ_3 (Fig. 4.5b and c). These results imply that the low-angle faults formed in a thrust-type tectonic regime. The principal stresses yielded by the fault-slip analyses of the first phase faults match in accordance with the principal stress orientation obtained by the independent analysis of the conjugate kink bands (Fig. 4.5). Such a dynamic compatibility between these structures substantiates the interpretation that the low-angle faults, and N-S trending kink bands and the large scale folds, such as Fort syncline, were all developed during a common deformation event.

The fault-slip analyses do not reveal absolute magnitudes of the principal stresses. The direct inversion method, however, yields the relative values of the principal stresses in terms of a shape factor Φ. As the direct inversion method applied to low-angle faults reveals that the value of Φ is close to 0.5, it is evident that the first phase of deformation occurred in a plane-deviatoric state of stress, i. e., $\sigma_2' = 0$. It is the consequence of such a plane-deviatoric state of stress that the first phase faults in the fault related deformation zone are pure dip-slip thrusts.

4.1.2 Second phase structures

Fractures, faults and en-échelon veins belonging to the second phase cut through the first phase structures throughout the Fort syncline. Furthermore, the second phase structures are consistent with respect to orientation, regardless of the variation in the orientation of bedding-surface due to the large scale F_2 folding. Finally, all the second phase structures are either vertical or dip at steep angles.

Fractures

Fractures cutting through the limestone-shale-sandstone sequence of the Fort Syncline are characterised by sub-vertical dips and lack of features such as plumose markings, arrest lines or slicken-lineations. Based on the relative orientation with respect to the N-S trending hinge lines of the large-scale folds, these fractures can be classified

127

into four sets: (i) a strike-set that consists of N-S striking fractures, (ii) a cross-fold set that consists of E-W striking fractures and, (iii) and (iv) the two sets of oblique fractures; namely, oblique set-I and oblique set-II striking NW-SE and NE-SW, respectively (Fig. 4.6a to d). Lack of consistent crosscutting and abutting relationships amongst the fractures of different sets points to their broadly synchronous origin.

Brittle-ductile shear zones

Conjugate pairs of brittle-ductile shear zones containing en-échelon vein-arrays cut through both the limbs and the hinge zone of the large scale F_2 fold typified by Fort Syncline (Fig. 4.2a). The direction of movement on these shear zones is sub-horizontal, because the line of intersection between the shear zone-boundary and the veins is invariably sub-vertical. At some outcrops, two or more contiguous shear zones occur in different orientations but imply the same sense of relative movement. Inconsistent overprinting relationship amongst such diversely oriented shear zones points to their coeval development as hybrid extensional-shear fractures. The angle between the veins and the shear zone-boundary ranges between 10-58°, although the modal value of this angle is 35-45° in most of the arrays.

The orientational and geometrical similarities between the en-échelon veins and fractures point to their dynamically compatible nature. Whereas the fractures of the cross-fold set and the oblique set-I match in orientation with the veins in the dextral shear zones, the fractures of the oblique set-II parallel the veins in the sinistral shear zones (compare Fig 4.6b and c with f and 4.6d with e).
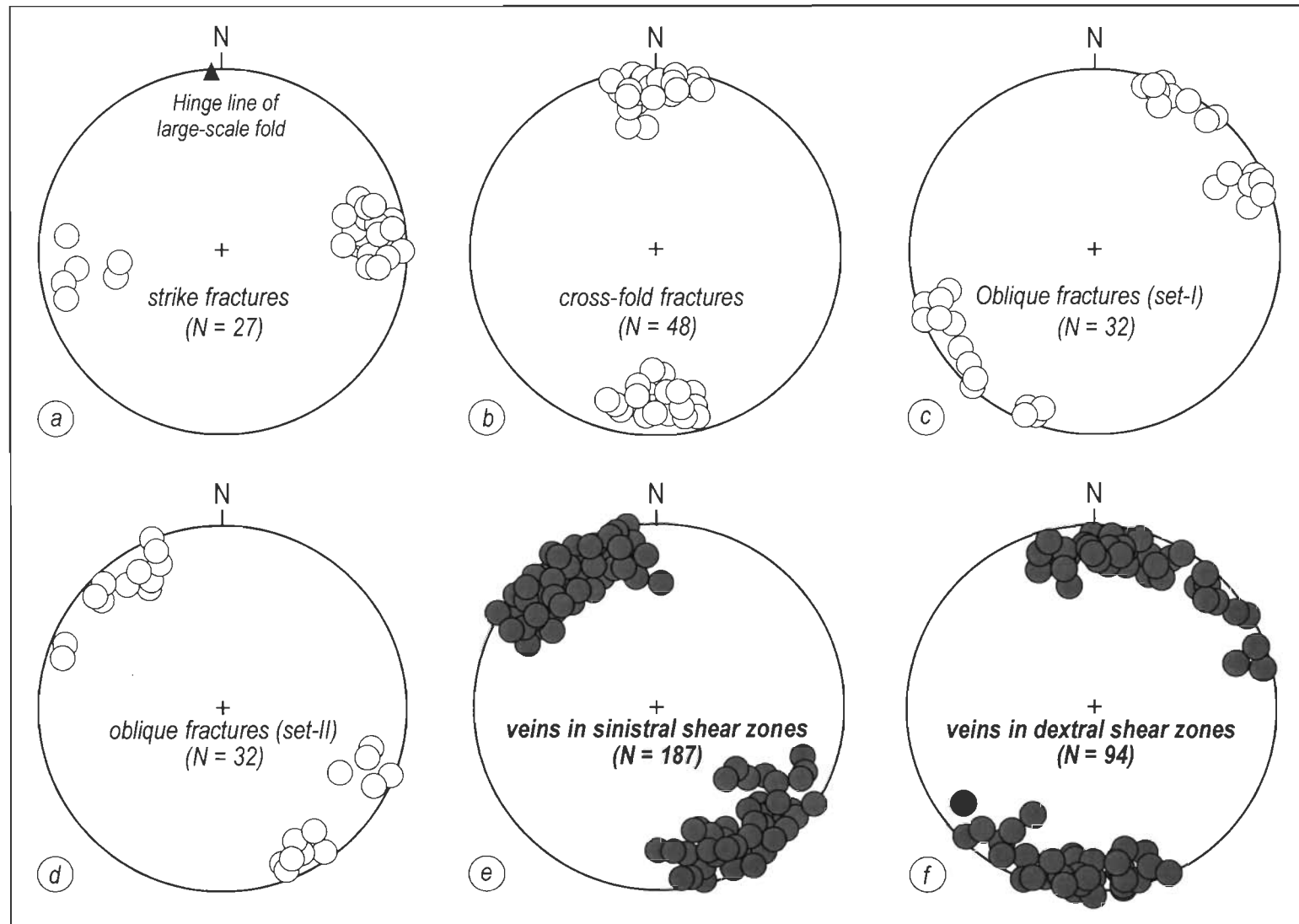
Fig. 4.6: Stereoplots showing the orientations of second phase structures. (***a-d***) fractures. (***e-f***) Veins. The orientations of the oblique fractures (set- II) and veins in the sinistral shear zones are identical (cf. fig. d and e). Similarly, the orientations of the cross-fold fractures and oblique fractures (set-I) are identical to the orientation of the veins in the dextral shear zones (cf. fig. b, c and f). Mesoscopic veins corresponding to strike fractures are absent.

Rectilinear fibres of quartz and calcite constitute the bulk of the infillings of veins cutting through the sandstone and limestone beds, respectively. These fibres are inclined at 60-80° with respect to the vein-margin and stretch in a characteristic optical continuity from one margin of the vein to the other (Fig. 4.7a and b). Most of these veins are of hybrid extensional-shear origin. In the rare veins that are of predominantly shear origin, the angle between fibres and vein-boundary is typically low ≤ 15°, although presumably there is some amount of extension across these veins, as well. Microstructures such as, the 'stretched' quartz crystal geometry of fibres, the occurrence of wall-parallel fluid inclusion bands and the irregular geometry of contacts between adjacent fibres imply that 'crack-seal' rather than 'taber-growth' model is the favored mechanism of vein development in the study-area (Ramsay, 1980; Means and Li, 2001).

Sub-vertical faults

Faults belonging to the second phase are characterised by sub-horizontal slip-lineations and sub-vertical or steeply-dipping fault surfaces (Fig. 4.2b). These faults occur in two conjugate sets that imply dextral and sinistral sense of relative movements. The dextral and sinistral faults are characteristically parallel the boundaries of the dextral and the sinistral brittle-ductile shear zones, respectively. The sense and direction of relative movement is invariably consistent on those faults and shear zones that are parallel to each other.
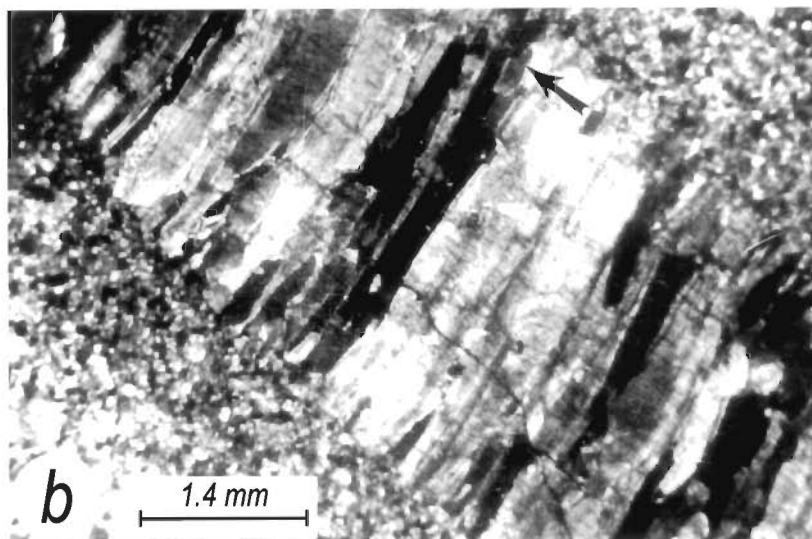
Fig. 4.7: Vein textures. (*a*) Plan view of a stretched crystal fibre type of vein. The vein infilling is characteristically made-up of rectilinear fibres that are oblique to the vein margins. (*b*) Wall-to-wall optical continuity in the fibres in a stretched fibre type of vein. One of the optically continuous fibres is indicated by arrow.

Paleostress analyses of the second phase structures

As the brittle-ductile shear zones and steeply-dipping faults are similar with respect to their orientations and kinematics, these two types of structures are grouped together for dynamic analysis by fault-slip techniques. Only those brittle-ductile shear zones that contain planar veins of simple geometry are considered for the fault-slip analysis. Shear zones containing sigmoidal, or geometrically complex veins, are not considered for the paleostress analysis because of the concentration of a significant amount of strain in such zones. The direction of movement on the shear plane is perpendicular to the line of intersection of the veins and the shear zone-boundary (Srivastava et al., 1995). The relative sense of movement is determined by the angular relationship between the veins and shear zone-boundary.

Results from both the P-T axes and the direct inversion methods consistently reveal that the second phase structures were developed in a strike-slip type tectonic-setting (Fig. 4.8). This tectonic regime comprised a horizontal maximum principal stress σ_1 trending ENE-WSW, a vertical intermediate principal stress σ_2, and a horizontal minimum principal stress σ_3 trending NNW-SSE. As the second phase structures occur in conjugate sets, these are independent of relative values of the principal stresses and the value of Φ yielded by the direct inversion method is insignificant in this case.
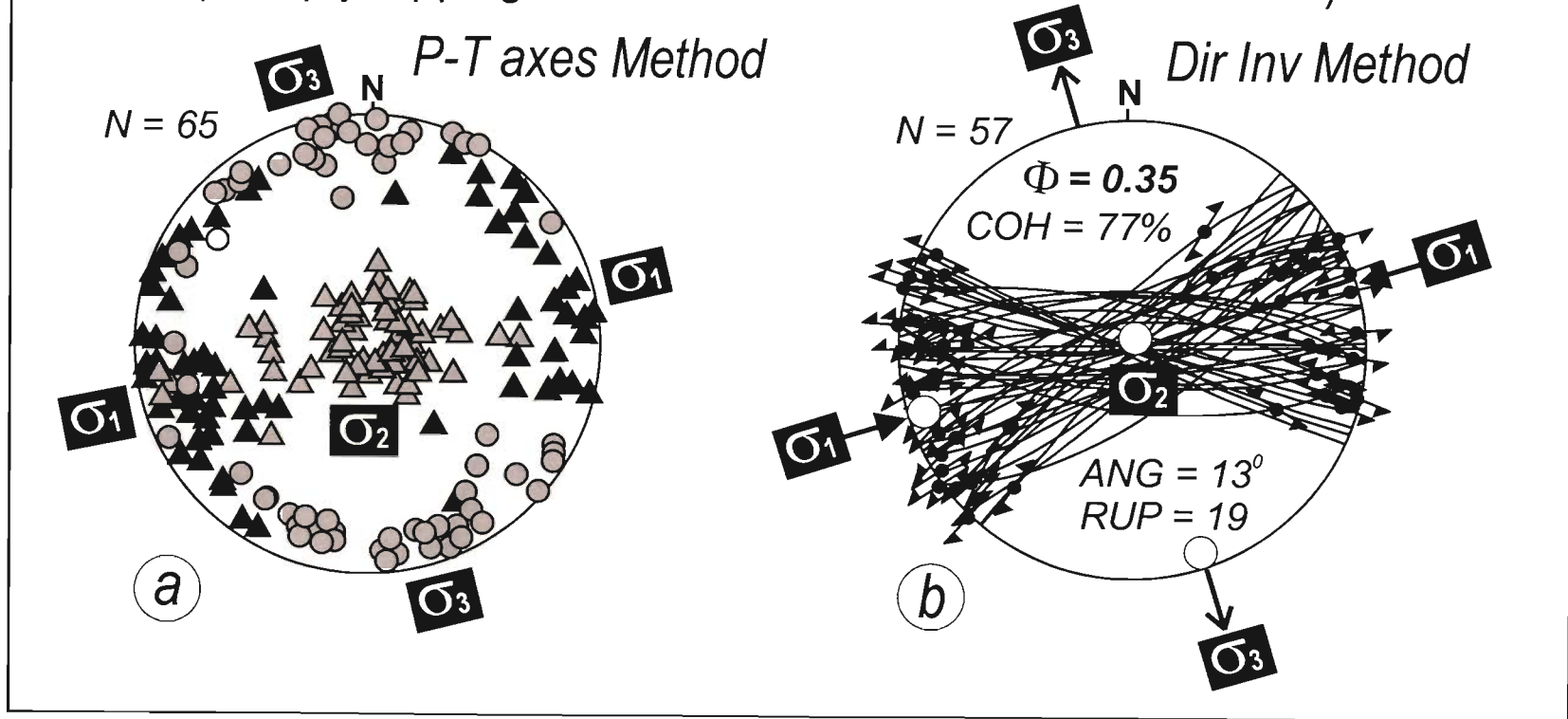
Fig. 4.8: Paleostress analyses of the second phase structures. (*a*) P-T axes method. Black triangle-σ_1; grey triangle-σ_2; and grey circle- σ_3. (*b*) Direct inversion method. Great circle- fault plane/shear zone; half arrows on dot- sense and direction of movement. White circles- principal stresses. See text for the definition of Φ, COH, RUP and ANG.

4.1.3 Third phase structures

Kink folds on E-W axes and thrust faults

The third phase structures are developed exclusively in those beds that are exposed in the vicinity of the Great Boundary Fault Zone. Whereas structures of the first and the second phase are abundant on both limbs of the Fort Syncline, those of the third phase are characteristically absent in the domains distant from the Great Boundary Fault Zone.

Although the kink folds of the third phase are also compressional in type and occur as conjugate pairs, these are distinct from the first phase kinks in the following respects. (i) Whereas the axes of the first phase kinks trend N-S, the axes of the third phase kinks trend E-W or ENE-WSW. (ii) The conjugate pairs of the first phase kinks imply top-to-the-east and top-to-the-west sense of relative movements, respectively. In contrast, the conjugate pairs of the third phase kinks imply top-to-the-north and top-to-the-south sense of relative movements, respectively. (iii) The first phase kinks are not directly associated with mesoscopic thrust faults. By contrast, the third phase kinks are almost always associated with the mesoscopic-scale thrust faults and their geometry is demonstrably controlled by the geometry of the thrust faults (Fig. 4.3a and b). Thin carbonate veins along such thrust surfaces trace the mesoscopic-scale flat and ramp and duplex structures, which occur in common association with the third phase kinks.

135

Independent Paleostress analyses of the kink folds and the thrust faults belonging to the third phase reveal that these two types of structures are dynamically compatible (Fig. 4.9). The stress configuration responsible for development of the third phase structures comprised a horizontal σ_1-axis trending NNW-SSE, a horizontal σ_2-axis trending ENE-WSW, and a vertical σ_3-axis. As the value of Φ for the third phase thrust faults is close to one ($\Phi = 0.88$), it can be inferred that the effective intermediate principal stress σ_2' was approximately equal to the effective maximum principal stress σ_1', and the state of stress approached axial extension ($\sigma_1' \approx \sigma_2' > 0$).

4.2 Mechanism of reactivation

It is well known that the pore-fluid pressure must exceed the lithostatic pressure for reactivation of a thrust or high angle normal fault and reverse fault into a reverse fault, provided friction co-efficient does not assume exceptionally low values (Sibson 1985; Boullier and Robert, 1992). That the condition of supralithostatic pore-fluid pressure, for reactivation of the Great Boundary Fault into a reverse fault, was satisfied during the first phase is evidenced by the occurrence of subhorizontal thrusts and flat veins in a tectonic setting of vertically directed minimum principal stress σ_3 Table 4.1.
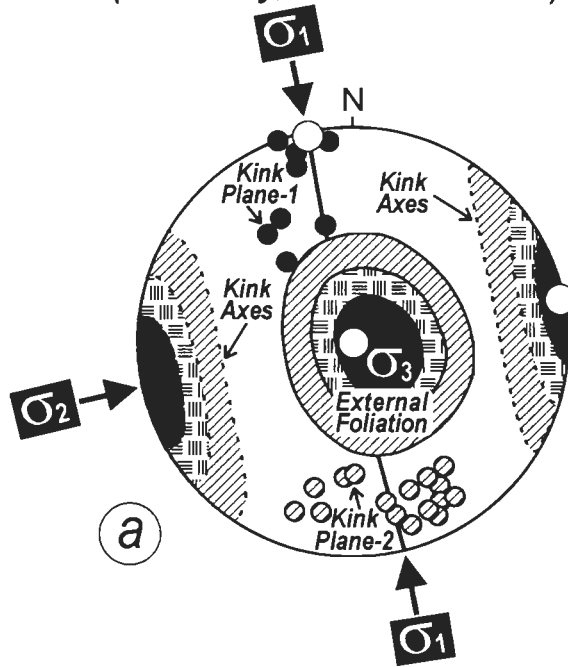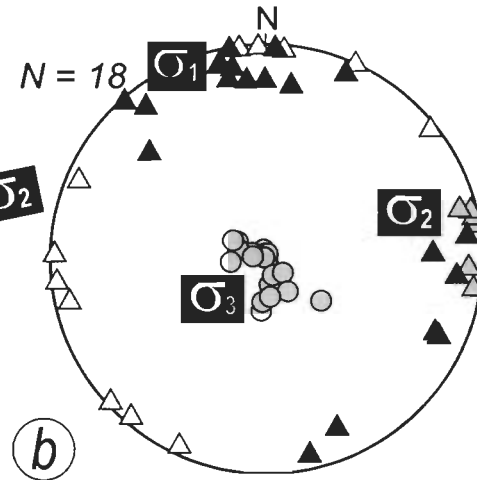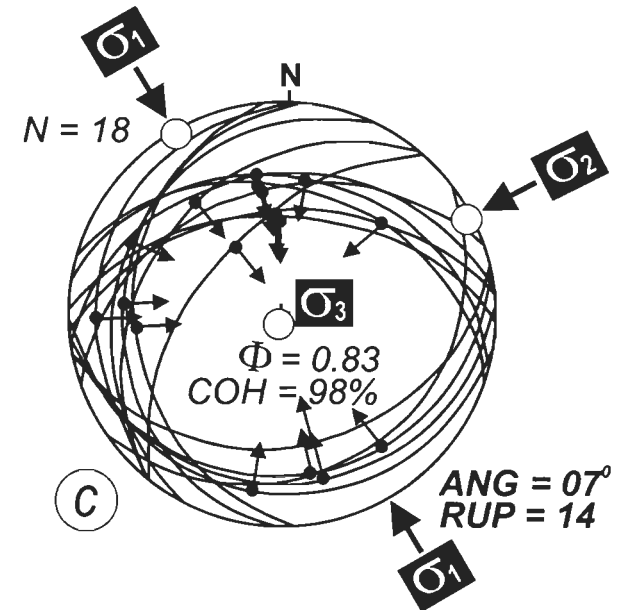
Fig. 4.5: Paleostress analyses of the third phase structures. (*a*) Kink plane-1 and kink plane-2 are complementary sets of conjugate pairs. Grey circles- poles to kink plane-1; N = 8. Hatched circles- poles to kink plane-2; N = 16 For externl foliation, N = 33 and Kamb contours at 5-10-15σ, σ = 1.18. For kink axes, N = 39 and Kamb contours at 6-12-18 σ, σ = 1.22. White circles- principal stresses. (*b*) and (*c*) Stress analyses of thrust faults. (*b*) P-T axes method; black triangle- σ_1- axis; grey triangle- σ_2 axis; grey circle- σ_3 axis. (*c*) Direct inversion method; great circle-fault plane; arrow on black dot- direction and sense of movement on the fault surface. White circles- principal stresses. See text for the definition of ϕ, COH, RUP and ANG.

Table 4.1: Summary of the results of paleostress analysis of different structures belonging to three phases. *Φ*– shape factor indicating relative amounts of principal stresses, *RUP, ANG and COH* are the indicators of the quality of solutions

Structure		Method	σ_1- axis	σ_2- axis	σ_3- axis	Φ	RUP	ANG	COH
First Phase	Kinks	Ramsay (1962)	265°/00°	178°/00°	subvertical	-	-	-	-
	Thrust	P-T Axes	270°/08°	180°/05°	subvertical	-	-	-	-
	Thrust	Dir Inv	260°/00°	170°/10°	352°/80°	0.48	20	06°	86%
Second Phase	Faults and shear-zones	P-T Axes	250°/10°	vertical	160°/10°	-	-	-	-
		Dir Inv	253°/04°	vertical	163°/04°	0.35	19	13°	77%
Third Phase	Kinks	Ramsay (1962)	348°/05°	078°/00°	vertical	-	-	-	-
	Thrust	P-T Axes	350°/10°	078°/03°	vertical	-	-	-	-
	Thrust	Dir Inv	334°/03°	064°/03°	195°/85°	0.83	14	07°	98%

Because of the total release of shear stress and sudden drop in the pore-fluid pressure during the post-seismic period of the first phase, the intermediate σ_2- and the minimum σ_3- principal stresses interchanged, and the thrust-type tectonic setting changed into a strike-slip type tectonic setting. This change in tectonic setting must have been facilitated by a low amount of differential stress and relatively high magnitudes of pore-

fluid pressure. Similar interpretations regarding reactivation due to swapping of stress axes during post seismic period have been put forward by Boullier and Robert (1992), Cox (1995) and Henderson and MacCaig (1996).

That the pore-fluid pressure was close to but less than the lithostatic pressure during the second event of the reactivation is indicated by the occurrence of numerous sub-vertical strike-slip faults and en-échelon veins of hybrid extensional-shear origin. This interpretation is consistent with the results of numerical modelling of Secor (1965) and Sibson (1996), who predict that strike-slip faulting in the earth's crust occurs at sublithostatic pore-fluid pressure conditions. Fluid inclusions in the second phase veins show a considerable range of homogenization temperature, which is due to variation in the fluid pressure during entrapment of syntectonic fluids. The presence of crack-seal microstructures in syntectonic veins and the fluctuation in pore-fluid pressure shown by fluid inclusion data substantiate that the dilatancy or seismic pumping, driven by stress cycling in response to seismic activity on the Great Boundary Fault, was the dominant mechanism of fluid flow within the Vindhyan sedimentary rocks (cf. Sibson, 1989; Grant et al., 1990; Massonet et. al., 1996).

During the third phase of seismic-slip on the Great Boundary Fault, the pore-fluid pressure again achieved supralithostatic values, the minimum principal stress (σ_3) changed from horizontal to vertical, and the maximum compressive stress (σ_1) switched from E-W/horizontal to N-S/horizontal orientation. Consequently, a renewed reverse movement occurred on the Great Boundary Fault and a new set of minor structures, namely, E-W trending thrusts and kink folds developed, concomitantly.

In summary, the successive events of reactivation, related to seismic-slips on the Great Boundary Fault, are regarded to control the fluid pressure fluctuation and stress cycling in the Vindhyan rocks. Each major event of seismic-slip on the Great Boundary Fault triggered the establishment of fluid pressure gradient, which resulted into rapid and focused flow of syntectonic fluids through high permeability channelways, namely, faults and fractures (Foster and Evans, 1991; Evans et. al., 1997; Cox, 1999). Post-seismic drop in fluid pressure resulted in decrease in solubility and deposition of silica and carbonate minerals within the fracture openings. With progressive decrease in the permeability of rupture zones, the fluid pressure increased to the levels of lithostatic or supralithostatic pressures and the conditions became favorable for the subsequent event of reactivation. The high temperatures preserved by the syntectonic fluid inclusions, the connate or formational water origin of the fluids, and the cm-m scale of permeability zones mean that the distance traveled by the syntectonic fluids was rather short and loss of temperature during the fluid migration was insignificant.

Summary: The structural style of the fault related deformation zone is, therefore, defined by large scale N-S trending upright non-plunging F_2 folds and three distinct sets of brittle faults. These three fault sets, developed during three successive phases of reactivation on the Great Boundary Fault, respectively are characterised by distinct paleostress conditions. Both first and third phase faults were developed due to vertically directed least compressive stress in thrust type of tectonic regimes. The second phase structures developed in a strike-slip setting with vertically directed intermediate principal stress.

Syntectonic fluid inclusions

Fluid inclusions, entrapped during deformation, represent important microscopic samples of syntectonic fluids. These fluid inclusions bear a great potential for constraining the physico-chemical conditions and pore-fluid evolution history of faulting (Srivastava and Engelder, 1990), and crustal exhumation history (Santosh et al. 2003). This chapter attempts at deciphering the pressure, temperature, paleogeothermal and pore-fluids conditions during the strike-slip movement on the Great Boundary Fault.

As described earlier, hybrid extensional-shear veins of quartz and calcite, formed during second phase of reactivation of the Great Boundary Fault, contain numerous fluid inclusions. Most of these fluid inclusions occur as transgranular arrays paralleling the cross-fold fractures, strike fractures and the two sets of the oblique fractures (Fig. 5.1a). Of the two phases present in all the fluid inclusions at the ambient temperature, the liquid phase and vapor phase occupy about 80-90% and 10-20% by volume, respectively (Figs. 5.1b and 5.2a and g). Microstructural studies show that these fluid inclusions are localized along the microfractures that eventually evolved as veins by crack-seal process (Ramsay, 1980; Roedder, 1984; Lespinasse and Pecher, 1986; Lespinasse, 1999)

5.1 Microthermometric experiments

More than 150 fluid inclusions, occurring in the doubly-polished wafers of 10 samples, were analyzed at Reynold's fluid inclusion stage- a modified version of the USGS gas flow type fluid inclusion stage. Microthermometric experiments are performed on the fluid inclusions within quartz infillings. Representative examples of important phase changes observed during the freezing-heating experiments are shown in Fig. 5.2a to j. As most of the fluid inclusions were small ($\leq$ 10-15μm), cycling technique was used extensively for detection of the phase changes. By mapping each chip of the doubly-polished wafers in detail, it was possible to perform both freezing and heating experiments on the same fluid inclusion in 104 cases. Though tedious, the approach yielded a paired set of freezing-heating data that are useful for making distinction between different populations of fluid inclusion and inferring the cause of scattering in the paired data set (Fig. 5.3a).

It was, however, not always possible to obtain a paired freezing-heating data on each and every fluid inclusion. For example, total homogenization could not be achieved due to leakage or decrepitation in some fluid inclusions during the heating experiments. Similarly, distinct phase changes could not be observed in very small ($\leq$ 4 μm) fluid inclusions during the freezing experiments. As the unpaired data cannot be plotted on a cartesian graph, these are grouped together with the paired data and represented on separate frequency histograms for each type of the phase change (Fig. 5.3b to f). Statistical means, or modes, although used routinely to represent temperatures of phase changes, are less reliable indicators of the fluid inclusion population than clusters on the
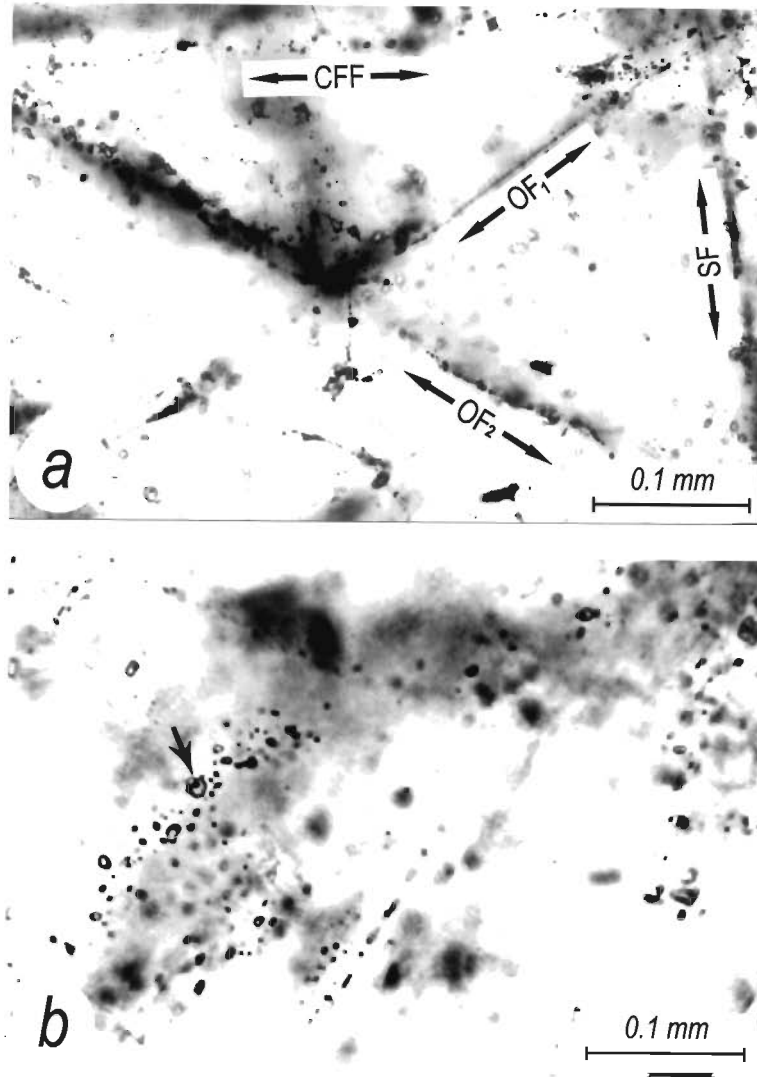
Fig. 5.1: Mode of occurrence of the fluid inclusions. (*a*) Four sets of secondary fluid inclusions occur in the transgranular arrays paralleling cross-fold (CFF), strike fractures (SF), oblique fractures of set-I (OF₁) and oblique fractures of set- II (OF₂). (*b*) Arrays of secondary fluid inclusions show the presence of liquid phase and vapor phase at the room conditions (marked by arrow).

26.8°C　　　　　　0.1 mm　　-62.5°C　　　　　　0.1 mm

a　　　　　　　　　　b

-48.0°C　　　　　　0.1 mm　　-31.0°C　　　　　　0.1 mm

c　　　　　　　　　　d

-20.8°C　　　　　　0.1 mm　　-19.7°C　　　　　　0.1 mm

e　　　　　　　　　　f
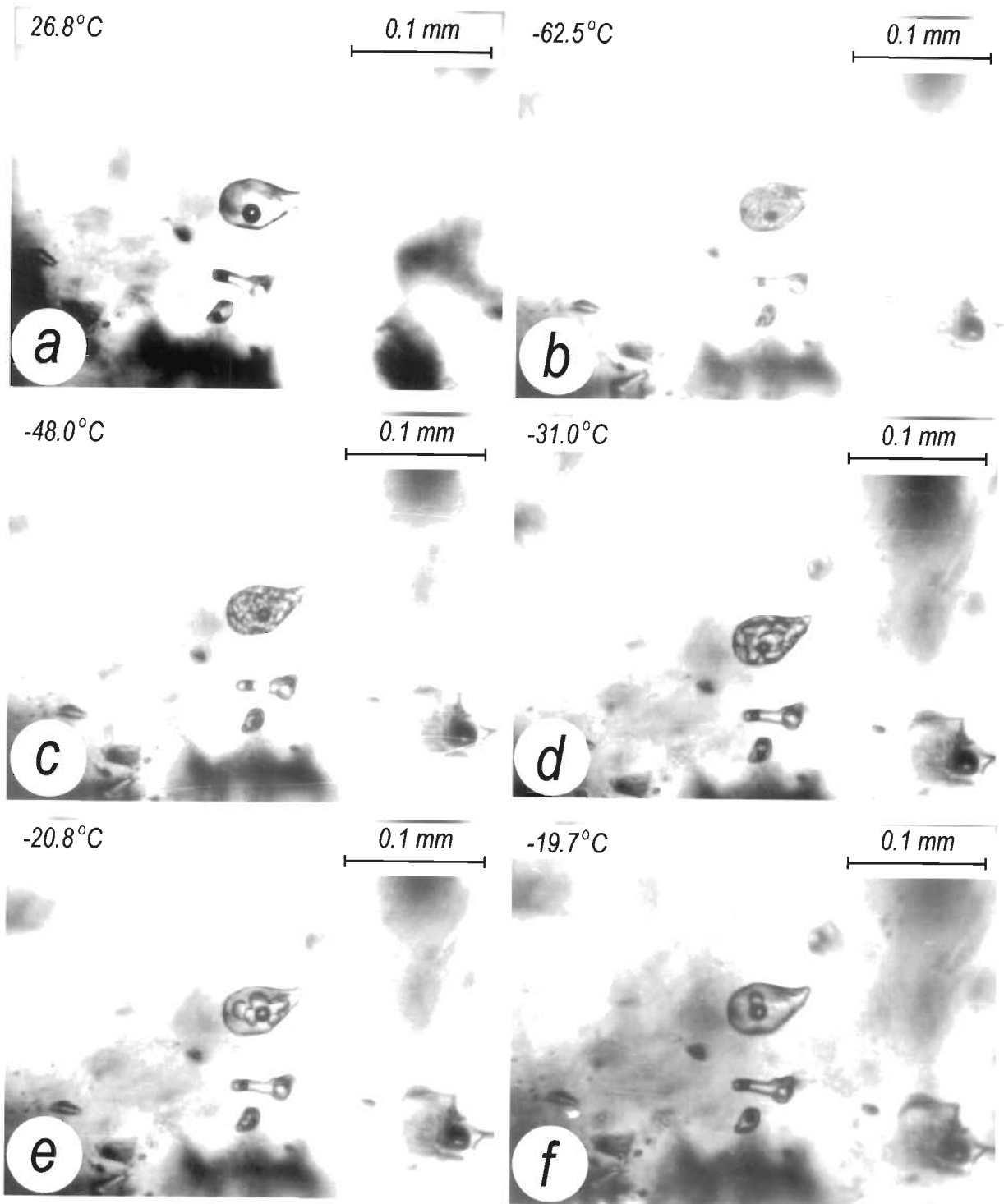
Fig. 5.2: *See captions on page 147.*

145
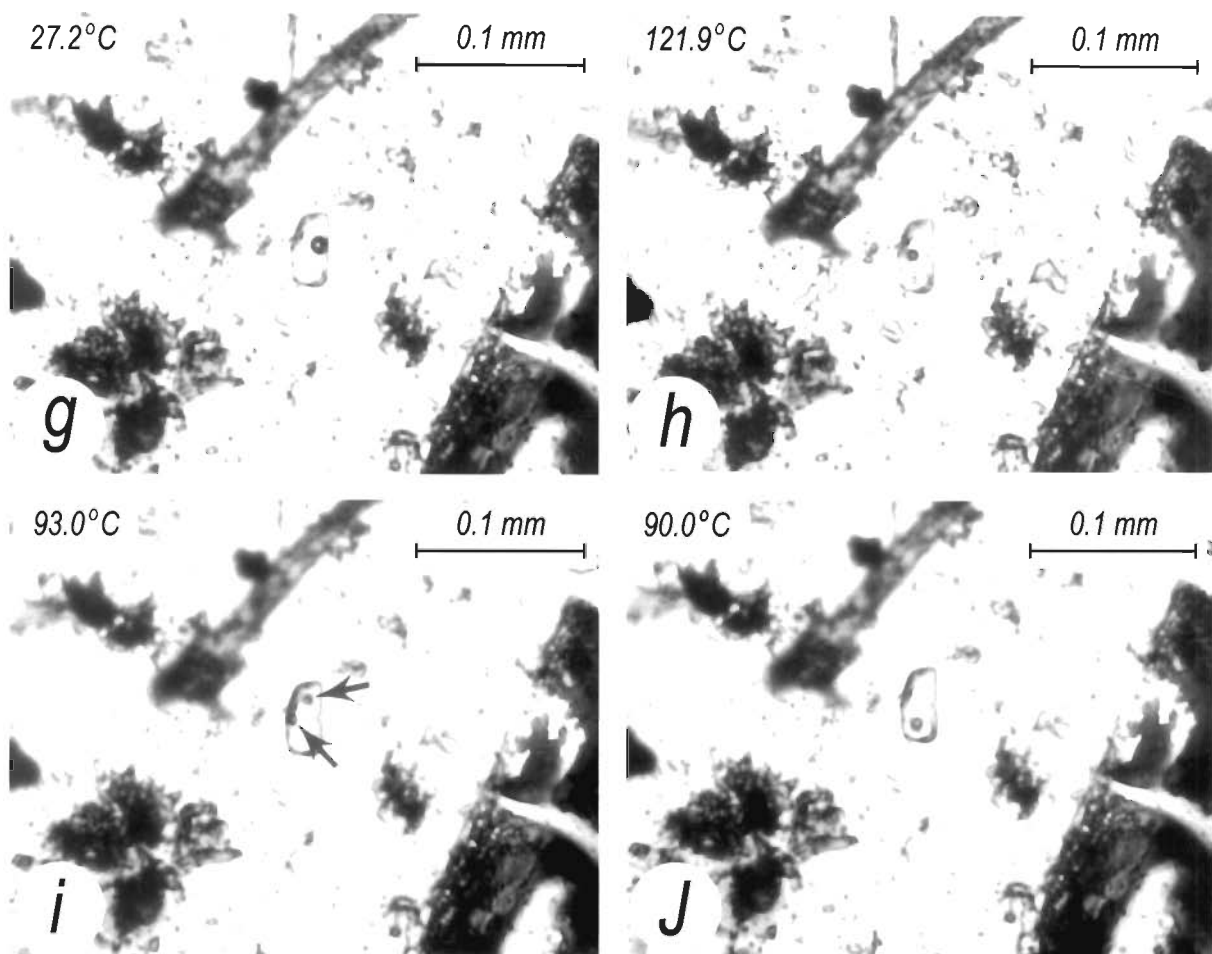
Fig. 5.2: (*a-f*) A typical sequence of phase changes during the freezing experiment. (*a*) A two phase fluid inclusion at room conditions. (*b*) The fluid inclusion shows pale-brown appearance, `mosaic texture` and the collapsed vapor bubble at -62.5^{0}C. (*c*) `Orange -peel texture indicating eutectic melting at a temperature close to -48^{0}C. Two types of solid phase; namely, fine grained euhedral hydrohalite and coarse grained rounded ice crystals, are observed at this stage. (*d*) Most of the hydrohalite crystals have melted at -31^0 C. (*e*) A few ice crystals which remain after the melting of all the hydrohalite crystals. Note that the inclusion is more clear, and the vapor bubble is bigger and more rounded as compared to the stage shown in (*d*). (*f*) The last cystal of ice is close to melting at -19.7^{0}C. (*g-j*) A typical sequence of phase changes during the heating runs. (*g*) A two-phase fluid inclusion at room conditions. (*h*) The vapor bubble is close to homogenization at 121.9^{0}C. (*i*) Two vapor bubbles, indicated by arrows, pop-up at 93^{0}C during the post-homogenization cooling. (*j*) The two popped-up vapor bubbles amalgamated into one bubble at 90^{0}C.

147
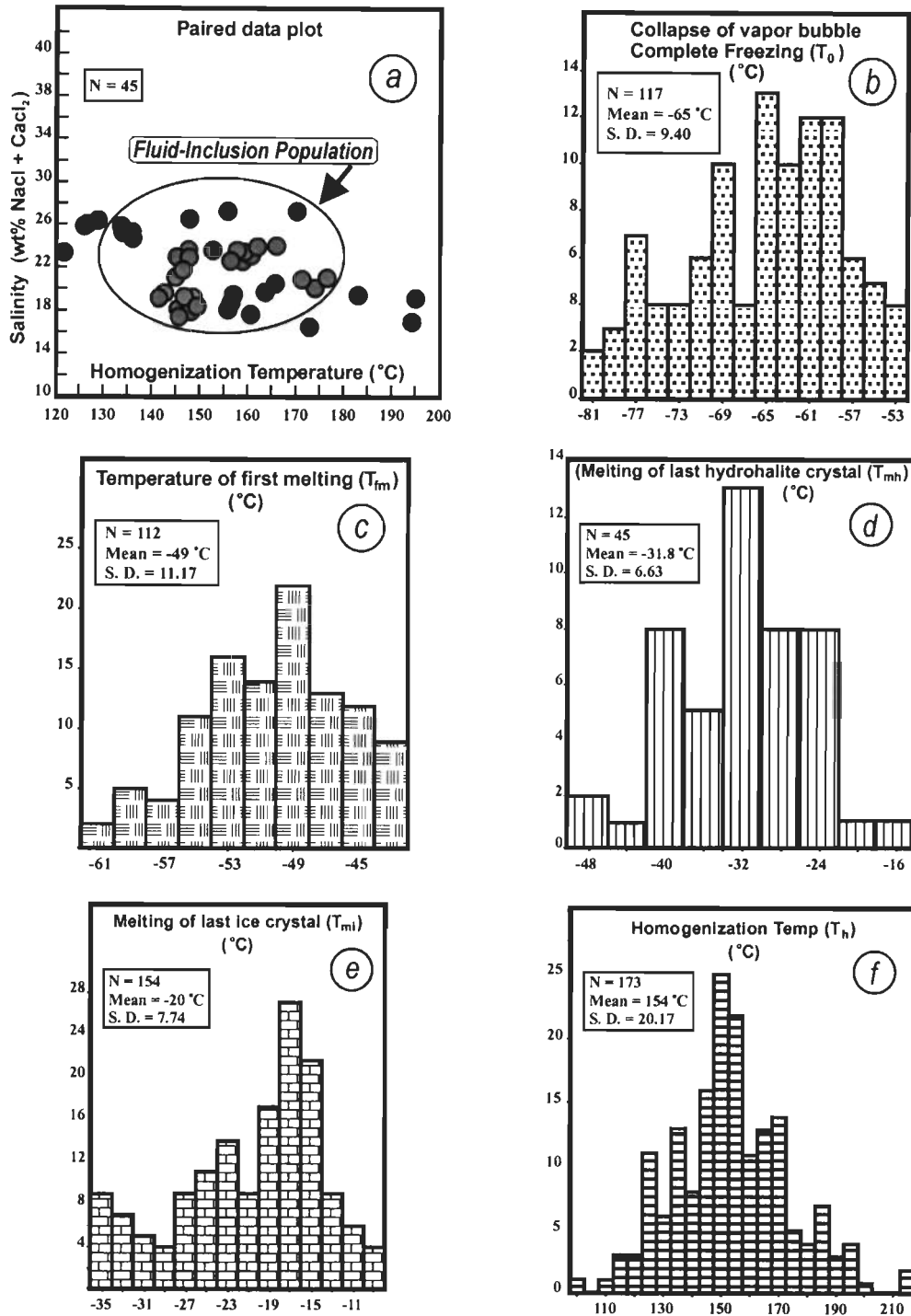
Fig. 5.3: (**a**) Paired plots between the salinity and homogenization temperature for the same fluid inclusion. these data are obtained from those fluid inclusions that show the melting of both the hydrohalite and the ice. The temperature population is encircled. (**b-e**) Histograms for the temperatures at which important phase changes occur during the freezing experiments. The temperature of collapse of vapor bubble (T_0) shown in (**b**) has no physico-chemical significance and the temperature of first melting (T_{fm}) shown in (**c**) is close to or slightly above the eutectic temperature (T_e). (**f**) Histogram for the temperature (T_h) at which the vapor phase homogenizes into liquid phase.

paired data plots. One limitation in considering the statistical mode is that the frequency of a particular class-interval may be spuriously high due to mixing of data from two or more populations. Furthermore, only one variable is taken into account in plotting a histogram. Besides being more reliable for distinction between different fluid inclusion populations, the paired data plots often display such patterns that are characteristic of the fluid evolution path (Goldstein and Reynolds, 1994).

5.1.1 Freezing experiments

Complete freezing of the inclusions was marked by the collapse of the vapor bubble with a sudden jerk at temperature T_0 (Fig. 5.3b). Upon slow and continued warming, the fluid inclusions turned pale-brown and showed a `mosaic texture` due to metastable reaction or solid state recrystallisation (Fig. 5.2b). This phenomenon occurred typically at a temperature which was, at least, 10°C lower than the eutectic temperature (Davis et al., 1990; Goldstein and Reynolds, 1994). With continued warming, the fluid inclusions showed an extremely granular or `orange-peel` texture signaling the commencement of melting of the solid phases (Fig. 5.2c). The temperature (T_{fm}) at which this texture is observed is close to or slightly above the eutectic temperature (T_e) which, in turn, is an indicative of the type of salts present within the brines. At this stage, most fluid inclusions contained a mixture of two types of solid-phases: (i) fine-grained and euhedral hydrohalite crystals, $NaCl. 2H_2O$, and (ii) coarse-grained and rounded ice crystals H_2O (Fig. 5.2c). A slight change in the shape of the vapor bubble with a sudden

150

jerk and an appreciable increase in the clarity of fluid inclusion marked the melting of the last crystal of hydrohalite at the temperature T_{mh}. The actual melting of the last hydrohalite crystal was, however, only rarely observed. Finally, ice was found to be the only solid-phase that remained in the fluid inclusion (Fig. 5.2d and e). The last crystal of ice was distinctly noticed in most of the fluid inclusions and its melting temperature T_{mi} could be recorded with an accuracy of $\pm 0.1^\circ$ C (Fig. 5.2f).

5.1.2 Heating experiments

During the gradual heating of the fluid inclusions, the vapor bubble progressively reduced in size and eventually got homogenized into liquid-phase at homogenization temperature T_h (Fig. 5.2g and h). No fluid inclusion was ever found to homogenize into vapor-phase. In order to minimize the effects of necking and stretching, homogenization temperatures were recorded only on those fluid inclusions that showed a consistent liquid/vapor ratio at room temperature. Subsequent to homogenization, the vapor bubble returned after several tens of degrees of cooling, and in some cases, the vapor bubble showed up only after a couple of days' cooling at the room temperature. In a few fluid inclusions, the vapor bubble returned in two small parts that amalgamated quickly to form a single bubble (Fig. 5.2i and j). All these phenomena are considered to indicate the metastable nature of the entrapped fluid. Table 5.1 gives a summary of the microthermometric observations and representative temperatures of the significant phase changes.

Table 5.1: Summary of the important observations during freezing-heating experiments. All the fluid inclusions are secondary, occur in transgranular arrays and contain two-phases (liquid/vapor) at room conditions.

Observation	Inference	No. of Observations	Temp. Range	Modal Temp.	Precision
Collapse of vapor bubble with sudden jerk.	Complete freezing of the fluid phase (T_0).	81	-52.0°C to -82°C	-65.0°C	± 0.5°C
'Orange-peel' texture (characteristic granular appearance).	Distinct melting at a few degrees above the eutectic temperature (T_e).	78	-42°C to -62°C	-49°C	+ 1.0°C
Sudden enhancement in the clarity of fluid inclusion/final melting of small euhedral grains.	Final melting of hydrohalite (T_{mh}).	45	-14°C to -50°C	-32°C	± 2.0°C
Melting of the last ice crystal.	Freezing point depression (T_{mi}).	114	-8°C to -36°C	-17.0°C	± 0.1°C
Disappearance of the vapor bubble.	Homogenization into liquid-phase (T_h).	173	87.5°C to 217.5°C	150°C	± 0.1°C

5.1.3 Fluid inclusion population

Final melting of both the solid phases, that is, hydrohalite and ice, could be detected during the freezing experiments on 45 inclusions. Using the *CalcicBrine*

152

program of Naden (1996), bulk salinities of these fluid inclusions are calculated and plotted against their respective homogenization temperatures (Fig. 5.3a). The paired plots of salinity versus homogenization-temperature as well as the histograms reveal that only one dominant population of the fluid inclusions is present in spite of the large scatters (cf. Fig. 5.3a and b to f). The scatter in salinity of fluids is within the standard deviation of the data (Fig. 5.3a). In addition, there is no geological line of evidence for chemical evolution of fluids with time. The cluster of data on the paired plot is in good agreement with the modal values of freezing point depression and homogenization temperature. As discussed later, the wide range of homogenization-temperature is due to fluid pressure variation during the entrapment, although the effects of thermal re-equilibration due to stretching and undetectable necking cannot be ruled out completely.

5.2 Nature of syntectonic fluid

Salinity, composition, density and isochores

As the first melting of solid phases in most of the fluid inclusions occurred around -49°C, it is evident that these fluid inclusions belong to $CaCl_2$-$NaCl$-H_2O system. Projections of modal values of melting temperatures of last crystals of the hydrohalite (T_{mh} = −31.8°C) and the ice (T_{mi} = -17°C) on the triangular graph, H_2O-$NaCl$-$CaCl_2$, reveal that the wt. ratio of salts, $NaCl$ / ($NaCl$ + $CaCl_2$), is 0.32 and the bulk salinity of the fluid is 19 wt% $NaCl$ + $CaCl_2$. (Oakes et al., 1990; Goldstein and Reynolds, 1994, p. 114). It is noteworthy that the values of salinity obtained by this graphical method

153

compare closely (± 0.2 wt.%) with those yielded by the program *CalcicBrine* of Naden (1996). Substitutions of the molalities of NaCl and CaCl₂ and the range of homogenization temperature (154 ± 20°C) in the equation given by Zhang and Frantz (1987) provide the density of the fluid as 0.9-1.0 gm/cm³, and the corresponding isochores.

Source of fluid

Highly saline, hot, dense and Ca-rich nature of the fluids implies that syntectonic brines are neither meteoric water, nor marine surface water, nor metamorphic water derived from dehydration of the Vindhyan sediments (Grant et al., 1990). The lack of acidic intrusives, either at local- or regional-scale, negates any possibility for magmatic origin of these fluids. The physico-chemical characteristics of the fluids are, however, consistent with connate or formational water origin. Several lines of geological evidence further support this interpretation. For example, without exception, the en-échelon veins in the sandstone beds are composed of quartz, whereas those in the limestone beds are composed of calcite. Strict lithological control on the composition of the vein-infillings, confinement of the veins within the individual beds and ubiquitous association of veins with pressure solution seams, all imply that the syntectonic fluids are the evolved connate water that were derived from the local and intraformational sources (Marquer and Burkhard, 1992).

Pressure-solution appears to be the dominant mechanism for generation of the mineralizing fluids in the host rocks. The drop in pressure due to fracturing results in

decrease in the solubility of silica and carbonates in the syntectonic brines (Srivastava and Engelder, 1991). Such a process must have been responsible for the precipitation of quartz and calcite in the fracture openings created during the brittle-ductile shearing.

5.3 Evidence for lithostatic pore-fluid pressure

The pore-fluid pressure conditions not only indicate the mechanism of fluid flow but also help constrain the trapping conditions from fluid inclusion data, particularly in situations where independent geothermometre or geobarometre are lacking. Since the fluid inclusion data reveal fluid pressure and not the rock pressure, it is crucial to ascertain whether the fluid pressure is due to hydrostatic or lithostatic load (Jenkin et al., 1994). The following lines of evidence suggest that the pore-fluid pressure achieved near-lithostatic to supralithostatic levels during the reactivation of the Great Boundary Fault. First, the compressional types tectonic settings, revealed by paleostress analyses of the structures of all the three phases, indicate that the pore-fluid pressures were close to lithostatic pressure (Figs. 4.4, 4.7 and 4.8; Table 4.1). Second, the local and formational water origin of the syntectonic fluids and small size of the closed system, point to lithostatic nature of pore-fluid pressure conditions. Third, occurrence of the impermeable shale beds at the tops and bottoms of both the Kaimur sandstone beds and the Nimbahera limestone beds, and the confinement of the entire sedimentary sequence by peripheral faults and the basement granite must have been conducive for building-up lithostatic pore-fluid pressure. Finally, the lack of fractures or faults connecting the polyphase

155

structures to the surface should rule out the possibility of hydrostatic pore-fluid pressure conditions.

5.4 Temperature and pressure of entrapment

Geothermal gradients in most sedimentary basins or diagenetic systems, vary between 20°C/km to 50°C/km (Mullis, 1979; Goldstein and Reynolds, 1994). If the average paleogeothermal gradient can be assumed as 35°C/km, it is then possible to construct a thermobaric gradient, 1.32°C/MPa, by using lithostatic geopressure gradient of 26.5 MPa/km. This thermobaric gradient intersects with the isochores at points, which define that the entrapment of syntectonic fluids occurred at 195-270°C temperature and 129-185 MPa pressure (Fig. 5.4a). An important implication of the trapping conditions, determined by this method, is the existence and denudation of 5-7 km thick column of overburden from the top of the Kaimur sandstone beds. Neither the occurrence of such a thick column of overburden is implied by any line of geologic evidence, nor the prevalence of large-scale vertical movement of the crust resulting into uplift of lithosphere, rather than lateral motion of the plates during the Proterozoic Era, is established beyond doubt. The trapping conditions, inferred by assuming a geothermal gradient of 35°C/km, are, therefore, unrealistic.

Geological cross-sections and available stratigraphic data imply that the maximum possible thickness of overburden above the Kaimur sandstone was approximately 2 km in the Chittaurgarh region (Prasad, 1984; Sinha-Roy et al., 1986b).

156
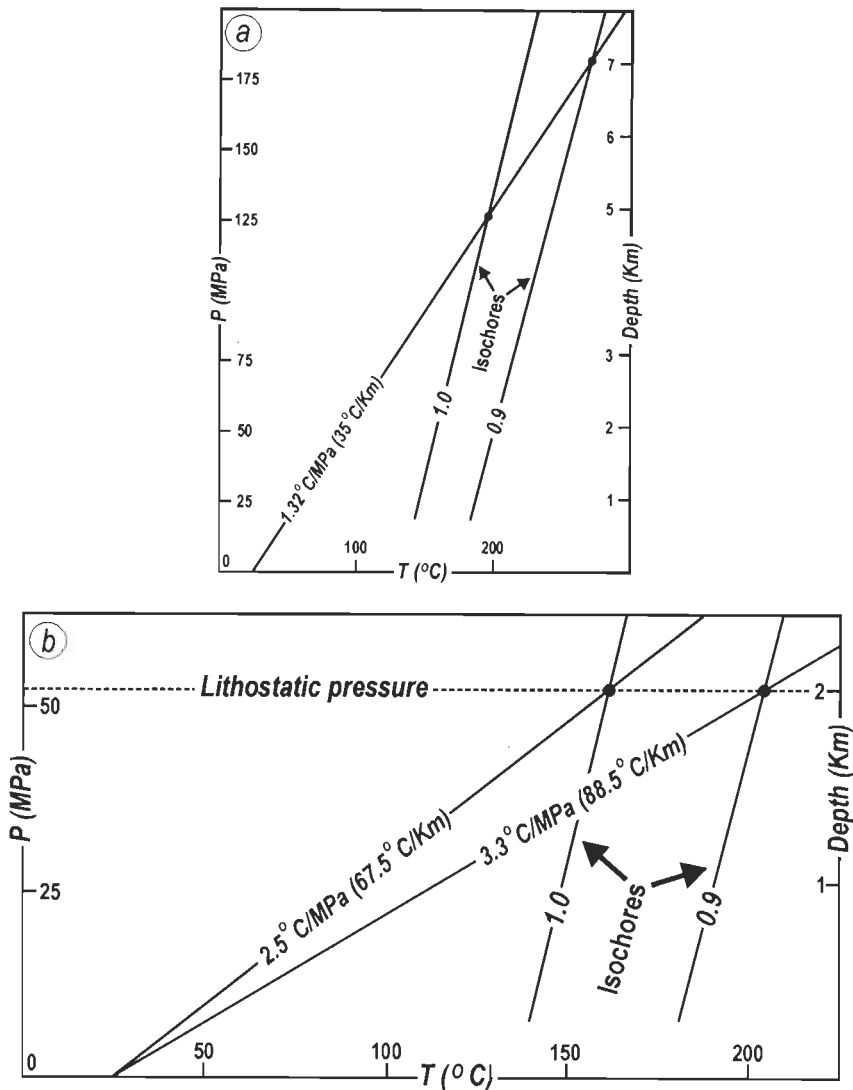
Fig. 5.4: (*a*) P-T plot displaying isochores of 0.9 gm/cm^3 and 1.0 gm/cm^3 densities corresponding to homogenization temperatures of 174^0 C and 134^0 C, respectively. These isochores would intersect the liquid-vapor curve at their respective homogenization tempertures (not shown in the figure). Thermobaric gradient is drawn for a geothermal gradient of 35^{0}C/Km and a geopressure gradient of 26.5 MPa/Km. The point of intersections of isochores with the thermobaric gradient constrain the lower and upper limits of the pressure and temperature of entrapment of the syntectonic fluid. (*b*) P-T plot displaying 53 MPa isobaric line for lithostatic pressure at 2 km depth, and isochores of 0.9 gm/cm^3 densities. The points of intersections of the isobaric line and isochores constrain P-T conditions for entrapment of the syntectonic fluid and imply paleogeothermal gradients of the order of 67.5-88.5^0 C/Km.

157

The intersection of the 53 MPa isobaric line, corresponding to lithostatic pressure at a depth of 2 km, and the iscohores suggest that the trapping temperature was 160-202°C. These trapping conditions reveal that the paleogeothermal gradient was of the order of 67.5-88.5°C/km, that is, (160-25)/2 to (202-25)/2 °C/km, where 25°C is the assumed surface temperature (Fig. 5.4b).

5.5 High paleogeothermal gradient

Homogenization temperature, regardless of the pressure correction, gives the minimum estimate of trapping temperature. Heating experiments on the fluid inclusions occurring in syntectonic veins yield a homogenization temperature of 154 ± 20°C, which is much higher than the temperature expected in sedimentary formation of about 2 km burial depth (Fig. 5.4). Such a condition is, however, not unique to the Vindhyan basin. Many recent studies on the Irish-type and Mississipi-Valley-type mineralization report the occurrence of anomalously high temperature fluid inclusions in the veins that are hosted by carbonate formations of shallow burial conditions (e. g., Kinsland, 1977; Friedman, 1987; Kontak and Sangster, 1995; Chi et al., 1998; Sangster et al., 1998). The occurrence of such a high temperature fluid inclusion population is commonly explained by anyone or some combination of the following three factors. (i) Post-entrapment changes in the fluid inclusions (Roedder, 1984; Goldstein and Reynolds, 1994), (ii) mixing of formational fluids with high temperature fluids derived from locally anomalous

heat sources, and (iii) entrapment of fluid inclusions in the geologic and tectonic settings of elevated geothermal gradients (Hitzman, 1995).

In this study, the effects of post-entrapment changes have been minimized by taking two precautions during the heating experiments. First, by analyzing the fluid inclusions exclusively in quartz, which is relatively less susceptible to thermal stretching than the carbonate minerals. Second, by restricting the measurement of homogenization temperatures on only those groups of fluid inclusions that show consistent liquid/vapor ratios. Existence of local heat sources is excluded by the geologic history of the area, and mixing of the connate fluid with the hot fluid of younger generation is not supported by any line of geologic evidence. By elimination, the elevated geothermal gradient is the main cause for the entrapment of high temperature fluid inclusions during the development of syntectonic veins within the Vindhyan basin.

Fluid inclusion data obtained in this study indicate a paleogeothermal gradient of about 67.5-88.5°C/km, which is ascribed to the continental rift type of tectonic setting of the Vindhyan basin and the Proterozoic age of the rifting process. Recent geophysical and geological studies confirm that the geological history of the Vindhyan basin begins with thinning of continental crust by stretching, rifting and basal volcanism during the Proterozoic Era (Mishra et al., 1996, Ram et al., 1996, Raza and Casshyap, 1996). It is due to higher concentration of radio isotopes, and more rapid and vigorous mantle convections during the Proterozoic Era that the paleogeothermal gradients in the Proterozoic rift terrains would have been much more elevated than the present day geothermal gradients of 30-40°C/km in the active continental rift terrains (Bridwell and Potzick, 1981).

Summary: The fluid inclusion study on quartz veins indicates that the syntectonic fluids were highly dense, Na-Ca-Cl brines of formational water origin. Interpretation of fluid inclusion data together with overburden thickness further imply that the reactivation of second phase of Great Boundary Fault occurred at relatively low depth (< 2km), temperatures of around 160-202° C and pressure of about 53 Mpa. These conditions point to high paleogeothermal gradients in the Vindhyan basin at the time of strike-slip reactivation of the Great Boundary Fault.

Discussions

6.1 Nature of deformation

As described earlier, the Great Boundary Fault runs close to the Vindhyan basin margin, and it cuts through the sandstone, the shale and the limestone beds occurring at various stratigraphic levels. The fault rocks within the Great Boundary Fault Zone, show both brittle and ductile nature of deformation, which is evidenced by intense fracturing, brecciation, veining and the development of cataclasite and mylonite in the different rock types. The nature of dominant deformation, in terms of the type of fault rocks, and characteristic structures in different rock types and the protoliths, arranged in the stratigraphic order, are given in the Table 6.1.

Table 6.1: Summary of nature of deformation in different rock types in the study area.

Rock type	Tectonic setting	Deformation
Kaimur sandstone	Fault related deformation zone	Folded into km scale F_2 folds. Mesoscopic scale kink-bands, fractures, striated faults and brittle-ductile shear zones are common.

Suket shale	Fault related deformation zone	Folded into km scale F_2 folds. Multiple sets of fractures.
Nimbahera limestone	Fault related deformation zone	Folded into km scale F_2 folds. Kink-bands, subhorizontal thrust, fractures and brittle-ductile shear zones containing en-échelon carbonate veins are common.
Nimbahera shale	Great Boundary Fault Zone	Three phases of successive (F_1 to F_2) folding at the mesoscopic scale. cm-dm scale ductile shear zones contain mylonitised quartz veins. Multiple sets of fractures are common.
Binota shale	Great Boundary Fault Zone	Scanty exposures show kink folding on steeply plunging axes.
Sawa shale-porcellanite	Great Boundary Fault Zone	Superposed folding is common. Intense fracturing, veining cataclasis,and mylonitisation are more pronounced in the relatively competent porcellanite beds.
Sawa sandstone	Great Boundary Fault Zone	Intense brecciation and development of cataclasite and mylonite.

Many deep seated faults are characterised by ductile deformation in depth and brittle deformation at the shallow crustal levels. Sibson (1977) suggests that the brittle-ductile transition zone occurs, in general, at 10-15 km depth. Ductile faulting and brittle faulting below and above the brittle-ductile transition zone results into the development of distinctive fault rocks, such as mylonite and breccia, respectively. Ramsay (1980) and Ramsay and Huber (1987, p. 617) show that the ductile shearing in the basement rocks can progressively change into brittle-ductile shearing and brittle faulting in the overlying cover rocks.

It is evident from Table 6.1 that different types of fault rocks, viz., mylonite, cataclasite and breccia are developed within the Great Boundary Fault Zone. The possibility that the mylonite represents a deeper section of the Great Boundary Fault is ruled out on the following two grounds. First, some of the older stratigraphic units, such as the Sawa sandstone beds show development of breccia/cataclasite, and relatively

younger stratigraphic units, such as Nimbahera shale beds show discrete, but well developed ductile shear zones containing mylonitised quartz veins. Second, the Great Boundary Fault is essentially a steeply dipping structure and there is no evidence of its folding that may expose the deeper part of the fault containing mylonite in some areas and shallower part containing breccia in the other areas.

The diversity in nature of fault rocks along the Great Boundary Fault is due to two factors. First, the nature of fault rocks is controlled by the relative competence of the protolith, the availability of fluids and the presence or lack of suitable conditions for crystal plastic deformation and recrystallisation. Second, the deformation occurred essentially in a brittle-ductile regime. For example, in the Berach river section, the incompetent Nimbahera shale beds, caught up within the Great Boundary Fault Zone, show well developed mylonite foliation within the mesoscopic ductile shear zones. These ductile shear zones were initiated due to the local circulation of pore-fluids and stress gradients, making suitable conditions for the crystal plastic deformation and recrystallisation of quartz veins in the Nimbahera shale beds. In the Lalji ka Khera and Bassi sections, where the Great Boundary Fault Zone contains both competent and incompetent beds, viz., Sawa sandstone-shale-porcellanite beds. In these sections, the fault rocks show a progressive development of breccia-cataclasite and mylonite, particularly in the relatively competent Sawa sandstone beds and the quartz veins cutting through the porcellanite beds.

In many fault zones, the processes leading to the development of fault rocks, such as breccia, cataclasite and mylonite has been shown to operate transiently or synchronously in brittle-ductile transition zone (Hadizadeh et al. 1991; Stewart et al.

2000). In this study, microstructural evidence show that the brittle fracturing and brecciation acts as a precursor to the mylonitisation (Guermani and Pennacchioni, 1998), and the cataclasite and mylonite formed in the alternate cycles- a feature suggesting that the fault rocks were developed in the brittle-ductile transition zone (Takagi et al., 2000). The interpretation that the fault rocks within the Great Boundary Fault Zone were developed in a low temperature regime is substantiated by the following lines of evidence: (i) Stratigraphic evidence implies that the overburden thickness above the rocks exposed in the fault zone was less than 3 km (Prasad, 1984), (ii) microscopic studies show that the deformation in the fault rocks is accommodated by microfractures, quartz filled veins, pressure solution seams, subgrains, serrated grain boundary and core and mantle texture and, (iii) lack of any appreciable metamorphism in the Vindhyan rocks in the Great Boundary Fault Zone, or, in fault related deformation zone, or, outside these two zones.

6.2 Evolution of the Great Boundary Fault

Existing opinions on the origin and age of the Great Boundary Fault are summarized in Table 6.2. Most of the studies assign the age of the Great Boundary Fault with respect to the age of the Vindhyan Supergroup, which ranges from 1400 to 600 Ma (Venkatachala et al. 1996).

Table 6.2: An outline of the existing opinions on the evolution and age of the Great Boundary Fault (modified after Verma, 1996).

Author(s)	Opinion
Medlicott (1868)	A feature of very ancient date.
Fermor (1930)	A pre-Vindhyan fault that reactivated during and after Vindhyan sedimentation.
Heron (1953)	Evolved with the uplift of the Aravalli range in Mesozoic Era (205-65 Ma).
Pascoe (1959)	Evolved as a result of earth movements, which gave rise to folding in the Aravalli Group and the Delhi Group of rocks (ca. 2000-1450 Ma, Roy, 1988)
Iqbaluddin et al. (1978)	Initiated as a normal fault along a pre-Vindhyan grain and acquired a reverse geometry during the Vindhyan sedimentation due to folding of the fault plane in Paleozoic Era (570 Ma).
Banerjee and Sinha (1981)	A zone of tectonic weakness that existed since the Aravalli Period (ca. 2000 Ma). The fault is related to horst and graben structures. It is developed during and after the deposition of the Vindhyan sediments.
Prasad (1981; 1984)	A post-Vindhyan fault, which marks a lineament after a fundamental grain comprising zone of fractures. It has been active since the end of the Vindhyan sedimentation (ca. 600). This fault truncates the various formations and structural trends in the Vindhyan sedimentary rocks.
Sinha-Roy et al. (1986a)	Related to indentation tectonics caused by impingement of the Bundelkhand massif with the Vindhyan cover rocks. This impingement is a result of crustal deformation in the Indian plate after its collision with the Asian plate (ca. 60 Ma).
Verma (1996)	A pre-Vindhyan fault that initiated as a normal fault ca. 2500 Ma, and acquired a reverse geometry during Delhi orogeny ca. 1400 Ma.
Choudhuri and Guha (2004)	A post-Vindhyan fault that originated as a thrust in brittle-ductile regime and reactivated as a normal fault.

The proponent of one school hypothesize that the Great Boundary Fault acts as reverse fault near the surface or at shallow depth, and gradually changes into a normal fault at depth (Iqbaluddin et al. 1978 and Ramasamy, 1995). This change in nature of faulting with depth has been ascribed to the change in the direction of dip of the Great Boundary Fault due to folding triggered by the hydroplastic behaviour of the basement and the Vindhyan sedimentary rocks in the peripheral part of the basin (Fig. 6.1).
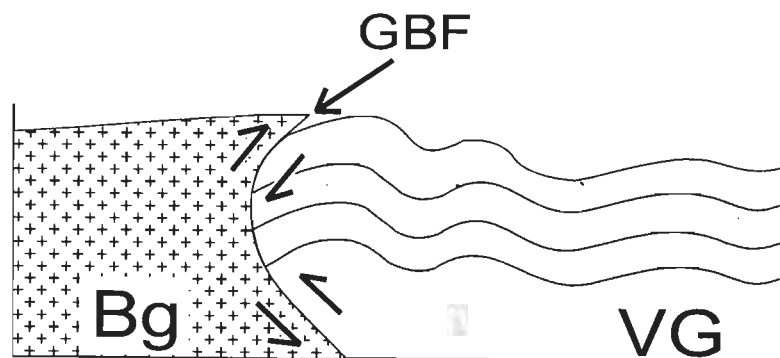
Fig. 6.1: Model showing evolution of the Great Boundary Fault (after, Ramasamy, 1996). Bg- Berach granite; VG- Vindhyan Supergroup.

This model also argues that the intense deformation of the Vindhyan rocks, along the basin margin near the Great Boundary Fault, is due to centrifugal nature of stresses radiating from the central portion of the Vindhyan basin. Following are the main limitations of this model: (i) the recent seismic reflection and magnetotelluric studies do not reveal any change in dip direction or folding of the Great Boundary Fault, (Tiwari, 1995; Gokarn, 1995), (ii) the reason for the change in dip direction of the Great Boundary Fault from depth to surface is not known, (iii) the model does not account for different types of fault rocks occurring within the Great Boundary Fault Zone and, (iv) the concept

of centrifugal forces fails to explain the deformation in some of the central parts of the basin.

Present investigations around Chittaurgarh, reveal that the Great Boundary Fault is a probably syn to post-Vindhyan structure, and it records an early event of ductile shearing, which is overprinted by, at least, three successive events of brittle reactivation. Whereas the event of ductile shearing is related to the initiation of the Great Boundary Fault, the development of fractures and striated faults is related to the successive phases of reactivation. It is difficult to establish the exact nature and sense of movement on the Great Boundary Fault during its initiation, because the stretching lineation/striations on the ductile shear zones and the microscopic shear sense indicators have been rotated during the successive phases of folding. However, the fact that the ductile shear zones contain well developed mylonite, which is a typical fault rock that commonly develops in a thrust tectonic setting, indicates that the Great Boundary Fault initiated as a thrust/reverse fault. It was during this initiation pf the Great Boundary Fault that the basement granite was brought up to rest over the younger Vindhyan rocks, now occurring on the footwall side of the Great Boundary Fault.

Several contributions imply that the Great Boundary fault is a reactivated structure (Table 6.2; Fermor, 1930; Verma, 1996; Choudhuri and Guha 2004). This study shows that, at least, three different phases of brittle reactivation occurred on the Great Boundary Fault during its long tectonic history. Each of these reactivation phases, is characterised by a unique stress regime, i. e., thrust type, strike-slip type and thrust type during the first, second and third phase of reactivation, respectively.

Fluid inclusion analyses on strike-slip veins reveal that the syntectonic fluids were essentially highly dense Na-Ca-Cl brines of intraformational origin. Interpretation of fluid inclusion data, together with estimates of the thickness of overburden above the

Kaimur sandstone beds, not only support the inference that the reactivation occurred at shallow depth but also argue in favour of a high paleogeothermal gradient in the Vindhyan basin during the evolution of the Great Boundary Fault. The condition of high paleogeothermal gradient is attributed to the continental rifting during the Proterozoic Era, and the occurrence of additional heat sources in the Vindhyan basin, for example, basal and intermittent volcanism (Chakraborty et al. 1996) and high heat-producing basement granite (Hand and Sandiford, 1999).

The age of initiation and reactivation on the Great Boundary Fault is difficult to constrain due to lack of reliable geochronological data for a large part of the Vindhyan section. The available age data open to criticism and the debate on the age of Vindhyan rocks has responded recently (Ray et al., 2002) . Despite these limitations, the possible ages of the deformational events along the Great Boundary Fault are inferred on the basis of the stratigraphic portions of the beds containing different phases of structures and available age data. These inferences are admittedly tentative.

The development of structures related to the initiation of the Great Boundary Fault is confined only to the Lower Vindhyan Group of rocks (1400-1140 Ma, Venkatachala et al. 1996) and there is no development of these structures in the Upper Vindhyan Group of rocks (< 900 Ma). The Great Boundary Fault, therefore, must have initiated after the deposition of the Lower Vindhyan Group of rocks but before the deposition of the Upper Vindhyan rocks i. e., 1400-900 Ma. Although the first and the second phase brittle structures are developed abundantly in the Kaimur sandstone beds exposed around the Chittaurgarh area, these structures are not observed in the Lower Bhander Group rocks exposed in Satur area (Fig. 2.1). The first and second events of reactivation on the Great Boundary Fault can, therefore, be inferred to have occurred between 900 and 750 Ma, which are probable ages of the Kaimur Group and the Bhander

Group, respectively (Venkatachala et al., 1996; Ray et al. 2002). As the Lower Bhander Group is also the youngest stratigraphic horizon bearing the imprints of the third phase brittle structures, the third event of reactivation must be younger than 750 Ma probably post-Vindhyan in age. The upper limit for the age of the third event is difficult to ascertain due to lack of geochronological data for a substantial section of the Vindhyan sequence. Although it is possible that the Great Boundary Fault is presently active due to movements in the Himalayan orogenic belt (Valdiya, 1998), there is no evidence to suggest that its development is related to the collision between the Indian and the Asian plates (Sinha-Roy et al. 1986a). A summary of the different groups of mesoscopic structures, developed during successive phases of reactivation on the Great Boundary Fault, along with their possible respective ages, are given in Table 6.3.

Table 6.3: Summary of the structural features, kinematics and age associated with the Great Boundary Fault.

Structures			Kinematics	Tentative age of deformation
Reactivation events	Third phase	Thrust related Kink-bands, and subhorizontal thrust	Brittle thrusting. Top-to-the-north and top-to-the south.	Younger than 750 Ma
	Second phase	Fractures, brittle-ductile shear zones containing en-échelon vein and subvertical faults	Brittle strike-slip faulting. Top to the east and top-to-the west.	900-750 Ma
	First phase	Kink-bands and low angle fault	Brittle thrusting. Top-to-the east and top-to-the west.	900-750 Ma

Initiation of the Great Boundary Fault	Fracture, veins breccia cataclasite ductile shear zones, mylonite, and successive groups of folds	Ductile thrusting. Probably top-to-the southeast.	Probably older than 900 Ma

6.3 Fault related folding

F_2 folds are most dominantly developed both at the mesoscopic and macroscopic scales, in the Vindhyan sedimentary rocks outcropping close to the Great Boundary Fault. As demonstrated by Sinha-Roy et al. (1986b) these folds have a genetic link with the development of the Great Boundary Fault both because the intensity and tightness of F_2 folding progressively increases towards the Great Boundary Fault.

This study shows that the F_2 folds were developed as a series of N-S trending open upright anticlines and synclines during the first phase of reactivation on the Great Boundary Fault. The original orientation and geometry including a characteristic orthorhombic symmetry of the F_2 folds is retained in the fault related deformation zone. This thesis negates the interpretation that the Great Boundary Fault athwart to the F_2 axial trace (Prasad, 1981; Choudhuri and Guha; 2004). In fact, it is due to clockwise rotation that these folds assume a NNE to NE trending geometry, monoclinic to triclinic symmetry and, a greater degree of tightness within the Great Boundary Fault Zone. The rotation of the F_2 folds from the fault related deformation zone to Great Boundary Fault Zone is a consequence of large scale dextral strike-slip movement, which relates to the second phase of the brittle reactivation (Fig. 6.2).
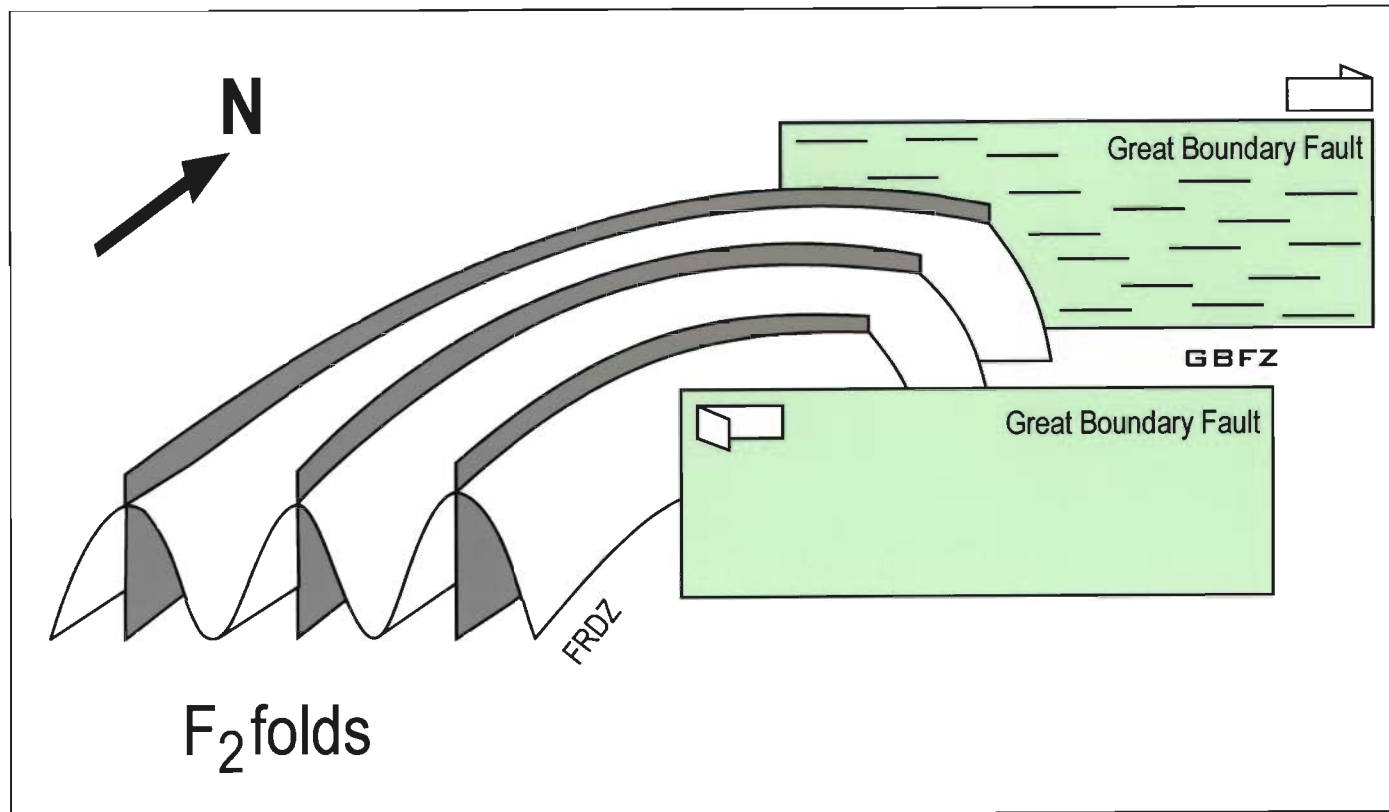
Fig. 6.2: Schematic model showing rotation of large scale N-S trending F_2 folds in the fault related deformation zone (FRDZ) to NE trending folds in the Great Boundary Fault Zone (GBFZ) due to dextral strike-slip movement during the second phase of reactivation.

Conclusions

The Great Boundary Fault in the northwestern India is a large scale tectonic lineament with well developed fault zone and fault related deformation zone. The relative thickness of the fault zone and fault related deformation zone vary in different segments of the Great Boundary Fault depending upon the relative competence of the rocks caught up within these fault zone. The development of these two types of zones is invariably confined to the Vindhyan sedimentary rocks occurring on the footwall side. The Berach granite occurring as basement on the hangingwall side does not bear any significant signatures of Great Boundary Fault related deformation. In the study area around Chittaurgarh, the fault zone varies in thickness from a few tens of metres to hundreds of metres, and the thickness of the fault related deformation zone is of the order of several km.

Three generations of successively developed folds F_1, F_2 and F_3 are common within the fault zone, particularly in those sections, where incompetent shale beds constitute a considerable part of the fault zone. Although the orientation and style of folding varies from one section of the fault zone to another, the predominance of F_2 folding and the development of the type-2 interference patterns are the most outstanding structural characteristics of the Great Boundary Fault Zone. The fault zone is also

characterised by the development of different types of fault rocks, namely, breccia, cataclasite and mylonite. Microstructural studies showing a cyclic development of cataclasite and mylonite indicate that the Great Boundary Fault developed in a brittle-ductile transition zone.

The fault related deformation zone is characterised by the large scale F_2 folding, faulting and fracturing at the mesoscopic scale. No distinctive fault rock occurs within the fault related deformation zone nor, there is any evidence of ductile shearing, nor F_1 or F_3 folding. In contrast to the Great Boundary Fault Zone, where F_2 folds are characteristically NNE to NE trending, the F_2 folds in the fault related deformation zone are N-S trending.

The development of ductile shear zones and different types of fault rocks, and F_1 folding are related to the initiation of the Great Boundary Fault, probably in a thrust regime under supralithosatic conditions. The subsequent structures are related to the reactivation events on the Great Boundary Fault. The first event of reactivation resulted into development of F_2 folds and low angle thrust due to E-W oriented maximum compression and vertically directed minimum compression.

Due to release of total shear stress and drop in pore-fluid pressure, the second event of reactivation occurred as a major strike-slip movement on the Great Boundary Fault. During this phase of reactivation, abundant mesoscopic scale structures, namely, the conjugate sets of brittle-ductile shear zones, the en-échelon veins, the striated faults and the fractures were developed in the Vindhyan rocks. There is distinct increase in the intensity of strike-slip faulting within the fault zone as compared to that in the fault related deformation zone. The N-S trending F_2 folds in the fault related deformation zone

rotate to NNE or NE because of a major dextral strike-slip movement during the second phase of reactivation.

Fluid inclusion studies on the veins in the strike-slip faults suggest that the syntectonic fluids were high density, high salinity brines of local formational water origin. The results of fluid inclusion analysis along with available estimates of overburden thickness also point a high paleogeothermal gradient of the order of 67.5°-88.5° C/km during the reactivation on the Great Boundary Fault. The third phase of reactivation occurred in a thrust regime in N-S oriented maximum compression, during which the striated thrust faults and kink folds developed abundantly.

In summary, amongst the four groups of mesoscopic scale structures, the earliest group records the initiation of the Great Boundary Fault in brittle-ductile transitional zone. The later three groups correspond to successive phases of reactivation of the Great Boundary Fault in brittle regime. Available stratigraphic and geochronological data suggest that the initiation of the Great Boundary Fault occurred between 1400-900 Ma. The first and the second phase of reactivation occurred probably between 900-750 Ma. Although the third phase of reactivation is younger than 750 Ma, its upper age limit is difficult to constrain due to lack of relevant geochronological data.

Angelier, J., 1990. Inversion of field data in fault tectonics to obtain the regional stress. III. A new rapid direct inversion method by analytical means. Geophysical Journal International 103, 363-376.

Angelier, J., 1994. Fault slip analysis and paleostress reconstruction. In: Hancock, P. L. (ed.), Continental Deformation, Pergamon Press, Oxford, 53-100.

Arlegui, L., Simon, J. L., 1998. Reliability of paleostress analysis from faults striations in near multidirectional extension stress field. Example from the Ebro basin, Spain. Journal of structural Geology 20, 827-840.

Banerjee, A. K., Singh, M. H. J., 1981. Palaeogeography and sedimentation of Vindhyans in eastern Rajasthan. In: Proceedings of the Symposium on Vindhyans of Central India. Geological Survey of India, Miscellaneous publication 50, 89-94.

Banerjee, A. K., Sinha, P. N., 1981. Structure and Tectonics of Vindhyans in Eastern Rajasthan. In: Proceedings of the Symposium on Vindhyans of Central India. Geological Survey of India, Miscellaneous publication 50, 41-47.

Bobyarchick, A. R., 1998. Evolving concepts in tectonics and the interpretive history of the Brevard Fault Zone. Geological Society of America Abstract with Programs 30, 4.

Bose, U., Sharma, A. K., 1992. The volcano-sedimentary association of the Precambrian Hindoli sipracrustals in southeastern Rajasthan. Journal Geological Society of India 40, 359-369.

Boullier, A. M., Robert, F., 1992. Palaeoseismic events recorded in Archaean gold-quartz vein networks, Val d'Or, Abitibi, Quebec, Canada. Journal of Structural Geology 14, 161-179.

Bridwell, R. J., Potzick, C., 1981. Thermal regimes, mantle diapirs and crustal stresses of continental rifts. Tectonophysics 73, 15-32.

Chakraborty, P. P., Banerjee, C., Das, N. G., Sarkar, S., Bose, P. K., 1996. Volcaniclastics and their sedimentological bearing in Proterozoic Kaimur and Rewa Groups in central India. In: Bhattacharyya, A. (ed.) Recent advances in Vindhyan geology. Memoir Geological Society of India 36, 59-75.

Chi, G., Kontak D. J., Williams-Jones, A. E., 1998. Fluid composition and thermal regime during Zn-Pb mineralisation in the Lower Windsor Group. Nova Scotia, Canada. Economic Geology 93, 883-895.

Choudhury, S. K., Dutta, A. N., 1975. Crustal thickness in north India and Himalayan region and its geological significance. Geophysical Research Bulletin 13, 29-37.

Choudhuri, A. R., Guha, D. B., 2004. Evolution of the Great Boundary fault: a re-evaluation. Journal Geological Society of India 64, 21-31.

Cox, S. F., 1995. Faulting processes at high fluid pressures: an example of fault valve behavior from the Wattle Gully Fault, Victoria, Australia. Journal of Geophysical Research 100 (B7), 12841-12859.

Cox, S. F., 1999. Deformational controls on the dynamics of fluid flow in mesothermal gold systems. In: McCafrey, K. J. W., Lonergan, L and Wilkinson, J. J. (eds.),

Fractures, fluid flow and Mineralisation. Geological Society, London, Special Publications, 155, 123-140.

Davis, D. W., Lowenstein, T. K., Spencer, R. J., 1990. Melting behavior of fluid inclusions in laboratory-grown halite crystals in the systems NaCl-H_2O, NaCl-KCl-H_2O, NaCl-$MgCl_2$-H_2O and NaCl-$CaCl_2$-H_2O. Geochimica et Cosmochimica Acta 54, 591-601.

Doblas, M., 1998. Slickenside kinematic indicators. Tectonophysics 295, 187-197.

Dubey, A. K., Cobbold, P. R., 1977. Non-cylindrical, flexural slip folds in nature and experiment. Tectonophysics 38, 223-239.

Dune, W. M., Hancock, P. L., 1994. Palaeostress analysis of small scale brittle structures. In: Hancock, P. L. (ed.), Continental Deformation, Pergamon Press, Oxford, 101-120.

Etchecopar, A., Vasseur, G., Daignieres, M., 1981. An inverse problem for the determination of stress tensors from fault striation analysis. Journal of Structural Geology 3, 51-65.

Evans, J. P., Forster, C. B., Goddard, J. V., 1997. Permeability of fault-related rocks, and implications for hydraulic structure of fault zones. Journal of Structural Geology 19, 1393-1404.

Fermor, L. L., 1930. On the age of Aravalli Range. Record, Geological Survey of India 62, 391-409.

Forster, C. B., Evans, J. P., 1991. Hydrogeology of thrust and crystalline thrust sheets: results of combined field and modeling studies. Geophysical Research Letter 18, 979-982.

Friedman, G. M., 1987. Deep-burial diagenesis: its implication for vertical movements of crust, uplift of the lithosphere and isostatic unroofing- a review. Sedimentary Geology 50, 67-94.

Ghosh, S. K., Ramberg, H., 1968. Buckling experiments on intersecting fold patterns. Tectonophysics 5, 89-105.

Ghosh, S. K., Chatterjee, A., 1985. Patterns of deformed early lineations over later folds formed by buckling and flattening. Journal of Structural Geology 7, 651-666.

Gokarn, S. G., Rao, C. K., Singh, B. P., 1995. Crustal structure in southeast Rajasthan using Magnetotelluric techniques. In: Sinha-Roy, S., Gupta, K. R. (eds.), Continental crust of northwestern India. Memoir Geological Society of India 31, 373-381.

Goldstein, R. H., Reynolds, T. J., 1994. Systematics of fluid inclusions in diagenetic minerals. SEPM short course 31, Society of Sedimentary Petrology, Oklahoma, USA, 198 pp.

Grant, N. T., Banks, D. A., McCaig, A. M., Yardley, B. W. D., 1990. Chemistry, source and behavior of fluids involved in Alpine thrusting of the Central Pyrenees. Journal of Geophysical Research 95 (B6), 9123-9131.

Greenly, E., 1919. The geology of Anglesey. Great Britain Geological Survey Memoir 1, 980p.

Groshong, R. H., 1988. Low-temperature deformation mechanisms and their interpretation. Geological Society of America Bulletin 100, 1329-1360.

Guermani, A., Pennacchioni, G., 1998. Brittle precursors of plastic deformation in a granite: an example from the Mont Blanc massif (Helvetic, western Alps). Journal of Structural Geology 20, 135-148.

Gupta, B. C., 1934. The geology of central Mewar. Memoir Geological Survey of India 65, 107-168.

Gupta, S. N., Arora, Y. K., Mathur, R. K., Iqballuddin, Prasad, B., Sahai, T. N., Sharma, S. B., 1981. Lithostratigraphic map of Aravalli region, south-eastern Rajasthan and northern Gujarat. Geological Survey India, Hyderabad.

Hacket, C. A., 1877. Note on Aravalli series in northeastern Rajputana. Records Geological Survey of India 10.

Hacket, C. A., 1881. On the geology of Aravalli region, central and eastern. Records Geological Survey of India 14, 279-303.

Hadizadeh, J., Babaie, H. A., Babaei, A., 1991. Development of interlaced mylonites, cataclasites and breccias: example from the Towaliga fault, south central Appalachians.

Hand, M., Sandiford, M., 1999. Intraplate deformation in central Australia, the link between subsidence and fault reactivation. Teconophysics 305, 121-140.

Henderson, I. H. C., McCaig, A. M., 1996. Fluid pressure and salinity variations in shear zone-related veins, central Pyrenees, France: implications for the fault-valve model. Tectonophysics 262, 321-348.

Heron, A. M, 1917. Synopsis of pre-Vindhyan Geology of Rajputana. Trans. Nat. Inst. Sci. India 2, 17-33.

Heron, A. M., 1936. The geology of southeastern Mewar, Rajputana. Memoir Geological Survey of India 68, 1-120.

Heron, A. M., 1953. The Geology of central Rajputana. Memoir Geological Survey of India 79.

Hills, E. S., 1956. A contribution to the morphotectonics of Australia. Journal Geological Society of Australia 3, 1-15.

Hitzman, M. W., 1995. Mineralization in the Irish Zn-Pb-(Ba-Ag) orefield. Society of Economic Geologists. Guide Book Series 21, 25-61.

Hobbs, B. E., Means, W. D., Williams, P. F., 1976. An outline of Structural Geology. John Wiley & Sons, Inc. New York.

Holdsworth, R. E., Butler, C. A., Roberts, A. M., 1997. The recognition of reactivation during continental deformation. Journal of the Geological Society, London 154, 73-78.

Iqbaluddin, Prasad, B., Sharma, S. B., Mathur, R. K., Gupta, S. N., Sahai, T. N., 1978. Genesis of the Great Boundary Fault of Rajasthan, India. Proceedings of the Third Regional Conference on Geology and Mineral Resources of South-East Asia, Bangkok, 145-149.

Jenkin, G. R. T., Craw, D., Fallick, A. E., 1994. Stable isotopic and fluid inclusion evidence for meteoric fluid penetration into an active mountain belt; Alpine Schist, New Zealand. Journal of Metamorphic Geology 12, 429-444.

Kale, A. S., Phansalkar, V. G., 1985. Sedimentological investigations of the Vindhyan rocks of Taraj area, Jhalawar district, Rajasthan. Journal of Indian Association of Sedimentalogist 5, 34-46.

Kinsland, G. L., 1977. Formation temperature of fluorite in the Lockport Dolomite in Upper New York State as indicated by fluid inclusion studies- with discussion of heat sources. Economic Geology 72, 849-854.

Kontak, D. J., Sangster, D. F., 1995. Aqueous and liquid petroleum inclusions in barite from the Walton deposit, Nova Scotia: a Carboniferous, carbonate-hosted Ba-Pb-Zn-Cu-Ag deposit. Economic Geology 93, 845-868.

Lespinasse, M., 1999. Are fluid inclusion planes useful in structural geology. Journal of Structural Geology 21, 1237-1243.

Lespinasse, M., Pecher, A., 1986. Microfracturing and regional stress field: a study of the preferred orientation of fluid-inclusion planes in a granite from the Massif Central, France. Journal of Structural Geology 8, 169-180.

Lisle, R. J., 1987. Principal stress orientations from faults: an additional constraints. Annales. Tectonicae 1, 155-158.

Lisle, R. J., Styles, P., Freeth, S. J., 1990. Fold interference structures: the influence of layer competence contrast. Tectonophysics 172, 197-200.

Lister, G. S., Snoke, A. W., 1984. S-C mylonites. Journal of structural Geology 6, 617-638.

Macinnes, E. A., Alsop, G. I., Oliver, G. J. H., 2000. Contrasting modes of reactivation in the Outer Hebrides Fault Zone, northern Barra Scotland. Journal of the Geological Society, London 157, 1009-1017.

Marquer, D., Burkhard, M., 1992. Fluid circulation, progressive deformation and mass-transfer processes in the upper crust: the example of basement-cover relationships in the External Crystalline Massifs, Switzerland. Journal of Structural Geology 14, 1047-1057.

Massonnet, D., Thatcher, W., Vadon, H., 1996. Detection of postseismic fault-zone collapse following the Landers earthquake. Nature 382, 612-616.

Means, W. D., Li, T., 2001. A laboratory simulation of fibrous veins: some first observation. Journal of Structural Geology 23, 857-863.

Medlicott, H. B., 1868. The boundary of Vindhyan series in Rajputana. Record, Geological Survey India 1, 69-72.

Mishra, D. C., Gupta, S. B., Vyaghreswara, R., Venkatrayudu, M., 1996. Crustal structure and basement tectonics under Vindhyan basin: Gravity-Magnetic study. Memoir Geological Society of India 36, 213-224.

Mullis, J., 1979. The system methane-water as a geologic thermometer and barometer from the external part of the central Alps. Bulletin de Mineralogie 102, 526-536.

Naden, J., 1996. CalcicBrine 1.5: a Microsoft Excel 5.0 Add-in for calculating salinities from microthermometric data in the system $NaCl-CaCl_2-H_2O$. *PACROFI VI*, University of Wisconsin (abs).

Newman, J., Mitra, G., 1993. Lateral variations in mylonite zone thickness as influenced by fluid-rock interaction, Linville Fall fault, North Carolina. Journal of Structural Geology 15, 849-863.

Nickelsen, R. P., 1986. Cleavage duplexes in the Marcellus shale of the Appalachian foreland. Journal of Structural Geology 8, 361-371.

Oakes, C. S., Bodnar, R. J., Simonson, J. M., 1990. The system $NaCl-CaCl_2-H_2O$. I. The ice liquidus at 1 atm total pressure, Geochimica et Cosmochimica Acta 54, 603-610.

Orife, T, Arlegui, L., Lisle, R. J., 2002. A QuickBasic stress inversion program for analysing, sets of faults without slip lineations. Computers and geosciences 28, 775-781.

Orife, T., Lisle, R. J., 2003. Numerical processing of palaeostress results. Journal of Structural Geology 25, 949-957.

Passchier, C. W., Trouw, R. A. J., 1998. Microtectonics. Springer-Verlag Berlin Heidelberg.

Pascoe, E. H., 1959. A Manual of Geology of India and Burma II, Govt. of India Press, Calcutta.

Pascoe, E. H., 1968. A manual of the geology of India and Burma II, reprint, 1st Geological Survey of India publicaiton.

Petit, J. P., 1987. Criteria for the sense of movement on fault surfaces in brittle rocks. Journal of Structural Geology 9, 597-608.

Prasad, B., 1981. A review of the Vindhyan Supergroup in southeastern Rajasthan. In: Proceedings of the Symposium on Vindhyans of Central India. Geological Survey of India, Miscellaneous publication 50, 31-40.

Prasad, B., 1984. Geology, sedimentation and paleogeography of the Vindhyan Supergroup, south-eastern Rajasthan. Memoir Geological Survey of India 116, 1-107.

Prasad, B., 1987. Geochemistry and petrogenesis of Berach granite, Rajasthan, India. Indian Mineral 41, 1-23.

Ragan, D. M., 1985. Structural Geology: An Introduction to Geometrical Techniques. 3rd edition. John Wiley & Sons, New York.

Ram, J., Shukla, S. N., Pramanik, A. G., Varma, B. K., Chandra, G., Murthy, M. S. N., 1996. Recent investigations in the Vindhyan basin: implications for the basin tectonics. In: Bhattacharyya, A. (ed.) Recent advances in Vindhyan geology. Memoir Geological Society of India 36, 267-286.

Ramasamy, SM., 1995. Lineament analysis and stress modeling of Vindhyan basin, Rajasthan, India. In: Sinha-Roy, S., Gupta, K. R. (eds.), Continental crust of northwestern India. Memoir Geological Society of India 31, 279-310.

Ramsay, J. G., 1962. Geometry of conjugate fold systems. Geological Magazine 99, 516-526.

Ramsay, J. G., 1967. Folding and fracturing of rocks. McGraw Hill, New York. 568p.

Ramsay, J. G., 1980. The crack-seal mechanism of rock deformation. Nature 284, 135-139.

Ramsay, J. G., 1980. Shear zone geometry: a review. Journal of structural Geology 2, 83-99.

Raja Rao, C. S., Poddar, B. C., Basu, K. K., Dutta, A. K., 1971. Precambrian stratigraphy of Rajasthan: a review. Record Geological Survey of India 101, 60-79.

Ramsay, J. G., Huber, M. I., 1987. The techniques of modern structural geology: folds and fracture, 2. Academic press, London.

Ray, J. S., Martin, M. W., Veizer, J., Bowring, S. A., 2002. U-Pb zircon dating and Sr isotope systematics of the Vindhyan Supergroup, India. Geology 30, 131-134.

Raymond, L. A., 1984. Classification of mélanges. In: Mélanges: Their nature, origin and significance. Geological Society of America, Special Paper 198, 7–20.

Raza, M., Casshyap, S. M., 1996. A Tectono-Sedimentary model of evolution of middle Proterozoic Vindhyan basin. In: Bhattacharyya, A. (ed.) Recent advances in Vindhyan geology. Memoir Geological Society of India 36, 287-300.

Reddy, P. R., Prasad, B. R., Rao, V. V., Khare, P., Rao, G. K., Murty, A. S. N., Sarkar, D., Raju, S., Rao, G. S. P., Sridher, V., 1995. Deep seismic reflection profiling along Nandsi-Kunjer section of Nagaur-Jhalawar transect: preliminary results. In: Sinha-Roy, S., Gupta, K. R. (eds.), Continental crust of northwestern India. Memoir Geological Society of India 31, 353-372.

Roedder, E., 1984. Fluid inclusions. Mineralogical Society of America. Reviews in mineralogy 12.

Rowley, D. B., 1996. Age of initiation of collision between India and Asia: a review of the stratigraphic data. Earth Planetary Science letters 145, 1-13.

Roy, A. B., 1988. Stratigraphic and tectonic framework of the Aravalli Mountain Range. In: Roy, A. B., (ed.), Precambrian of the Aravalli mountain Rajasthan, India. Memoir Geological Society of India 7, 3-31.

Sahay, A., Srivastava, D. C., 2005. Hourglass structure: an evidence of buckle folding. Journal of the Geological Society of India (*in press*).

Sangster, D. F., Savard, M. M., Kontak, D. J., 1998. A genetic model for mineralisation of Lower-Windsor (Visean) carbonate rocks of Nova Scotia, Canada. Economic Geology 93, 932-952.

Santosh, M., Tagawa, M., Tagichi, S., Yoshikara, S., 2003. The Nagercoil granulite block, southern India: petrology, fluid inclusions and exhumation history. Journal Asian Earth Sciences 22, 131-155.

Secor, D. T., 1965. Role of fluid pressure in jointing. American Journal of Science 263, 633-646.

Sharma, R. S., Roy, A. B., 1986. Evolution of Precambrian lithosphere, western India. The Indian Lithosphere, 1-14.

Sibson, R. H., 1977. Fault rocks and fault mechanisms. Journal of the Geological Society, London 133, 191-213.

Sibson, R. H., 1985. A note on fault reactivation. Journal of Structural Geology 7, 751-754.

Sibson, R. H., 1989. Earthquake faulting as a structural process. Journal of Structural Geology 11, 1-14.

Sibson, R. H., 1996. Structural permeability of fluid-driven fault-fracture meshes. Journal of Structural Geology 18, 1031-1042.

Sibson, R. H., Robert, F., Poulsen, K. H., 1988. High-angle reverse faults, fluid-pressure cycling, and mesothermal gold-quartz deposits. Geology 16, 551-555.

Simpson, C., Whitmeyer, S. J., De Paor, D. G., Gromet, P., Miro, R., Krol, M. A., Short, H., 2001. Sequential ductile to brittle reactivation of major fault zones along the accretionary margin of Gondwana in Central Argentina. In: Holdsworth, R. E., Strachan, R. A., Magloughlin, J. F., Knipe, R. J., (eds), The nature and tectonic significance of fault zone weakening. Geological Society, London, special publications 186, 233-255.

Sinha-Roy, S., 1986a. Himalayan collision and indentation of Aravalli orogen by Bundelkhand wedge: implications for neotectonics in Rajasthan. International symposium on neotectonics in south Asia, Dehradun, Feb. 18-21, 1986.

Sinha-Roy, S., Kirmani, I. R., Reddy, B. V. R., Sahu, R. L., Patel, S. N., 1986b. Fold pattern in the Vindhyan sequence in relation to Great Boundary Fault: example from Chittaurgarh area, Rajasthan. Quaternary Journal of Geological Mining and Metallurgical Society of India 58, 241-251.

Sinha-Roy, S., Malhotra, G., Guha, D. B., 1995. A transect across Rajasthan Precambrian terrain in relation to geology, tectonics and crustal evolution of south-central Rajasthan. In: Sinha-Roy, S., Gupta, K. R. (eds.), Continental crust of northwestern India. Memoir Geological Society of India 31, 63-89.

Sinha-Roy, S., Malhotra, G., Mohanty, M., 1998. Geology of Rajasthan. Geological Society of India, Banglore.

Srivastava, D. C., Engelder, T., 1990. Crack-propagation sequence and pore-fluid conditions during fault-bend folding in the Appalachian Valley and Ridge, central Pennsylvania. Geological Society of America Bulletin 102, 116-128.

Srivastava, D. C., Engelder, T., 1991. Fluid evolution history of brittle-ductile shear zones on the hanging wall of Yellow Spring thrust, Valley and Ridge Province, Pennsylvania, U.S. A. Tectonophysics 198, 23-34.

Srivastava, D. C., Lisle, R. J., Vandycke, S., 1995. Shear zones as a new type of plaeostress indicator. Journal of Structural Geology 17, 663-676.

Stewart, M., Holdsworth, R. E., Strachan, R. A., 2000. Deformation processes and weakening mechanisms within the frictional-viscous transition zone of major crustal-scale faults: insights from the Great Glen Fault Zone, Scotland. Journal of Structural Geology 22, 543-560.

Takagi, H., Goto, K., Shigematsu, N., 2000. Ultramylonite bands from cataclasite and pseudotachylyte in granites, northeast Japan. Journal of Structural Geology 22, 1325-1339.

Tandon, K., Lorenzo, J. M., O`Brien, G. W., 2000. Effective elastic thickness of the northern Australian continental lithosphere subducting beneath the Banda orogen (Indonesia): inelastic failure at the start of continental subduction. Tectonpophysics 329, 39-60.

Tiwari, S., 1995. Extension of the Great Boundary Fault (GBF) of Rajasthan in the Ganga Valley. In: Sinha-Roy, S., Gupta, K. R. (eds.), Continental crust of northwestern India. Memoir Geological Society of India 31, 311-328.

Turner, F. J., 1953. Nature of dynamic interpretation of deformation lamellae in calcite of three marbles. American Journal of Science 251, 276-298.

Valdiya, K. S., 1998. The Aravalli-Himalaya connection. In: Paliwal, B. S. (ed.), The Indian Precambrian. Scientific publishers (India), 118-127.

Vandycke, S., Bergerat, F., 2001. Brittle tectonic structures and palaeostress analysis in the Isle of Wight, Wessex basin, southern U. K. Journal of Structural Geology 23, 393-406.

Vandycke, S., 2002. Palaeostress records in Cretaceous formations in NW Europe: extensional and strike-slip events in relationships with Cretaceous-Tertiary inversion tectonics. Tectonophysics 357, 119-136.

Venkatachala, B. S., Sharma, M., Shukla, M., 1996. Age and life of the Vindhyans-facts and conjectures. In: Bhattacharyya, A. (ed.) Recent advances in Vindhyan geology. Memoir Geological Society of India 36, 397-165.

Verma, P. K., Greiling, R. O., 1995. Tectonic evolution of the Aravalli orogen (NW India): an inverted Proterozic rift basin. Geol Rundsch 84, 683-696.

Verma, P. K., 1996. Evolution and age of the Great Boundary Fault of Rajasthan. Memoir Geological Society of India 36, 197-212.

Zhang, Y., Frantz, J. D., 1987. Determination of the homogenization temperatures and densities of supercritical fluids in the system $NaCl-KCl-CaCl_2-H_2O$ using synthetic fluid inclusions. Chemical Geology 64, 335-350.

Wang, C., Ludman, A., 2004. Deformation conditions, kinematics and displacement history of shallow crustal ductile shearing in the Norumbega fault system in the Northern Appalachians, eastern Maine. Tectonophysics 384, 129-148.

Wiedenbeck, M., Goswami, J. N., Roy, A. B., 1996. Stabilization of the Aravalli craton of northwestern India at 2.5 Ga: an ion microprobe zircon study. Chemical Geology 129, 325-340.